ON THE COMBINATORICS OF EXTERNAL RAYS IN THE DYNAMICS OF THE COMPLEX HENON MAP.

A Dissertation

Presented to the Faculty of the Graduate School

of Cornell University

in Partial Fulfillment of the Requirements for the Degree of

Doctor of Philosophy

by

Ricardo Antonio Oliva

May 1998

Addendum.

This is a slightly revised version of my doctoral thesis: some typing and spelling mistakes have been corrected and a few sentences have been re-worded for better legibility (particularly in section 4.3). Also, to create a nicer pdf document with hyperref, the title of section 3.3.2 has been made shorter. The original title was *A model for a map with an attracting fixed point as well as a period-3 sink: the (3-1)-graph*.

ON THE COMBINATORICS OF EXTERNAL RAYS IN THE DYNAMICS OF THE COMPLEX HENON MAP.

Ricardo Antonio Oliva , Ph.D.

Cornell University 1998

We present combinatorial models that describe quotients of the solenoid arising from the dynamics of the complex Hénon map

$$f_{a,c} : \mathbf{C}^2 \to \mathbf{C}^2, \qquad (x, y) \mapsto (x^2 + c - ay,\, x).$$

These models encode identifications of external rays for specific mappings in the Hénon family. We investigate the structure of a region of parameter space in $\mathbf{R}^2$ empirically, using computational tools we developed for this study. We give a combinatorial description of bifurcations arising from changes in the set of identifications of external rays. Our techniques enable us to detect, predict, and locate bifurcation curves in parameter space. We describe a specific family of bifurcations in a region of real parameter space for which the mappings were expected to have simple dynamics. We compute the first few bifurcation curves in this family and label them combinatorially. Our computer experiments also indicate the existence of gaps within the region of real parameter space where Hénon family $f_{a,c}$ has connected Julia set $J_{a,c}$. We show why the verification of this gap would imply the existence of values of a for which the level-a Mandelbrot set, $M_a = \{c \in \mathbf{C} : J_{a,c} \text{ is connected}\}$, is not connected.

BIOGRAPHICAL SKETCH

Ricardo Oliva was born in Valparaíso, Chile, where he hopes to return some day. He came to the US with his parents just before entering high school; three years later he moved to Ithaca, NY, to study at Cornell University where he has been for nearly half of his life and where he also hopes to return some day. At Cornell Ricardo also completed B.S. degree in Applied & Engineering Physics and a M.S. degree in Computer Science. After leaving Cornell Ricardo will spend a year at the Institute for Mathematics and its Applications, University of Minnesota, in the program on Emerging Applications of Dynamical Systems.

Since the Spring equinox of 1986 Ricardo has shared his life with his wife Marta del Campo who has been in his heart since 4th grade of elementary school, and who also will be receiving her Doctorate from Cornell this year; their son Manuel was born two months after Ricardo entered graduate school and already has earned a "doctorate in patience".

A Manuel,

por todos esos días que no pateamos la pelota.

A Marta,

por todo lo que esto nos costó.

Y a la memoria de Aragrev,

con quién yo esperaba compartir estas locuras

pero no alcancé a decírcelo.

Lo más terrible se aprende enseguida

y lo hermoso nos cuesta la vida.

– Silvio Rodríguez.

ACKNOWLEDGEMENTS

I would like to begin by thanking my advisor, Professor John Smillie, for his guidance and encouragement throughout the duration of this project, and for his generous support during my later years as a graduate student. This thesis is also a product of his efforts and not just in an indirect way. We held many discussions in which not only he shared his ideas but also he helped focus mine; I am grateful for his dedication as a mentor.

Much of my gratitude goes also to Professor John Hubbard, who almost exactly four years ago showed me a picture of an unstable manifold for a complex Hénon map and invited me into the problem of studying the combinatorics of these mappings. His enthusiasm for this subject and his initial guidance were pivotal in my choice of topic. It was in his office and his Macintosh where I began the investigations which develop into this thesis, and I thank him for the many ideas he shared with me.

Also I would like to thank Professor John Guckenheimer who welcomed me as an extra student at Cornell's Center of Applied Math. The excellent computer facilities at CAM facilitated the the computer investigations on which much of this work is based.

The Cornell Theory Center grants DMS931236C and DMS980217C provided me with access to the SP2 supercomputer where we produced most of the pictures used in this study.

I am also grateful to to Professor Eric Bedford of Indiana University for helpful discussions while I worked in this project. His questions and suggestions led us to consider the idea of scanning parameter space to detect regions of stability. Bernd Krauskopf got us thinking about ways in which bifurcations curves could be traced in parameter space. Both ideas played a central role in this project.

During my initial years as a graduate student I benefited from the advice and encouragement of many people. In particular, I would like to thank Professor Marshall Cohen who served in my original graduate student Committee; Tom Rishell who taught me my first serious math course when I was still an engineering student and who motivated me to pursue graduate studies in Mathematics; and Ernesto Acosta who took time from his busy last year as a graduate student to answer the many math questions I asked him during my first year.

Finally, to my family and friends, thanks for always being there, especially at the end when things got tough in so many ways.

Table of Contents

List of Tables

List of Figures

Chapter 1

Introduction

One of the main goals in complex dynamics is the description of the set where the "chaotic" dynamics are concentrated. This set is called the Julia set and is denoted by J. For polynomials on $\mathbf{C}$, the Julia set coincides with the boundary of the set K, consisting of points with bounded orbit. Douady and Hubbard introduced "external rays" as a powerful tool for understanding the topology of J in one-dimensional complex dynamics. In one sense external rays are geometric objects: field lines of the Greens function of the set K. Rays are parameterized by the circle and they model the dynamics of $\mathbf{C} - K$ under a polynomial of degree n, in terms of dynamics of the circle under the map $z \mapsto z^n$. The later can be described in terms of symbolic dynamics, and in this sense rays are also combinatorial objects. For expanding polynomials with connected Julia sets each ray has a well defined limit as it approaches J. This defines a "landing map" by which the topology of J can be described as a quotient of the circle. This model of J is known as the "pinched-disk"

model. The combinatorics of external rays have proved very useful in studying the structure of the Julia set as well as the Mandelbrot set ([Br, DH, A]).

Hubbard also introduced sets analogous to K and J for studying the dynamics of the Hénon map

$$f_{a,c}(x, y) \to (x^2 + c - ay,\, x)$$

as a mapping of $\mathbf{C}^2$. Although the definitions of the invariant sets in $\mathbf{C}^2$ are analogous to those for dynamics in one-complex variable, the study of mappings of $\mathbf{C}^2$ requires different mathematical tools and, in general, proves more difficult than the parallels with the one-dimensional theory would suggest. Some of the main advances in the dynamics of the complex Hénon map have been carried out in the works of Hubbard & Oberste-Vorth, Fornaess & Sibony, and Bedford & Smillie.

One of the difficulties of dynamics in $\mathbf{C}^2$ is that, unlike their counterparts in $\mathbf{C}$, the sets J and K can not be "seen" or drawn directly on a computer. Bedford and Smillie proved that for general polynomial diffeomorphisms of $\mathbf{C}^2$ many of the properties of J, in particular its connectivity, can be deduced from "slices" of $\mathbf{C}^2$ by unstable manifolds of points in J. These invariant manifolds are parameterized by $\mathbf{C}$ and can be drawn by computer [1]. Furthermore, it is shown in [BS7] that when J is connected and f is hyperbolic, there exists a combinatorial model for the dynamics of $f|_J$ defined in terms of external rays. For the Hénon map, the external rays are not parameterized by the circle but instead by its inverse limit under the doubling map. This inverse limit construction is known as a solenoid.

[1] This experimental approach had been suggested by Hubbard, who produced the first computer pictures of the unstable manifold of the fixed saddle point of complex Hénon mappings.

In this thesis we study the combinatorics of external rays for the Hénon map. We will present specific examples of quotients of the solenoid resulting from identifications of external rays. These examples give new combinatorial models for the dynamics of polynomial diffeomorphisms of $\mathbf{C}^2$. The quotients of the solenoid are described by means of bi-labeled directed graphs on which paths correspond to pairs of binary sequences representing identified rays.

Another part of this thesis is experimental in nature. We investigate the combinatorial structure of parameter space using computer tools that we developed for the visualization of unstable manifolds and external rays. We describe how the combinatorics of rays changes as parameter values are varied. Changes in the identifications of rays take place through bifurcations in which pairs of identified rays change partners. We can predict these combinatorial changes using the models that encode the identifications. In addition, we implement algorithms to locate the corresponding bifurcations curves in parameter space. These bifurcations correspond to tangencies of invariant manifolds. Some correspond to tangencies of invariant manifolds in $\mathbf{R}^2$, while other bifurcations occur outside $\mathbf{R}^2$ and have not been described before.

A surprising discovery resulting from our computer investigations is that there appear to be thin bands in parameter space where the Julia set is disconnected. A consequence of the rigorous confirmation of this discovery would be the existence of parameter values $a > 0$ for which the level-a Mandelbrot set $\mathcal{M}_a = \{c : J_{a,c} \text{ is connected}\}$ is not connected, in contrast with the classic theorem of Douady and Hubbard which proved that the Mandelbrot set $\mathcal{M}_0$ is connected.

1.1 Thesis Summary.

In Chapter 2 we review the essential background for the dynamics of the Hénon map as a polynomial diffeomorphisms of $\mathbf{C}^2$. In §2.2 we present the main definitions from [HOV1, BS7]. We discuss the complex solenoid as the space of rays and as a symbolic dynamical system (§2.3). In §2.4 we present the theorems of Bedford and Smillie which provide the semi-conjugacy from the solenoid. In §2.5 we discuss the information encoded in the computer pictures of unstable manifolds.

In Chapter 3 we construct the combinatorial models in term of directed labeled graphs representing equivalence relations in the space of symbol sequences. We show how to construct these graphs for the pinched-disk model a quadratic polynomials $z \mapsto z^2 + c$ when c is in a real hyperbolic component of the Mandelbrot set (§3.2). In §3.3 we present two graphs that model Hénon mappings whose combinatorics differ from those arising from polynomials on $\mathbf{C}$. There are restrictions in the possible quotients of the solenoid that can arise from identifying external rays. Section §3.3.3 is devoted to proving that the quotients produced by our models satisfy the known combinatorial conditions given in [BS7].

In Chapter 4 we examine the structure of a region in real parameter space. We associate changes in the identifications of specific rays with bifurcations curves separating regions of apparent stability. We present computer evidence supporting our conjecture that the combinatorics of Hénon mappings within two of these stable regions are those given by specific models presented in chapter 3. From the differences in the set of identifications given by these models, we deduce other bifurcations

that must occur between the regions in parameter space were each model applies. A complete combinatorial description for the minimum set of bifurcations between two of the models is given in section 4.3. We then verify some of these predictions and describe "fans" of bifurcation lines in parameter space associated with specific families of rays (§4.3.2). In section §4.4 we present the computer evidence for the thin bands of disconnectivity in parameter space, and show why they would imply the disconnectivity of the connectivity locus $\mathcal{M}_a$.

Some details of the algorithms used to compute the unstable manifold pictures and external rays are given in the appendix.

Chapter 2

Preliminaries.

2.1 External rays for polynomials on C.

We begin with a quick overview of some well known concepts from dynamics in one complex variable which have useful analogies in the study of polynomial mappings on $\mathbf{C}^2$.

Let $K_c \subset \mathbf{C}$ be the set of points that remain bounded under iteration by the polynomial $P_c : z \mapsto z^2 + c$. The set $J_c = \partial K_c$ is known as the Julia set of P_c and carries the chaotic dynamics: the iterates of P_c form a normal family in $\mathbf{C} - J_c$. J_c is non-empty, compact, and either connected or totally disconnected. The connectivity locus $\mathcal{M} = \{c : J_c \text{ is connected } \}$ is known has the Mandelbrot set.

When K_c is connected, the Böttcher coordinate in a neighborhood of infinity can be extended to give a holomorphic bijection $\varphi_c : \mathbf{C} - K \to \mathbf{C} - \overline{\Delta}$ which conjugates the dynamics of P_c outside K_c to the action of $z \mapsto z^2$ outside the unit disk. This

endows $\mathbf{C} - K$ with a natural system of polar coordinates "imported" from $\mathbf{C} - \overline{\Delta}$ via the homeomorphism $\psi_c := \varphi_c^{-1}$. The images under ψ_c of circles centered at the origin are termed equipotentials, and the images of lines of constant angle are called external rays. The ray with angle θ is said to "land" at the point z_θ if z_θ is the limit of $\psi(re^{i\theta})$ as r approaches 1. The landing lemma of Douady and Hubbard shows that rays with rational angle always land. When ψ extends to a continuous map on the boundary the landing map $\theta \mapsto \psi(e^{2\pi i\theta})$ induces a semi-conjugacy between the doubling map on $S^1 = \partial\Delta$ and the action of P_c on $J_c = \partial K_c$. As a result, the parameterization of external rays by their angular coordinate induces a parameterization of J_c. The equivalence relation on S^1 induced by the landing map provides an abstract topological description for the Julia set, known as the "pinched disk" model ([D]). This model can be given a combinatorial description via the natural semi-conjugacy between the doubling map on the circle and the left-shift map on the space of right-infinite binary sequences where points in S^1 are represented by the binary expansion of their angular coordinate. This leads to a combinatorial model of J_c as a quotient of the space of one-sided binary sequences for the case of expanding polynomials with J_c connected.

2.2 Complex Hénon Mappings and their Julia set.

By a theorem in [FM] every polynomial diffeomorphisms of $\mathbf{C}^2$ with interesting dynamics is conjugate to a finite composition of maps of the form

$$f : (x, y) = (P(x) - ay, x)$$

where P is a monic polynomial in x of degree at least two, and $a \neq 0$. These are called generalized Hénon mappings. In this sense the Hénon map, when $P = P_c$, is a fundamental family to consider.

The relevant sets for the dynamics of polynomial diffeomorphisms of $\mathbf{C}^2$ are defined in a similar way as for polynomials in one-dimensional complex dynamics, but both forward and backwards orbits of points have to be considered. In particular, K_c and J_c have the following analogs for for a polynomial diffeomorphism of $\mathbf{C}^2$:

$$K^{\pm} = \{p \in \mathbf{C}^2 \,:\, f^{\pm n}(p) \not\to \infty \text{ as } n \to +\infty\}, \tag{2.1}$$

$$J^{\pm} = \partial K^{\pm}, \quad \text{and} \tag{2.2}$$

$$J = J^{-} \cap J^{+}. \tag{2.3}$$

The set J will be referred to as "the Julia set" of f, as it corresponds to the locus of points where the dynamics are expected to be "chaotic". Points in $U^{\pm} = \mathbf{C}^2 - K^{\pm}$ escape to infinity under forward/backward iteration at a rate measured by the Green function of $K^{\pm}$, respectively, which can be defined as

$$G^{\pm}(p) = \lim_{n\to\infty} \frac{1}{d^n} \log^{+} ||f^{\pm n}(p)|| = \lim_{n\to\infty} \frac{1}{d^n} \log^{+} |\pi_x\, f^{\pm n}(p)| \tag{2.4}$$

where π_x is the projection to the first coordinate [HOV1]. It follows that

$$G^{\pm} \circ f^{\pm} = d\, G^{\pm}. \tag{2.5}$$

The recurrent dynamics occur in a bounded part of $\mathbf{C}^2$. In fact, for sufficiently

large R the regions defined

$$V^+ = \{|x| \geq |y|,\, G^+ \geq \log R\}, \tag{2.6}$$

$$V^- = \{|x| \leq |y|,\, G^- \geq \log R\} \quad \text{and} \tag{2.7}$$

$$V = \{G^+,\, G^- < \log R\} \tag{2.8}$$

provide a partition of $\mathbf{C}^2$ such that, relative to these regions, the forward orbit of any point behaves as indicated in figure 2.1: points in V^+ never escape V^+ and belong to U^+, the forward orbit of any point in V^- enters V or V^+; and the forward orbit of a point in V either belongs to V, in which case the point is in K^+, or enters V^+. If R is large enough, the picture for backward orbits is the same with V^+ and V^- interchanged. Then, $U^\pm = \cup_{n>0} f^{\mp n}(V^\pm)$, $J^\pm \subset V \cup V^\mp$, and $J \subset V$. Note in particular that $J^- \cap \{G^+ > R\} \subset V^+$.

In $V^+ \subset U^+$ one can define a "direction of escape" function $\varphi^+ : V^+ \to \mathbf{C}$ by

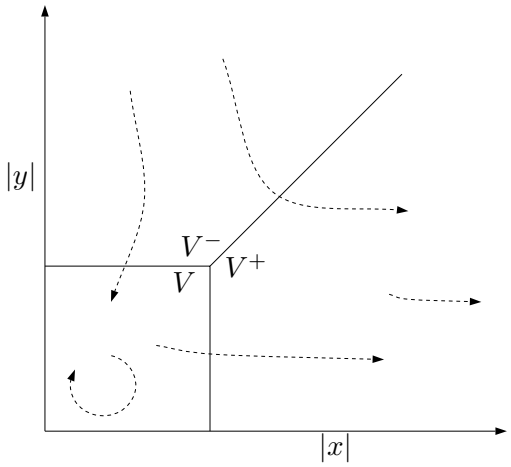

Figure 2.1:

the uniformly converging sequence

$$\varphi^+(x,y) = \lim_{n\to\infty} \left(\pi_x \circ f^n(x,y)\right)^{1/d^n}, \tag{2.9}$$

where π_x is the projection to the first coordinate and the root is chosen such that $\varphi^+ \approx \pi_x$ at infinity. This definition is analogous to that of the function φ_c which conjugates the action of the polynomial P_c in a neighborhood of infinity to the action of $z \mapsto z^2$, and which is used in the definition of external rays in the one-dimensional theory. Thus, φ^+ gives an analogous semi-conjugacy for f on V^+, namely $\varphi^+ \circ f = (\varphi^+)^d$. Hubbard and Oberste-Vorth showed that φ^+ can not be extended analytically to all of U^+ ([HOV1]). In [BS6] Bedford and Smillie give topological conditions under which φ^+ extends analytically to $J_+^- := J^- \cap U^+$, inducing a semi-conjugacy Φ between f on J_+^- and the inverse limit of $\mathbf{C} - \overline{\Delta}$ under $z \mapsto z^d$. Accordingly, J_+^- is equipped with "external rays" and plays a role analogous to that played by of exterior of K_c for the polynomial P_c.

2.3 The complex solenoid

Let $\sigma : X \to X$ be a dynamical system. The inverse limit of X under σ defines an invertible dynamical system, $\hat{\sigma} : \hat{X} \to \hat{X}$, where $\hat{X}$ is the space of (bi)-infinite sequences of histories under σ of points in X:

$$\hat{X} = \left\{\xi \in X^{\mathbf{Z}} \,:\, \xi_{i+1} = \sigma(\xi_i) \;\forall\; i \in \mathbf{Z}\right\}$$

with the product topology, and $\hat{\sigma}$ is the homeomorphism induced by σ:

$$[\hat{\sigma}(\xi)]_n = \sigma(\xi_n) = \xi_{n+1}$$

Thus, a point in $\hat{X}$ is specified by a sequence of consecutive pre-images under σ of a point in X, and $\hat{\sigma}$ is the map that shifts sequences to the left. Although we write $\xi \in \hat{X}$ as a bi-infinite sequence, the specification of any coordinate ξ_n determines ξ_m for all $m > n$. The projections to the n-th coordinate of a point, $\hat{\pi}_n : \hat{X} \to X,\ \xi \mapsto \xi_n$, are continuous and satisfy $\hat{\pi}_n \circ \hat{\sigma} = \sigma \circ \hat{\pi}_n$. When X is a topological group with identity element 1, then $\hat{X}$ is also a topological group with group operation defined coordinatewise and with the constant sequence $\mathbf{1} = (\dots, 1, 1, 1, \dots)$ as identity element. In any topological group, the the path component of $\mathbf{1}$ is a subgroup and its topology determines the topology of the whole group ([Hig]). If $H_{\mathbf{1}}$ denotes the component of $\mathbf{1}$, then the path component of any other element in the group is given by the coset $\hat{s}\, H_{\mathbf{1}}$.

The degree-d complex solenoid, denoted by Σ, is the inverse limit of $\mathbf{C}^*$ under $\sigma_d : z \mapsto z^d$, $d \geq 2$. From $\mathbf{C}^*$, Σ inherits the structure of a topological group under multiplication. The unit element will be denoted by $\mathbf{1}$. The subgroup

$$\Sigma_0 = \{\xi \in \Sigma \,:\, |\xi_0| = 1\}$$

is the topological space usually known as the solenoid[1]. We will refer to the subspace that projects to the exterior of the unit disk,

$$\Sigma_+ = \{\xi \in \Sigma \,:\, |\xi_0| > 1\}$$

as the "exterior" solenoid. The exterior solenoid plays a fundamental role as a model for the dynamics "outside" K^+, much like the role played by the exterior of

[1]Smale introduced the solenoid as an example of a hyperbolic dynamical system $F : \hat{T} \to \hat{T}$, where F maps the solid torus $T \subset \mathbf{R}^3$ strictly inside itself d times around its "hole" without intersections, and $\hat{T} = \cap_{n>0} F^n(T)$. This is also discussed in [Shu].

the unit disk under $z \mapsto z^2$ in the study of quadratic polynomials in the plane. The main tool from that theory are external rays: lines of constant angular coordinate in the plane. Below we introduce their natural analogs in Σ_+.

2.3.1 External rays on the complex solenoid.

We write $\Sigma_{\mathbf{R}_+}$ for the subgroup of the solenoid consisting of points with all coordinates in the positive real numbers, namely

$$\Sigma_{\mathbf{R}_+} = \{\xi \in \Sigma \,:\, \xi_n = |\xi_n| \;\forall n \in \mathbf{Z}\}.$$

The "inclusion" map defined by

$$\mathbf{R}_+ \ni r \mapsto \hat{r} \in \Sigma_{\mathbf{R}_+} \quad \text{with} \quad \hat{r}_n = r^{d^n}$$

is a homeomorphism (with inverse $\hat{\pi}$). The pair of maps

$$\rho : \Sigma \to \Sigma_{\mathbf{R}_+} \qquad [\rho(\xi)]_n = |\xi_n| \tag{2.10}$$

$$\Theta : \Sigma \to \Sigma_0 \quad [\Theta(\xi)]_n = \xi_n/|\xi_n| \tag{2.11}$$

are continuous and surjective. Clearly $\xi = \rho(\xi)\Theta(\xi)$ for all $\xi \in \Sigma$ hence

$$\Sigma = \Sigma_{\mathbf{R}_+}\Sigma_0.$$

It follows that Σ is homeomorphic to the product $\mathbf{R}_+ \times \Sigma_0$, with $\Sigma_+ = \{r > 1\} \times \Sigma_0$. In this sense ρ and Θ are the natural "polar" coordinates of Σ. The external ray above $\omega \in \Sigma_0$ is the path in the exterior solenoid Σ_+ having "constant Θ coordinate":

$$\mathcal{R}_\omega = \{\xi \in \Sigma_+ \,:\, \Theta(\xi) = \omega\} = \{\hat{r}\,\omega \,:\, r > 1\}$$

The point ω is said to be the landing point of $\mathcal{R}_\omega$, and the ray $\mathcal{R}_\omega$ is said to pass through $\xi \in \Sigma_+$ if $\xi \in \Sigma_+ \cap \mathcal{R}_\omega$.

Since both ρ and Θ commute with $\hat{\sigma}$, rays are preserved by the shift map and the action of $\hat{\sigma}$ on rays reduces to the action of $\hat{\sigma}$ on Σ_0.

For any $\xi \in \Sigma_+$ there is a unique ray that passes through ξ, and this ray lands at $\Theta(\xi)$. In particular, the external ray above $\mathbf{1} \in \Sigma_0$ is given by

$$\mathcal{R}_{\mathbf{1}} = \{\hat{r} \ : \ r > 1\} = \Sigma_{\mathbf{R}_+} \cap \Sigma_+.$$

Next we discuss how path components in Σ_+ can be given a global parameterization by the complex half-plane in which rays correspond to horizontal lines.

2.3.2 Parameterization of components.

Let $\Omega(\omega, \Sigma_0)$ denote the path component of Σ_0 containing ω. Then, $\Omega(\omega, \Sigma_0)$ is the coset $\omega\, \Omega(\mathbf{1}, \Sigma_0)$. As shown below, path components in Σ_0 are not closed.

The complex exponential $\mathbf{C} \ni z \to e^z \in \mathbf{C}^*$, is a (universal) covering map that covers $\mathbf{C}^* - \Delta$ by the half-plane $\mathbf{H} = \{z \in \mathbf{C} : \text{Real}\, z > 0\}$, and $S^1 = \partial\Delta$ by the imaginary axis $i\mathbf{R} = \{z \in \mathbf{C} : \text{Real}\, z = 0\}$. Given a point z above $e^z \in \mathbf{C}^*$, there is a natural choice of $\omega \in \Sigma$ such that $\hat{\pi}(\omega) = e^z$, namely $\omega_n = (e^z)^{d^n}$. We denote such point by $\boldsymbol{e}^z$. This defines a map $\mathbf{C} \to \Sigma$.

Lemma 1 (Parameterization via exp). *The function* $\mathbf{exp} : \mathbf{C} \to \Sigma$ *defined by*

$$\mathbf{exp}(z) = \boldsymbol{e}^z \qquad \textit{where} \quad [\boldsymbol{e}^z]_n = (e^z)^{d^n}$$

is continuous and injective, and satisfies the "rule of exponents" $\boldsymbol{e}^{z_1}\boldsymbol{e}^{z_2} = \boldsymbol{e}^{z_1+z_2}$.

Proof. Each coordinate function $[\boldsymbol{e}^z]_n = e^{zd^n}$ is continuous and obeys the law of exponents, hence so does **exp**. To verify injectivity suppose $\boldsymbol{e}^{x+iy} = \boldsymbol{e}^{u+iv}$. Then $e^{(x+iy)d^n} = e^{(u+iv)d^n}$ for every n. Taking norms it follows that $x = u$ since the real exponential is injective. We are left with $e^{iyd^n} = e^{ivd^n}$ for every n, which implies that the product $(y-v)d^n$ is an integer multiple of 2π for each n. But $(y-v)d^{-n} < 1$ for n large enough, therefore $(y-v)d^{-n} = 0$ for some n, hence $y = v$. □

Clearly $\boldsymbol{e}^{i\mathbf{R}} \subset \Sigma_0$ so the path component of $\mathbf{1} = \boldsymbol{e}^0$ in Σ_0 contains a copy of $\mathbf{R}$ parameterized by $y \mapsto \boldsymbol{e}^{iy}$. In fact, this parameterizes all of $\Omega(\mathbf{1}, \Sigma_0)$.

Lemma 2. *The path components of* Σ_0 *are homeomorphic to* $\mathbf{R}$ *and agree with the unstable manifolds, namely*

$$\mathbf{exp}(i\mathbf{R}) = \Omega(\mathbf{1}, \Sigma_0) = W^u(\mathbf{1}, \Sigma_0).$$

Proof. Let $\gamma : [0,1] \to \Sigma_0$ be a path in the solenoid with initial point $\gamma(0) = \mathbf{1}$ and terminal point ω. We want to show that $\omega = \boldsymbol{e}^{it}$ for some $t \in \mathbf{R}$. The projections $\gamma_n = \pi_n \circ \gamma$ are paths in S^1 with initial point $\gamma_n(0) = 1$, and such that $\gamma_n(t)^d = \gamma_{n+1}(t)$. Let $\tilde{\gamma}_n$ be the lift of γ_n to the universal cover of S^1. Then $\tilde{\gamma}_n$ is a path in $\mathbf{R}$ with initial point $\tilde{\gamma}_n(0) = 0$, and such that $\tilde{\gamma}_n(t)\, d = \tilde{\gamma}_{n+1}(t)$. Let $t_0 = \tilde{\gamma}_0(1)$. Then $\tilde{\gamma}_n(1) = t_0 d^n$ for any n; then for N large enough we have $t_0 d^{-N} < 2\pi$, implying $\gamma_{-N}(1) = \omega_{-N} = e^{it_0/2^N}$. This shows $\gamma(1) = \boldsymbol{e}^{it_0}$, hence $\Omega(\mathbf{1}, \Sigma_0) \subset \mathbf{exp}(i\mathbf{R})$. In addition, $\omega_{-n} = \gamma_{-n}(1) = e^{it_0/d^n} \to 1$ as $n \to \infty$. This implies $\hat{\sigma}^{-n}(\omega) \to \mathbf{1}$ as $n \to \infty$, hence $\omega \in W^u(\mathbf{1})$. This shows $\Omega(\mathbf{1}, \Sigma_0) \subset W^u(\mathbf{1})$, and we have

$$\Omega(\mathbf{1}, \Sigma_0) = \boldsymbol{e}^{i\mathbf{R}} \subset W^u(\mathbf{1}).$$

Now let $x \in W^u(\mathbf{1})$. Then $\hat{\sigma}^{-n}(x) \to \mathbf{1}$ implies $x_{-n} \to 1$, as $n \to \infty$. Hence, for any given $\varepsilon > 0$ there exist $n_0 < 0$ such that

$$x_n \in \{e^{it} \ : \ t \in (-\varepsilon, \varepsilon)\} \quad \text{for} \ \ n \leq n_0.$$

Let $x_n = e^{it_n}$. Then t_n satisfies $t_{n-1}d = t_n \mod (1)$ for each n, thus

$$t_{n-1} \in \{(t_n + k)/d \ : \ k = 0, \ldots, d-1\}.$$

This together with t_n, $t_{n-1} \in (-\varepsilon, \varepsilon)$ for $n < n_0$, with ε small enough, imply that

$$t_{n-1} = t_n/d \quad \text{for } n \leq n_0 < 0.$$

But then $t_{n_0-k} = t_{n_0}/d^k$ for $k \in \mathbf{Z}$, and therefore $x = \boldsymbol{e}^{it_0}$ with $t_0 = t_{n_0} d^{|n_0|}$. This shows $W^u(\mathbf{1}) \subset \mathbf{exp}(i\mathbf{R})$. □

It follows that the path component of $\mathcal{R}_{\mathbf{1}}$ in Σ_+, denoted $\Omega(\mathbf{1}, \Sigma_+)$, is parameterized by $\mathbf{H}$ via $\mathbf{exp}$, and we call $\mathbf{exp}(\mathbf{H})$ the canonical parameterization of $\Omega(\mathbf{1}, \Sigma_+)$. With this choice of coordinates, the external ray above $\mathbf{1}$ is given by

$$\mathcal{R}_{\mathbf{1}} = \{\boldsymbol{e}^r \ : \ r > 0\} = \mathbf{exp}(\mathbf{R}_+)$$

and the external rays above any other $\omega \in \Omega(\mathbf{1}, \Sigma_0)$ is given by $\{\boldsymbol{e}^r \boldsymbol{e}^{iy_0} \ : \ r > 0\}$ where $\omega = \boldsymbol{e}^{iy_0}$. More generally, the external ray above any $\omega \in \Sigma_0$ correspond to the path

$$\mathcal{R}_\omega = \{\omega \boldsymbol{e}^r \ : \ r > 0\} = \omega \, \mathbf{exp}(\mathbf{R}_+),$$

and the path component of Σ_+ containing $\mathcal{R}_\omega$ can be parameterized as $\omega \, \mathbf{exp}(\mathbf{H})$, choosing ω as a base point. This is not unique, but if ω and υ are in the same path component of Σ_0, then $\upsilon = \omega e^{iy}$ in the parameterization given by ω, therefore both parameterizations agree up to multiplication by an element of $\Omega(\mathbf{1}, \Sigma_0)$.

2.3.3 Binary Representation of Σ_0

The degree-2 solenoid has a natural representation as a quotient of the shift on the space of binary sequences $\{0,1\}^{\mathbf{Z}}$, with the word "natural" justified by the fact that the map $z \mapsto z^2$ on S^1 corresponds to "shifting" the base-2 expansion of the angular polar coordinate: $0.b_0b_1b_2\cdots \mapsto 0.b_1b_2b_3\cdots$. Thus, a choice of an inverse image under $z \mapsto z^2$ for a point $z = e^{2\pi i\theta}$ with $\theta = 0.b_0b_1b_2\ldots$ in base 2, corresponds to a choice of $b_{-1} \in \{0,1\}$ for $0.b_{-1}b_0b_1b_2\cdots$. More generally, a history

$$(\cdots, z_{-3},\, z_{-2},\, z_{-1}), \qquad (z_{-n})^{2^n} = z,$$

of such z corresponds to a specific choice of b_{-1}, b_{-2}, $b_{-3}, \cdots$, each $b_i \in \{0,1\}$, for the sequence

$$(\cdots (0.b_{-3}b_{-2}b_{-1}\ldots),\, (0.b_{-2}b_{-1}b_0\ldots),\, (0.b_{-1}b_0b_1\ldots))\,.$$

This suggests how each point in $s \in \Sigma_0$ can be specified by a point $b \in \{0,1\}^{\mathbf{Z}}$, and how the shift on the solenoid agrees with the shift on $\{0,1\}^{\mathbf{Z}}$. Below we outline the semi-conjugacy in detail and introduce notation that will be used in later section.

Finite binary sequences will be referred to as *words*, and the length of the word x will be denoted $|x|$. The word resulting from the concatenation of two words x and y is written xy, and the concatenation of x with itself n-times is written x^n so that the usual rule of exponents applies: $x^nx^m = x^{n+m}$ with the convention that $x^0 = \varepsilon$, the empty word. The space bi-infinite binary sequences will be denoted by $\mathcal{S}_2$. It will be convenient to also use $\mathcal{S}_2^+$ and $\mathcal{S}_2^-$ to denote, respectively, the space

of left- and right-infinite sequences written as

$$\mathcal{S}_2 = \{(\cdots b_{-1}.b_0 b_1 \cdots) \,:\, b_i \in \{\mathtt{0},\mathtt{1}\}\},$$

$$\mathcal{S}_2^+ = \{(b_0 b_1 \cdots) \,:\, b_i \in \{0,1\}\}$$

$$\mathcal{S}_2^- = \{(\cdots b_{-2} b_{-1}) \,:\, b_i \in \{0,1\}\}.$$

so that the indices agree naturally with $\mathcal{S}_2 = \mathcal{S}_2^- \times \mathcal{S}_2^+$. As customary, a period is used to indicate the 0-th term within a specific sequence. If x is a (non-empty) word the notations ${}^{\infty}x$ and x^{∞} denote, respectively, the element of $\mathcal{S}_2^-$ and $\mathcal{S}_2^+$ in which x repeats infinitely often. A bi-infinite sequence is periodic of period k if it can be written as ${}^{\infty}z.z^{\infty}$ with z a word of minimal length k. The constant sequences ${}^{\infty}\mathtt{0}.\mathtt{0}^{\infty}$ and ${}^{\infty}\mathtt{1}.\mathtt{1}^{\infty}$ will also be denoted by $\underline{\mathtt{0}}$ and $\underline{\mathtt{1}}$, respectively. A word occurring within a sequence is called a sub-word of b, or block of b. We use interval sub-indices, such as $b_{[n,m]}$, $b_{(-\infty,n]}$ and $b_{[n,\infty)}$, to denote a subword or left/right subsequences, for instance,

$$b_{[n,n+k]} = b_n b_{n+1} \cdots b_{n+k}, \tag{2.12}$$

$$b_{[n,n+k)} = b_n b_{n+1} \cdots b_{n+k-1}, \quad \text{and} \tag{2.13}$$

$$b_{[n,\infty)} = (b_n b_{n+1} \cdots) \in \mathcal{S}_2^+. \tag{2.14}$$

The central n-block of $b \in \mathcal{S}_2$ refers to $b_{[-n,n]}$.

We consider $\mathcal{S}_2$ (also $\mathcal{S}_2^+$ and $\mathcal{S}_2^-$) as having the product topology and metric given by

$$d_2(a,b) = \begin{cases} 2^{-|k|-1} & \text{where } \exists\, k \,:\, a_k \neq b_k \text{ and } a_n = b_n \text{ for } |n| < |k| \\ 0 & \text{otherwise.} \end{cases}$$

hence a neighborhood about b of size less than $1/2^k$, $k \geq 1$, consists of sequences that agree with b in an initial k-block. This gives $\mathcal{S}_2$ (also $\mathcal{S}_2^+$ and $\mathcal{S}_2^-$) the topology of a Cantor set ([KH, LM]). On $\mathcal{S}_2$ the left shift $\sigma : b \mapsto b'$ defined by $b'_n = b_{n+1}$ gives a homeomorphism. The natural projection $\mathcal{S}_2 \ni b \mapsto b_{[0,\infty)} \in \mathcal{S}_2^+$ is continuous.

The usual binary representation of the circle by $\mathcal{S}_2^+$ has a natural generalization to $\mathcal{S}_2$ in which the angle function simply "ignores" the left-part of a bi-infinite sequence. Namely, the map

$$\theta : \mathcal{S}_2 \to S^1, \qquad \theta(b) = e^{i2\pi\vartheta(b)}$$

where

$$\vartheta(b) = \sum_{i=0}^{\infty} \frac{b_i}{2^{i+1}} \quad (= 0.b_0b_1b_2\cdots \text{in base } 2),$$

is continuous and satisfies $\sigma\theta = (\theta)^2$. Hence, θ defines a semi-conjugacy between the shift map on $\mathcal{S}_2$ and the squaring map on S^1, and this induces a semi-conjugacy with the solenoid

$$\hat{\theta} : \mathcal{S}_2 \to \Sigma_0, \qquad [\hat{\theta}(b)]_n = \theta(\sigma^n b).$$

Thus, under $\hat{\theta}$, a bi-infinite sequence $b = b_{(-\infty,-1]}.b_{[0,\infty)}$ determines a point in the circle from the angle specified by $b_{[0,\infty)}$ (interpreted as a binary expansion), and also a history of this point from its digits to the left, $b_{(-\infty,-1]}$. More specifically, the subword $b_{[-n,-1]}$ selects a choice of 2^n-th root of $\hat{\pi}\hat{\theta}(b) = [\hat{\theta}(b)]_0 \in S^1$ as specified in the next lemma.

Lemma 3. *Let $\vartheta(b) = t$. For each $n \geq 0$, $[\hat{\theta}(b)]_n = e^{i2\pi t2^n}$ (by definition), and $[\hat{\theta}(b)]_{-n} = e^{i2\pi(t+k)/2^n}$ where $b_{[-n,-1]}$ gives the binary representation of the integer k.*

Proof. By definition, $[\hat{\theta}(b)]_{-n} = e^{i2\pi\vartheta(\sigma^{-n}b)}$ and $\vartheta(\sigma^{-n}b) = \sum_{j=0}^{\infty} b_{j-n}/2^{i+1}$ can be rewritten as

$$\begin{aligned}\vartheta(\sigma^{-n}b) &= \left(\frac{b_{-n}}{2} + \cdots + \frac{b_{-1}}{2^n}\right) + \sum_{j=0}^{\infty} \frac{b_i}{2^n 2^{i+1}} \\ &= \frac{1}{2^n}\left(b_{-n}2^{n-1} + \cdots + b_{-1}2^0\right) + \frac{t}{2^n} \\ &= \frac{1}{2^n}\left(k + t\right).\end{aligned}$$

□

Lemma 4. *The mapping $\hat{\theta}$ is continuous, onto, and satisfies $\hat{\theta}\sigma = \hat{\sigma}\hat{\theta}$.*

Proof. Each coordinate function $\hat{\theta}_n$ is continuous being a composition of continuous functions, surjectivity follows from Lemma 3, and the conjugation relation follows directly from the definition:

$$\left[\hat{\theta}(\sigma b)\right]_n = \theta(\sigma^n \sigma b) = \theta(\sigma^{n+1} b) = \left[\hat{\theta}(b)\right]_{n+1} = \left[\hat{\sigma}\hat{\theta}(b)\right]_n.$$

□

Therefore Σ_0 is homeomorphic to the quotient

$$\tilde{\mathcal{S}}_2 = \mathcal{S}_2/\sim \quad \text{where} \quad a \sim b \iff \hat{\theta}(a) = \hat{\theta}(b) \tag{2.15}$$

and $(\Sigma_0, \hat{\sigma})$ is conjugate to $(\tilde{\mathcal{S}}_2, \sigma)$.

Lemma 5. *If $a \neq b$ but $a \sim b$ then either a and b are the constant sequences, $\{a, b\} = \{\underline{0}, \underline{1}\}$, or there is an index m such that $\{a_{[m,\infty)},\ b_{[m,\infty)}\} = \{10^\infty, 01^\infty\}$ and $a_{(-\infty,m)} = b_{(-\infty,m)}$.*

Proof. Suppose $a, b \in \mathcal{S}_2$ satisfy $\hat{\theta}(a) = \hat{\theta}(b)$ and $a \neq b$. Then, there is $m \in \mathbf{Z}$ such that $a_m \neq b_m$; without loss of generality suppose $a_m = \mathtt{0},\ b_m = \mathtt{1}$. Now, $\hat{\theta}(a) = \hat{\theta}(b) \iff \theta(\sigma^n a) = \theta(\sigma^n b)$ for each n; in particular $\theta(\sigma^m a) = \theta(\sigma^m b)$. This is equivalent to $\vartheta(\sigma^m b) = \vartheta(\sigma^m a) \mod (1)$. However, as $a_m = \mathtt{0}$ and $b_m = \mathtt{1}$,

$$\vartheta(\sigma^m a) \in [0, \tfrac{1}{2}] \qquad \text{and} \qquad \vartheta(\sigma^m b) \in [\tfrac{1}{2}, 1].$$

Therefore $\vartheta(\sigma^m b) = \vartheta(\sigma^m a) \mod (1)$ only if

$$\vartheta(\sigma^m a) = 0 \text{ and } \vartheta(\sigma^m b) = 1, \qquad \text{or} \qquad \vartheta(\sigma^m a) = \tfrac{1}{2} = \vartheta(\sigma^m b).$$

From these two cases, respectively, and the definition of ϑ it follows that either

$$a_{[m+1,\infty)} = \mathtt{0}^\infty \text{ and } b_{[m+1,\infty)} = \mathtt{1}^\infty, \quad \text{or} \qquad a_{[m+1,\infty)} = \mathtt{1}^\infty \text{ and } b_{[m+1,\infty)} = \mathtt{0}^\infty.$$

Therefore, $a_{[m,\infty)} \in \{\mathtt{00}^\infty, \mathtt{01}^\infty\}$ and $b_i \neq a_i$ for $i \geq m$. Reversing the assumption $a_m = \mathtt{0},\ b_m = \mathtt{1}$ to $a_m = \mathtt{1},\ b_m = \mathtt{0}$ interchanges the role of a and b. In either case, we conclude that a and b are constant for $n > m$ with opposite symbols:

$$\{a_{[m+1,\infty)},\ b_{[m+1,\infty)}\} = \{\mathtt{0}^\infty, \mathtt{1}^\infty\}. \qquad (*)$$

But m is an arbitrary index such that $a_m \neq b_m$, so either $(*)$ holds for all m, in which case a and b are the constant sequences, or there is some integer $m' \leq m$ such that $a_i = b_i$ for $i < m'$ and $\{a_{[m',\infty)},\ b_{[m',\infty)}\} = \{\mathtt{10}^\infty, \mathtt{01}^\infty\}$. □

We say that $\omega \in \Sigma_0$ has (binary) coding b if $\hat{\theta}(b) = \omega$. According to Lemma 5 any $\omega \in \Sigma_0$ has a unique coding b such that $b_{[n,\infty)} \neq \mathtt{1}^\infty$ for any n. If b is of this form then ω_0 has an angle $\vartheta(b) \in [0, \frac{1}{2})$ if, and only if, $b_0 = \mathtt{0}$. By considering the shifted sequence $\sigma^n b$, the same conclusion applies to b_n and ω_n. This defines an inverse to $\hat{\theta}$ relative to $\tilde{\mathcal{S}}_2$. We let $\measuredangle(z)$ denote the angle of $z \in \mathbf{C}$ measured in turns.

Lemma 6 (Binary coding of Σ_0). *The map $\boldsymbol{\beta} : \Sigma_0 \to \tilde{\mathcal{S}}_2$ defined by*

$$[\boldsymbol{\beta}(\omega)]_n = \begin{cases} \mathtt{0} & \text{if } \measuredangle(w_n) \in [0, \frac{1}{2}) \\ \mathtt{1} & \text{otherwise} \end{cases} \tag{2.16}$$

satisfies $\hat{\theta} \circ \boldsymbol{\beta}(\omega) = \omega$ for $\omega \in \Sigma_0$, and $\boldsymbol{\beta} \circ \hat{\theta}(b) = b$ for $b \in \tilde{\mathcal{S}}_2$ not ending in $\mathtt{1}$'s.

The conjugacy between Σ_0 and a quotient of the symbolic space $\mathcal{S}_2$ makes it easy to see some of its dynamical characteristics. For instance, since the distance between points in $\mathcal{S}_2$ is determined from the central block in which they agree, it is clear that the set of periodic orbits is dense. Similarly, it is clear that unstable manifolds in $\mathcal{S}_2$ consists of sequences that agree sufficiently far to the right, and stable manifolds are given by sequences that agree to the left:

$$\begin{aligned} W^s(b, \mathcal{S}_2) &= \{a \,:\, \exists\, n \;\; a_{[n,\infty)} = b_{[n,\infty)}\}. \\ W^u(b, \mathcal{S}_2) &= \{a \,:\, \exists\, n \;\; a_{(-\infty,n]} = b_{(-\infty,n]}\} \end{aligned}$$

It follows from Lemma 5 that $W^u(b, \tilde{\mathcal{S}}_2) = W^u(b, \mathcal{S}_2)$ if b is not constant, otherwise the unstable manifold consists of sequences that are eventually constant to the left:

$$W^u(\underline{\mathtt{0}}, \tilde{\mathcal{S}}_2) = W^u(\underline{\mathtt{0}}, \mathcal{S}_2) \cup W^u(\underline{\mathtt{1}}, \mathcal{S}_2) = W^u(\underline{\mathtt{1}}, \tilde{\mathcal{S}}_2).$$

The symbolic characterization of unstable manifolds also tells us the following:

Lemma 7. *Path components are dense in Σ_0 and each contains at most one periodic point.*

Proof. Path components correspond to unstable manifolds (Lemma 2). For arbitrary $a, b \in \tilde{\mathcal{S}}_2$ and $n > 1$, the point $b' = b_{(-\infty,-n)})a_{[-n,\infty)}$ belongs to $W^u(b)$ and

and to the $1/2^n$-neighborhood of a, so components are dense. Next, two sequences that agree "to the left" and are periodic also agree "to the right", hence are equal, or if both are "constant to the left" and are periodic they are both constant, hence equal in $\tilde{\mathcal{S}}_2$. □

The subset of $\tilde{\mathcal{S}}_2$ consisting of sequences that are eventually zero to the left provides a natural representation of $\{\mathbf{R} \geq 0\}$ (via the standard binary representation of real numbers). The same is true of the subset of sequences that are eventually ones to the left (as $b \mapsto \overline{b}$ is a homeomorphism). This makes evident the fact that $W^u(\underline{0}, \tilde{\mathcal{S}}_2)$ is a copy of $\mathbf{R}$, with the map $\chi : W^u(\underline{0}, \tilde{\mathcal{S}}_2) \to \mathbf{R}$ continuous and bijective:

$$\chi(b) = \begin{cases} \sum_{i=-\infty}^{\infty} \frac{b_i}{2^{i+1}} & \text{if } \exists\ n \quad b_{(-\infty,n]} = {}^{\infty}\mathtt{0}, \\ -\chi(\overline{b}) & \text{if } \exists\ n \quad b_{(-\infty,n]} = {}^{\infty}\mathtt{1}, \end{cases}$$

Then, the point in the unstable manifold $W^u(\underline{0}, \tilde{\mathcal{S}}_2)$ that corresponds to $x \in \mathbf{R}$ is given by the binary expansion of x,

$$[\boldsymbol{\beta}_{\mathbf{R}}(x)]_n = \begin{cases} \mathtt{0} & \text{if} \quad 2^n x \pmod 1 \in [0, \frac{1}{2}) \\ \mathtt{1} & \text{if} \quad 2^n x \pmod 1 \in [\frac{1}{2}, 1) \end{cases}$$

if $x \geq 0$, and by $\boldsymbol{\beta}_{\mathbf{R}}(x) = \overline{\boldsymbol{\beta}_{\mathbf{R}}(-x)}$ for $x < 0$.

In terms of the standard parameterization of the component of $\mathbf{1} \in \Sigma_0$ via the map $\mathbf{exp}$, recall that $W^u(\mathbf{1}, \Sigma_0) = \mathbf{exp}(i\mathbf{R})$, hence

$$\boldsymbol{\beta}(\mathbf{exp}(i\mathbf{R})) = W^u(\underline{0}, \tilde{\mathcal{S}}_2) = \boldsymbol{\beta}_{\mathbf{R}}(\mathbf{R}).$$

The connection between the map $\mathbf{exp}$ and binary sequences is is as suggested by the notation: for $t \in \mathbf{R}_+$, and $\boldsymbol{e}^{i2\pi t} = \mathbf{exp}(i2\pi t) \in \Omega(\mathbf{1}, \Sigma_0)$

$$\boldsymbol{\beta}(\boldsymbol{e}^{i2\pi t}) \iff \chi(b) = t \iff \boldsymbol{\beta}_R(t) = b,$$

so that binary coding of $\boldsymbol{e}^{i2\pi t}$ is the expansion of t in base 2 not ending in 1's. For negative t we use the expansion of $-t$ reversed.

2.4 The solenoid as a model for J_+^-.

The existence of a semi-conjugacy from J_+^- to Σ_+ when J_+^- satisfies certain topological conditions was proved by Bedford & Smillie in [BS6]. The construction of this semi-conjugacy depends on extending φ^+ from $V^+ \subset U^+ - V$ to $J_+^- = J^- \cap U^+$. One major result shows that the existence of such an extension depends on the topology of the intersection of U^+ with unstable manifolds. In addition, these concepts are shown to be related to the geometric structure of J_+^-, as well as with the connectivity of J:

Theorem 1 (Bedford & Smillie). *If* $\det(Df) \leq 1$, *the following are equivalent:*

1. φ^+ *extends to a continuous map on* J_+^- *satisfying* $\varphi^+ \circ f = (\varphi^+)^d$.
2. *For some periodic saddle point* p, *some component of* U_p^+ *is simply connected.*
3. *For any periodic saddle point* p, *some any component of* U_p^+ *is simply connected.*
4. J *is connected*
5. J_+^- *has a lamination by simply connected Riemann surfaces, (then each component of* U_p^+ *is a leaf of this lamination, and* φ^+ *restricted to any leaf is a holomorphic covering of* $\mathbf{C} - \overline{\Delta}$.*)*

The hypothesis in the theorem is not restrictive, as it holds for either f or f^{-1}. If any of the equivalent conditions in Theorem 1 are satisfied, then the map

$$\Phi : J_+^- \to \Sigma_+, \qquad [\Phi(p)]_n = \varphi^+(f^n(p)), \tag{2.17}$$

provides a semi-conjugacy

$$\Phi \circ f = \hat{\sigma} \circ \Phi. \tag{2.18}$$

It is shown in [BS6] that Φ maps each component bijectively and holomorphically. It follows that every component $\mathcal{O}$ of J_+^- is conformally equivalent to a half plane with canonical coordinates given by $\log|\hat{\pi}\Phi| = \log|\varphi^+| = G^+$ and a choice of harmonic conjugate, denoted here by H^+. The function H^+ is a real valued function on $\mathcal{O}$ such that

$$\varphi^+ = e^{G^+ + iH^+}$$

where e^z denotes the complex exponential (this specifies H^+ up to addition of an integer multiple of 2π). Then $\Phi(p) = s$ is equivalent to

$$s_n = \varphi^+ \circ f^n(p) = (\varphi^+(p))^{d^n} = e^{[G^+(p) + iH^+(p)]d^n}$$

or $s = \mathbf{exp}(G^+(p) + iH^+(p))$. External rays in J_+^- can be defined as the inverse images of rays in Σ_+, and on each component of J_+^- they corresponds to points where H^+ is constant. The choice of H^+ corresponds to choosing the ray $\gamma \in \mathcal{O}$ where $H^+ \equiv 0$, then $\Phi|_{\mathcal{O}}$ gives the parameterization of the component $\omega\,\mathbf{exp}(\mathbf{H}) \in \Sigma_+$ where $\Phi(\gamma) = \mathcal{R}_\omega$.

By (2.18) the action of f on rays in J_+^- is given by the dynamics of rays in Σ_+, which is equivalent to the action of $\hat{\sigma}$ on Σ_0. The later has been given a symbolic

dynamics description as the shift on the quotient $\tilde{\mathcal{S}}_2 = \mathcal{S}_2/\sim$ where the equivalence $\sim$ is as in Lemma 5.

We say a ray γ in J_+^- has solenoidal coding $b \in \tilde{\mathcal{S}}_2$ if b is the binary coding of its corresponding ray in Σ_+, namely if $\hat{\theta}(b) = \omega$ and $\mathcal{R}_\omega = \Phi(\gamma)$.

From a computational point of view it is worth noting that if q is point in J_+^-, then $\Phi(q)$ is a point in the ray $\mathcal{R}_\omega \in \Sigma_+$ where $\omega = \Theta \circ \Phi(q) \in \Sigma_0$, or

$$\omega_n = \frac{\varphi^+ \circ f^n(p)}{|\varphi^+ \circ f^n(p)|}, \quad n \in \mathbf{Z} \tag{2.19}$$

For n large enough $f^n(q)$ will have entered V^+ where $\varphi^+ \simeq \pi_x$. Then, $\measuredangle(\pi_x f^n(q)) \simeq \measuredangle(\omega_n)$ which determines $[\boldsymbol{\beta}(\omega)]_n$ by the rule given in Lemma 6.

2.4.1 Hyperbolic maps with connected J.

Under the additional hypothesis that f is hyperbolic, it is shown in [BS7] that the mapping Φ is a covering map of finite degree, and this fact is used to establish the existence of a conjugacy

$$\Psi \,:\, (\sigma, \Sigma_+) \to (f, J_+^-)$$

that maps rays in Σ_0 to rays of J_+^-. In addition, when f is hyperbolic rays in J_+^- actually land on J, and the landing map induces a semi-conjugacy

$$\boldsymbol{\psi} \,:\, (\sigma, \Sigma_0) \to (f, J) \tag{2.20}$$

defined as follows: for $\omega \in \Sigma_0$, the external ray above ω, $\mathcal{R}_\omega \in \Sigma_+$, maps under Ψ to a ray $\gamma \in J_+^-$ whose landing point q_γ is in J. Then, the assignment $\boldsymbol{\psi} : \omega \mapsto q_\gamma$ gives a continuous extension of Ψ to Σ_0. It is shown that $\boldsymbol{\psi}$ is onto and finite-to-one.

Hence, the map $\boldsymbol{\psi}$ represents J as a quotient of the solenoid

$$\Sigma_0/\overset{\psi}{\sim} \quad \text{where} \quad \omega \overset{\psi}{\sim} \upsilon \iff \boldsymbol{\psi}(\omega) = \boldsymbol{\psi}(\upsilon). \tag{2.21}$$

Let $\{s_1, \ldots, s_\nu\} \subset \Sigma_0$ be the pre-images of the point $q \in J$ under $\boldsymbol{\psi}$ and write R_j for the ray $\mathcal{R}_{s_j} \in \Sigma_+$. Let H_j denote the component of Σ_+ containing R_j, and let I_j be the components of Σ_0 containing s_j. Then $\{\Psi R_j : j = 1, \ldots, \nu\}$ is the set of the rays that land at q. A result in [BS7] shows that every component of U_q^+ corresponds to a unique ray landing at q. Namely if $\mathcal{O}_j = \Psi(H_j)$ then $U_q^+ = \{\mathcal{O}_j : j = 1, \ldots, \nu\}$ with the components of J in K_q^+ given by $\partial\mathcal{O}_j = \boldsymbol{\psi}(I_j)$. From the fact that each O_j is a homeomorphic image of $\mathbf{H}$ sitting in $W^u(q)$, itself a copy of $\mathbf{C}$, it follows that there are topological restrictions in the possible elements of the solenoid that can be identified under $\boldsymbol{\psi}$. In particular, it is shown in [BS7] that the following planarity conditions must hold

Planarity Conditions. Let Ω and Ω' denote distinct components of Σ_0, parameterized by $\mathbf{R}$ with orientations determined by $\hat{\pi}$ and a orientation of S^1.

- **Non-linking.** If $r_1, r_2, r_3, r_4 \in \Omega$ are such that $\boldsymbol{\psi}(r_1) = \boldsymbol{\psi}(r_2) \neq \boldsymbol{\psi}(r_2) = \boldsymbol{\psi}(r_4)$, then $r_1 < r_2 < r_3$ implies $r_1 < r_4 < r_3$.

- **Orientation.** If $r_1, r_2 \in \Omega$ and $r_1', r_2 \in \Omega'$ are such that $\boldsymbol{\psi}(r_1) = \boldsymbol{\psi}(r_1') \neq \boldsymbol{\psi}(r_2) = \boldsymbol{\psi}(r_2')$, then, $r_1 < r_2$ implies $r_1' > r_2'$.

- **Localization.** If $r_1, r_2 \in \Omega$ and $r_1', r_2' \in \Omega'$ are such that $\boldsymbol{\psi}(r_1) = \boldsymbol{\psi}(r_1') \neq \boldsymbol{\psi}(r_2) = \boldsymbol{\psi}(r_2')$ and $r \in (r_1, r_2) \subset \Omega$ is such that $\boldsymbol{\psi}(r_1) \neq \boldsymbol{\psi}(r) \neq \boldsymbol{\psi}(r_2)$, then $\boldsymbol{\psi}(r) = \boldsymbol{\psi}(s)$ implies $s \in (r_1, r_2) \cup (r_1', r_2')$.

In addition to the planarity conditions, $\boldsymbol{\psi}$ satisfies the following properties with respect to stable manifolds:

- **Injectivity.** If ω and υ are distinct points in the same stable manifold of Σ_0 then $\boldsymbol{\psi}(\omega) \neq \boldsymbol{\psi}(\upsilon)$.
- **Matching.** If $\boldsymbol{\psi}(\omega) = \boldsymbol{\psi}(\upsilon)$, then $\forall\ \omega' \in W^s(\omega)\ \exists\ \upsilon' \in W^s(\upsilon)$ such that $\boldsymbol{\psi}(\omega') = \boldsymbol{\psi}(\upsilon')$.

According to the matching property, two identified rays belonging to distinct stable manifolds imply that the stable manifolds are identified.

2.5 The unstable manifold "picture" of a periodic saddle.

Next we consider the parameterization of the unstable manifold of a periodic point as a tool to explore the connectivity of J and the combinatorics of external rays by computer. We assume that f is hyperbolic and that $p \in J$ is periodic.

The unstable manifold of any point $q \in J$ admits an analytic parameterization by $\mathbf{C}$. There is an analytic bijective map

$$\phi_p : \mathbf{C} \to W^u(q), \qquad \phi_p : 0 \mapsto p, \tag{2.22}$$

which is unique if we specify a derivative at 0.

If $q_k = f^k(q)$, the map λ that makes the following diagram commute

$$\begin{array}{ccc} \mathbf{C} & \xrightarrow{\phi_q} & W^u(q) \\ {\scriptstyle F}\downarrow & & \downarrow{\scriptstyle f^k} \\ \mathbf{C} & \xrightarrow{\phi_{q_k}} & W^u(q_k) \end{array}$$

is holomorphic bijection of $\mathbf{C}$ with 0 as a fixed point, hence $F(z) = \lambda z$ for some $\lambda \in \mathbf{C}^*$. When p is periodic of period N, we can talk about the action of f^N on $W^u(p)$, which "as seen" in $\mathbf{C}$ becomes multiplication by λ, the expanding eigenvalue of Df^N at p,

$$\phi_p^{-1} \circ f^N \circ \phi_p(z) = \lambda z. \tag{2.23}$$

Lemma 8. *If $p \in J$ is periodic of period N, then the rays landing at p are all periodic of period kN for some $k \in \mathbf{N}$ and f^N preserves their cyclic ordering within $W^u(p)$.*

Proof. The set of rays landing at p is a finite set mapped to itself by f^N, hence some least k-th iterate of f^N maps each ray to itself. The action of f^N on $W^u(p)$ corresponds to multiplication by λ so rays are either rotated or fixed by f^N. □

Corollary 1. *If $p = \boldsymbol{\psi}(\mathbf{1})$ then U_p^+ consists of a single component.*

We will refer to the fixed point of $f_{a,c}$ for which $Df(p)$ has the largest eigenvalue as the β-fixed point of f. If f is hyperbolic $\boldsymbol{\psi}(\mathbf{1})$ coincides with the β-fixed point.

The fact that the parameterization ϕ_p from 2.22 can be approximated numerically makes $W^u(p)$ a particularly useful slice of $\mathbf{C}^2$ for obtaining information about

the structure of J using a computer. Properties of $W^u(p)$ can be pulled back to $\mathbf{C}$ via the map ϕ_p, and can be observed on a computer rendered picture of the plane. In particular, the partition of $W^u(p)$ into $K_p^+ := W^u(p) \cap K^+$ and its complement, $U_p^+ := W^u(p) - K_p^+$, can be approximated from the dynamics of points under finite iteration, to give a partition of $\mathbf{C}$ by $\phi_p^{-1}(K_p^+)$ and $\phi_p^{-1}(U_p^+)$. In the resulting computer picture, the connectivity of $\phi_p^{-1}(K_p^+)$ is indicative of the connectivity of J, by Theorem 1, and from $\phi_p^{-1}(U_p^+)$ we obtain information about the external rays and the combinatorics of their identification as explained below[2]. These experiments were first suggested and carried out by Hubbard.

We will call the image of the partition of $\mathbf{C}$ by $\phi_p^{-1}(K_p^+)$ and $\phi_p^{-1}(U_p^+)$ the unstable manifold picture of f at p, or W_p^u-picture for short. When p is the β-fixed point we also write W_β^u. By a minor abuse of notation we will use K_p^+ and U_p^+ to denote the subsets of $W^u(p)$ in $\mathbf{C}^2$ and their respective inverse images under ϕ_p in the W_p^u picture.

Examples. Figure 2.2 shows the W_p^u picture for two mappings. In each picture the set K_p^+ is colored black and U_p^+ is shaded gray/white. In the images on the left the shading depicts level curves of G^+ as the boundary between the grey/white regions, and in the images on the right external rays are made visible by a binary-decomposition of the level sets which we explain below. For the first example (top images) the picture is rather simple with K_p^+ and U_p^+ both being topologically half-planes. The second example illustrates how external rays "pinch" K_p^+ when $\boldsymbol{\psi}$ is not injective.

[2] Some details of the algorithms are given in the appendix.

$a = .201, c = -0.673$

$a = .01, c = -1.0$

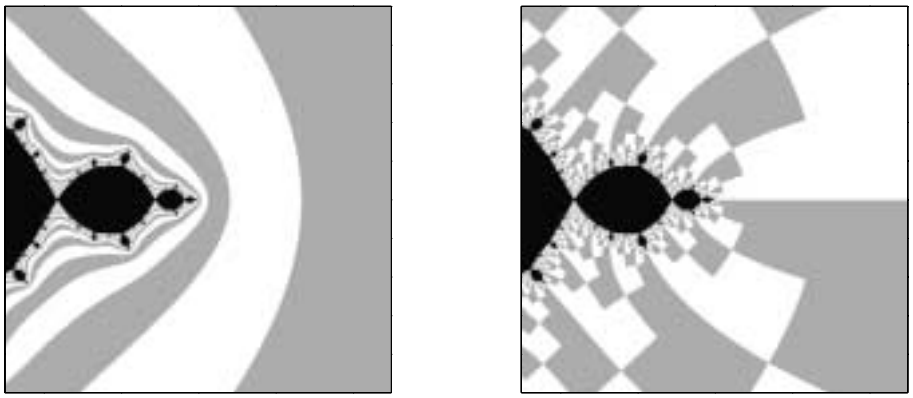

Figure 2.2:

The W^u_p picture in the second example, where $a = 0.01$ and $c = -1$, resembles the picture of the filled-in Julia set of the polynomial $P_{-1} : z \mapsto z^2 - 1$ (see figure 3.4). In general, if c is in the interior of the Mandelbrot set, there will be some small enough $|a|$ such that the the picture of $K^+ \cap W^u(\beta)$ for $f_{a,c}$ is topologically the same as the picture of K_c at the β-fixed point of the polynomial P_c. This is a consequence of a theorem in [HOV2] about Hénon mappings that are "perturbations of quadratic polynomials" to be discussed in more details in Chapter 3. In Chapter

4 we will consider the question of how the W^u_β picture changes as the value of $|a|$ increases.

2.5.1 Reading the W^u_p picture.

In the W^u_p-picture we color U^+_p to depict the following information. Let $U_n = f^n(V^+) \cap U^+_p$ for each $n \in \mathbf{Z}$. Then, $q \in U_n$ if $G^+(f^n(q)) \geq \log R$. We call the set $L_n = U_n - U_{n-1}$ the n-th level set. By (2.5) the boundaries of each level set correspond to level curves between which G^+ decreases by a factor of 2,

$$q \in L_n \quad \iff \quad \frac{1}{2^n} < \frac{G^+(q)}{\log R} < \frac{1}{2^{n-1}}.$$

Next, the binary decomposition of U^+_p shown in the in the right-hand-side of figures 2.2 is obtained by a partition of each level set L_n into $L^{\mathtt{0}}_n$ (colored light) and $L^{\mathtt{1}}_n$ (colored dark) according to the criteria

$$q \in L^{\mathtt{0}}_n \quad \text{if} \quad \measuredangle\left(\varphi^+ \circ f^n(q)\right) \in [0, \tfrac{1}{2}), \quad \text{else} \quad q \in L^{\mathtt{1}}_n$$

This rule is also what defines n-th entry in the solenoidal coding of the ray through q, as in (2.19). Thus,

$$\gamma \cap L^\ell_n \quad \iff \quad [\boldsymbol{\beta}(\gamma)]_n = \ell. \tag{2.24}$$

Accordingly, the solenoidal coding of a ray $\gamma \in U^+_p$ can be read from the picture by looking at the label (light/dark) of the region through which the ray passes on each level set.

The boundary of any component $\mathcal{O}$ of U^+_p is the image of a single component of Σ_0 under $\boldsymbol{\psi}$. Let γ_p denote the ray in $\mathcal{O}$ that lands at $0 = \phi_p^{-1}(p)$ in the W^u_p-picture.

In general, $\boldsymbol{\beta}(\gamma_p)$ is periodic and its coding and can be determined from its initial repeating word. Since components in Σ_0 are unstable manifolds, it follows that that the solenoidal coding of any ray $\gamma \in \mathcal{O}$ agrees sufficiently far to the left with the coding of γ_p, or is eventually constant if p is the β-fixed point.

Now, by (2.23) the the geometry of the W^u_p picture is invariant under multiplication by λ. Therefore knowledge of L_0 is irrelevant: to locate any specific ray γ with given coding b, we can assume the picture is at a scale showing the first coordinate where b and $\boldsymbol{\beta}(\gamma_p)$ disagree. Equivalently, in the W^u_β picture the geometry of any ray γ the same as the geometry of $\lambda^k\gamma$ for any $k \in \mathbf{Z}$. If $\gamma \neq \gamma_p$ we refer to the region between γ and $\lambda\gamma$, including either of these two rays, as a fundamental domain of the component $\mathcal{O}$ of U^+_p containing γ. A computed W^u_p picture showing the origin will contain a largest fundamental domain on each side of γ_p. To examine the behavior near K^+ of any ray in $\mathcal{O}$ we use its λ-scaled representative inside this domain. In particular, the topology of $\partial\mathcal{O}$ is determined by the identifications involving rays in these fundamental domains.

When p is the β-fixed point, $\boldsymbol{\beta}(\gamma_p) = \underline{0} = \underline{1}$, and U^+_p has one component. Multiplication by λ in the W^u_β-picture corresponds to the action of f on $W^u(\beta)$ and to the shift σ the solenoid. Thus, in terms of symbol sequences, a fundamental domain in the W^u_β-picture is determined by rays with coding b and σb for any $b \neq \underline{0}$. Figure 2.3 shows an example.

Combining the planarity conditions with the shift invariance of the geometry of rays gives the following restriction for the identifications of rays within a fundamental domain. On a parameterization of a component of Σ_0 by $\mathbf{R}$ the action of the

shift corresponds to multiplication by 2.

Lemma 9. *Let Ω be a component of Σ_0 parameterized by $\mathbf{R}$ with 0 corresponding to a periodic point. If $r, s \in \Omega$ are such that $rs > 0$ and $\boldsymbol{\psi}(r) = \boldsymbol{\psi}(s)$, then $2^{-1}r \leq s \leq 2r$.*

Proof. Without loss of generality suppose $r, s > 0$. Assume $s > 2r$. The interval $[r, 2r]$ is a fundamental domain so there is $k > 0$ such that $2^{-k}s \in [r, 2r]$. By invariance under the shift, $2^{-k}s \sim 2^{-k}r$. This identification together with $r \sim s$ violate the non-liking condition. Replacing r by s we conclude $2^{-1}r < s$. □

This tells that two rays in the same side of the periodic point can be identified only if both are within a fundamental domain, hence not too far apart. But as the W^u_β-picture in figure 2.3 illustrates, there are also identifications involving rays located

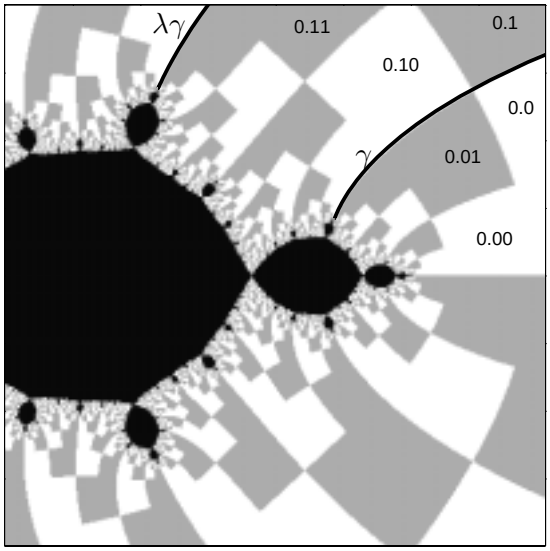

Figure 2.3: A fundamental domain in U^+_β.

on opposite sides of the fixed ray. In this case, the examples we have seen indicate that the rays also have opposite solenoidal coordinates, $\boldsymbol{\psi}(r) = \boldsymbol{\psi}(-r)$, and can be noted as the rays that land on the real axis in the W^u_β-picture. In fact this has to be the case when there is symmetry with respect to complex conjugation.

The W^u_β-pictures in figure 2.2 are symmetric with respect to reflection about the real-axis. This is due to the fact that the fixed point p is in $\mathbf{R}^2$ and the eigenvalues of $Df(p)$ are real, for then the coefficients of ϕ_p can be chosen to be real. Since f and ϕ_p commute with complex conjugation the same holds for the Greens function on U^+_p. Thus rays in come in conjugate pairs. It follows that the fixed ray is in $\mathbf{R}$ in the W^u_β-picture, as suggested in the images of figure 2.2. By (2.16), the solenoidal coding of complex conjugate rays have opposites symbols,

$$\boldsymbol{\beta}(\overline{\gamma}) = \overline{\boldsymbol{\beta}(\gamma)}.$$

When there is symmetry with respect to complex conjugation, then we have

Lemma 10. *Let Ω be a component of Σ_0 parameterized by $\mathbf{R}$ with 0 corresponding to a periodic point. If the identifications are symmetric about 0, (such as when there is symmetry with respect to complex conjugation), and if $r, s \in \Omega$ are such that $rs < 0$ and $\boldsymbol{\psi}(r) = \boldsymbol{\psi}(s)$ then $s = -r$.*

Proof. Without loss of generality assume $r > 0$. By the symmetry, $r \sim s$ implies $-r \sim -s$. Then either of $r > -s$ or $r < -s$ violate the non-linking condition. □

When the W^u_β-picture is symmetric with respect to complex conjugation we will say that rays that land on the real axis form a real identification. For instance, in

the fundamental domain specified in figure 2.3 there is only one real identifications arising from the ray ${}^{\infty}\mathtt{0}.(\mathtt{10})^{\infty}$ and its complex conjugate ray.

If γ lands on z in the W^u_p-picture and $\boldsymbol{\beta}(\gamma)$ is periodic sufficiently far to the right, then $\phi_p(z) \in W^s(p')$ where p' is periodic. If the W^u_β picture is symmetric with respect to complex conjugation and both γ and $\overline{\gamma}$ land on z in the W^u_β-picture, then p' is in $\mathbf{R}^2$ as it is the limit of $f^n(\phi_p(z)) \in \mathbf{R}^2$. For example, in the W^u_β-picture of figure 2.3, the rays that land on $\mathbf{R}$ are identified only with their conjugate rays and have solenoidal coding that eventually becomes either $(\mathtt{01})^\infty$ or $(\mathtt{10})^\infty$. This tells us that the landing point of these rays map to $W^u(p) \cap W^s(p')$ under ϕ_p, where $p' \in \mathbf{R}^2$ is the landing point of a pair of rays which have coding ${}^{\infty}(\mathtt{01}).(\mathtt{01})^\infty$ and ${}^{\infty}(\mathtt{10}).(\mathtt{10})^\infty$, respectively. Since these period-2 rays are identified under the landing map but map to each other under the shift, it follows that p' is the other fixed point of f.

A second mapping having real identifications is the mapping for $a = 0.3$ and $c = -1.17$, whose W^u_β-picture is shown in figure 2.4. The coding of rays landing on $\mathbf{R}$ eventually becomes either $(\mathtt{011})^\infty$ or $(\mathtt{100})^\infty$. This tell us that there is a period-three orbit $\{p'_1, p'_2, p'_3\} \subset J \cap \mathbf{R}^2$, where

$$\boldsymbol{\psi}({}^{\infty}(\mathtt{011}).(\mathtt{011})^\infty) = p'_1 = \boldsymbol{\psi}({}^{\infty}(\mathtt{100}).(\mathtt{100})^\infty)$$

$$\boldsymbol{\psi}({}^{\infty}(\mathtt{110}).(\mathtt{110})^\infty) = p'_2 = \boldsymbol{\psi}({}^{\infty}(\mathtt{001}).(\mathtt{001})^\infty)$$

$$\boldsymbol{\psi}({}^{\infty}(\mathtt{101}).(\mathtt{101})^\infty) = p'_3 = \boldsymbol{\psi}({}^{\infty}(\mathtt{010}).(\mathtt{010})^\infty).$$

The study of this map was suggested by Hubbard. In the next chapter we will present a combinatorial model for this mapping.

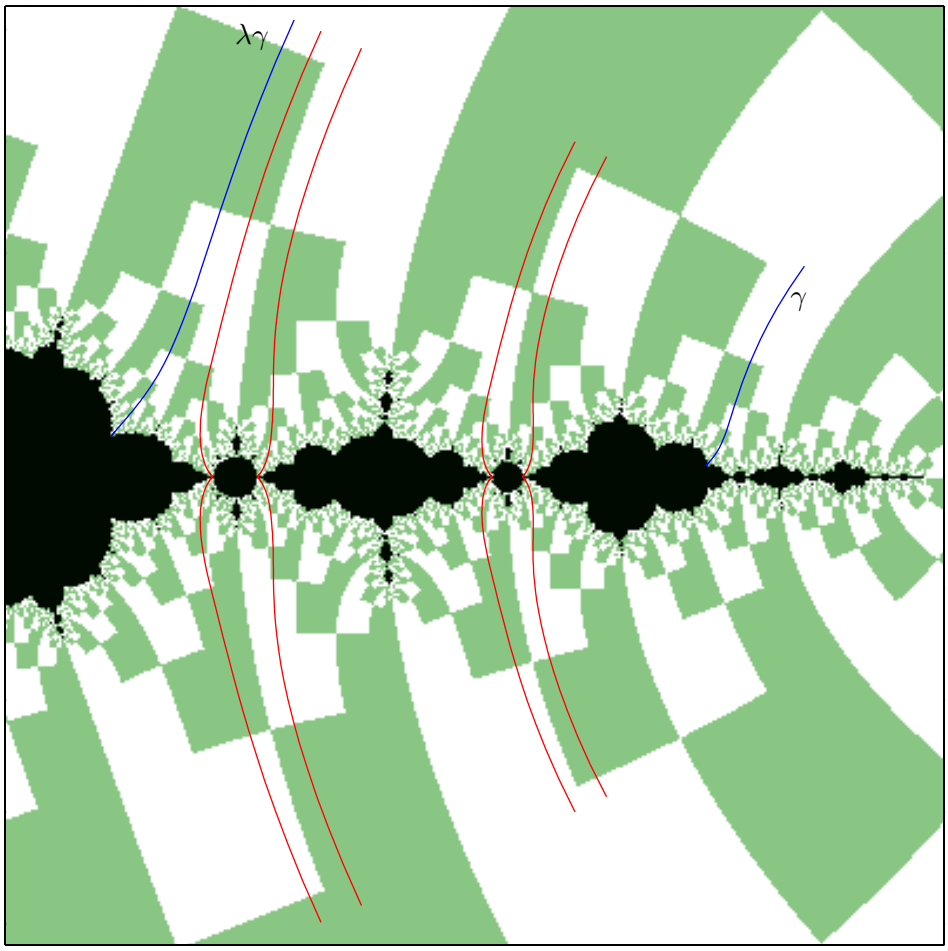

Figure 2.4: W^u_β picture with four real identifications in a fundamental domain.

Chapter 3

Combinatorial Models for Hénon Mappings

3.1 Graph representation of quotients of $\mathcal{S}_2$.

In this chapter we will consider the set J as a quotient of the combinatorial space $\Sigma_0 \simeq \mathcal{S}_2/\hat{\theta}$. We will make use of the fact that the equivalence relation E_{ψ} induced on $\mathcal{S}_2$ by $\boldsymbol{\psi} \circ \hat{\theta}$ is a subshift of finite type ([Fr]). This allows E_{ψ} to be described by a finite directed graph whose edges carry an ordered pair of binary labels.

A finite directed graph whose edges are labeled with an ordered pair of elements of $\{0, 1\}$ will be called a bi-labeled graph. We will write the labels of the edges positioned vertically relative to each other, for instance as $\left[\begin{smallmatrix}0\\1\end{smallmatrix}\right]$. The notation top and bot will refer to the top and bottom labels of an edge, respectively. A path in a directed graph is a sequence of consecutive edges: $\gamma = (\ldots, \gamma_k, \gamma_{k+1}, \ldots)$ where

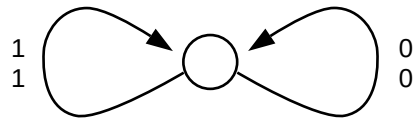

Figure 3.1: The diagonal graph.

the terminal node of γ_k is the initial node of γ_{k+1}. If γ is a path, we let $[\gamma]_k$ denote the pair of labels of the edge γ_k, namely $[\gamma]_k = \left[\begin{smallmatrix} \mathsf{top}\,\gamma_k \\ \mathsf{bot}\,\gamma_k \end{smallmatrix}\right]$. Any bi-infinite path on a bi-labeled graph produces an ordered pair of elements in $\mathcal{S}_2$, given by the sequences of top and bot labels along the path. A bi-labeled graph is said to describe the equivalence relation E there exist a path on the graph producing the pair $\left[\begin{smallmatrix} \mathtt{A} \\ \mathtt{B} \end{smallmatrix}\right]$ if and only if $(\mathtt{A}, \mathtt{B}) \in E$. We will refer to an element of E_ψ as an identification. If $\mathtt{A} \overset{\psi}{\sim} \mathtt{B}$ the identification $(\mathtt{A}, \mathtt{B}) \in E_\psi$ will also be written $\left[\begin{smallmatrix} \mathtt{A} \\ \mathtt{B} \end{smallmatrix}\right]$, a notation that facilitates comparing the identified sequences.

Without loss of generality we may write the graphs describing E_ψ so that they are left-deterministic: the set edges incident on a given node carry distinct pairs of labels [LM]. When this condition holds there is at most one backward path starting at a given node ν that produces a given pair of left-infinite sequences $\left[\begin{smallmatrix} \mathtt{A}_{(-\infty,-1]} \\ \mathtt{B}_{(-\infty,-1]} \end{smallmatrix}\right]$.

Example 1 (the diagonal graph). The graph consisting of a single node and two edges labeled $\left[\begin{smallmatrix} 0 \\ 0 \end{smallmatrix}\right]$ and $\left[\begin{smallmatrix} 1 \\ 1 \end{smallmatrix}\right]$, respectively, will be called the diagonal graph (figure 3.1). The diagonal graph expresses the identification of every possible sequence with itself.

We will use the diagonal graph to encode the identifications due to the reflexivity property of the equivalence relation E_ψ. The symmetry property of the equivalence

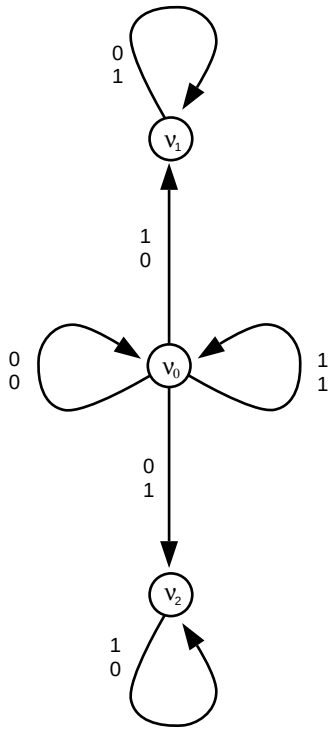

Figure 3.2: The solenoid graph Γ_{Σ_0}.

relation will be evident in our graphs that represents E_ψ, for the existence of a path γ encoding $\left[\begin{smallmatrix}\mathtt{A}\\ \mathtt{B}\end{smallmatrix}\right] \in E_\psi$ implies the existence of a symmetric path γ' encoding $\left[\begin{smallmatrix}\mathtt{B}\\ \mathtt{A}\end{smallmatrix}\right]$ which must consists of edges with `top` and `bot` labels interchanged relative to those of γ.

Example 2 (The solenoid graph). We have seen that the solenoid is a quotient of the full shift in section 2.4. This equivalence relation identifies a sequence terminating in $\mathtt{10}^\infty$ with one terminating on $\mathtt{01}^\infty$ as described in Lemma 5. The graph in figure 3.2 encodes exactly the identifications representing the solenoid: paths that never leave the node ν_0 correspond to the trivial identifications; paths that stay

only in the ν_1 node or only the ν_2 node correspond to the identification of the two constant sequences ${}^{\infty}\mathtt{1.1}^{\infty}$ and ${}^{\infty}\mathtt{0.0}^{\infty}$; and any path containing either of the edges (ν_0, ν_1) or (ν_0, ν_2), correspond to the identification of $\mathtt{X10}^{\infty}$ with $\mathtt{X01}^{\infty}$, where $\mathtt{X}$ is a left infinite sequence. It follows that Γ_{Σ_0} is the complete graph describing $E_{\boldsymbol{\psi}}$ when the landing map on rays $\boldsymbol{\psi}$ is injective. As we are interested in identifications when $\boldsymbol{\psi}$ is not injective, we will also refer to the identifications produced by the solenoid graph as being trivial.

Next, we discuss the graph for simplest non-trivial equivalence relation on Σ_0. In fact, this will be the graph arising from a well known one-dimensional map.

Example 3 (The graph Γ_2). As we will show in the next section, the graph in Figure 3.3 is the graph that describes the pinched-disk model of J_c for the quadratic polynomial $P_c : z \mapsto z^2 - c$ when c is in the period-2 hyperbolic component of the Mandelbrot set. The center of this hyperbolic component is at $c = -1$. Figure 3.4 shows a drawing of the set K_c for $c = -1$ with a few external rays identified in the pinched-disk model.

It follows from a theorem in [HOV2] that the topology of the Julia set of P_c determines the topology of the Julia set of the Hénon mapping $f_{a,c} : (x, y) \mapsto (x^2 + c - ay, x)$ when a is small enough and c belongs to a hyperbolic component of the Mandelbrot set. We will show in the next section that, in this case, the graph describing identifications of rays under the pinched-disk model for the polynomial P_c is the same graph describing identifications of rays in the solenoid for the complex Hénon mapping $f_{a,c}$. We will also outline a method for constructing such graph.

In the graph of figure 3.3 we can distinguish three kinds of identifications pro-

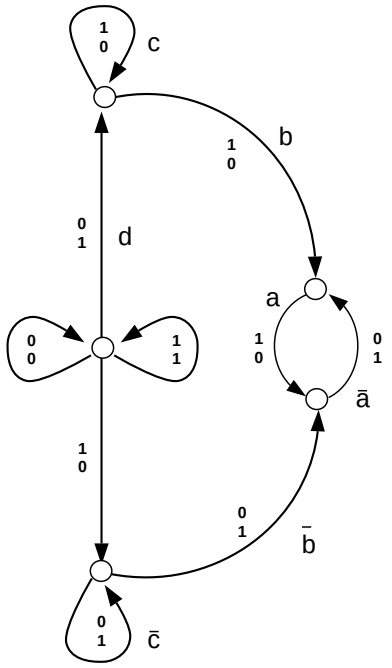

Figure 3.3: The graph Γ_2.

duced by paths outside the solenoid subgraph.

(i) Paths that always stay in the 2-cycle (edges $\mathtt{a}$ and $\overline{\mathtt{a}}$). These produce the identification of the period-2 sequences ${}^{\infty}(\mathtt{01}).(\mathtt{01})^{\infty}$ and ${}^{\infty}(\mathtt{10}).(\mathtt{10})^{\infty}$.

(ii). Paths that include edge $\mathtt{b}$ but do not include edge $\mathtt{d}$. These identify pairs of sequences of the form ${}^{\infty}\mathtt{0}(\mathtt{01})^{\infty}$ and ${}^{\infty}\mathtt{1}(\mathtt{10})^{\infty}$.

(iii). Paths that include edges $\mathtt{b}$ and $\mathtt{d}$. These identify pairs of sequences of the form $\mathtt{X01}^n(\mathtt{10})^{\infty}$ and $\mathtt{X10}^n(\mathtt{01})^{\infty}$, where $n \in N$ and $\mathtt{X}$ is a left-infinite sequence corresponding to a path in the diagonal subgraph.

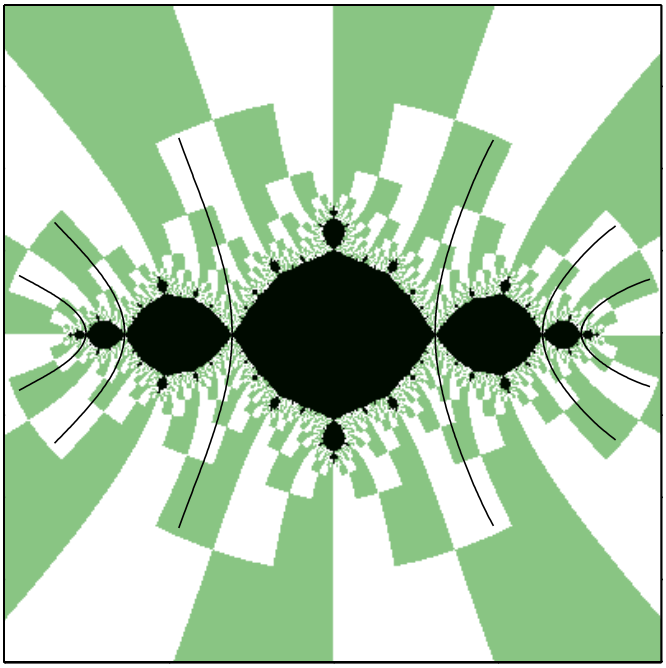

Figure 3.4: The set K_c for $c = -1$.

Note that by the matching property of $\boldsymbol{\psi}$ with respect to stable manifolds, (§2.4.1), the identification in *(i)* implies that every ray in the stable manifold of $^{\infty}(\mathtt{01}).(\mathtt{01})^{\infty}$ is identified with a ray in the stable manifolds $^{\infty}(\mathtt{10}).(\mathtt{10})^{\infty}$. The question of which ray is the "partner" of any given ray in these stable manifolds is specified in *(ii)* and *(iii)*. In particular, the only non-trivial identifications encoded by this graph correspond to rays in these two stable manifolds.

3.2 Perturbations of hyperbolic polynomials.

In this section we show that a Hénon map that is a perturbation of a hyperbolic polynomial is described by the same graph that describes the polynomial, and we give a method of constructing the later in the case that the polynomial is a complexified real polynomial.

When $a = 0$ the Hénon map $f_{a,c}$ is not invertible: it maps all of $\mathbf{C}^2$ to the "parabola" $y = P_c(x)$ in $\mathbf{C}^2$. In this "degenerate" case, the dynamics of points $\{(x, P_c(x)\}$ under $f_{0,c}$ coincides with the dynamics $\mathbf{C}$ under P_c. If $|a|$ is small but non-zero, the dynamics of the Hénon mapping $f_{a,c}$ and the polynomial P_c are still closely related if the polynomial is hyperbolic. In this case, $f_{a,c}$ can be thought of as a perturbation of the "polynomial" $f_{0,c}$. This idea was made precise by Hubbard & Oberste-Vorth in [HOV2] where the following theorem is proven:

Theorem 2 (Hubbard & Oberste-Vorth). *If the polynomial $P_c : z \mapsto z^2 + c$ is hyperbolic, there is some $\varepsilon > 0$ such that for $0 < |a| < \varepsilon$ there is a homeomorphism Φ^- conjugating the inverse limit of $\mathbf{C}$ under P_c to the dynamics of J^- under the Hénon mapping $f_{a,c} : (x, y) \mapsto (P_c(x) - ay, x)$.*

Moreover, it is shown in [HOV2] that Φ^- can be made analytic when restricted to the inverse limit of $\mathbf{C} - K$, which we denote $\hat{U}_c$. The set $\hat{U}_c$ is homeomorphic to the exterior solenoid, Σ_+, via the map induced by φ_c (cf. §2.1). Since external rays can be defined from the complex structure, the map Φ^- preserve external rays.

We will write $f \approx \varprojlim P_c$ when there is a conjugacy Φ between the mapping $f_{a,c}$ restricted to J^- and the inverse limit of $\mathbf{C}$ under the polynomial P_c such that the

restriction of Φ to $\hat{U}_c$ takes external rays to external rays.

By restricting the homeomorphism Φ^- to the non-wandering set, theorem 2 implies the existence of a conjugacy between the inverse limit of the polynomial's Julia set, $\hat{J}_c$, and the Julia set of the Hénon mapping:

$$\Phi : \hat{J}_c \to J_f, \qquad \Phi \circ \hat{P}_c | J_c = f_{a,c} \circ \Phi.$$

This provides a representation of $J_{a,c}$ as a quotient of the solenoid or, equivalently, as a quotient of the the 2-shift, as summarized in the following diagram where $\hat{\sigma}_c$ denotes the shift on $\hat{J}_c$ induced by P_c.

$$\begin{array}{ccccccc}
\mathcal{S}_2 & \xrightarrow{\hat{\theta}} & \Sigma_0 & \xrightarrow{\hat{\psi}_c} & \hat{J}_c & \xrightarrow[\simeq]{\Phi} & J \\
\downarrow{\scriptstyle \sigma} & & \downarrow{\scriptstyle \hat{\sigma}} & & \downarrow{\scriptstyle \hat{\sigma}_c} & & \downarrow{\scriptstyle f_{a,c}} \\
\mathcal{S}_2 & \xrightarrow{\hat{\theta}} & \Sigma_0 & \xrightarrow{\hat{\psi}_c} & \hat{J}_c & \xrightarrow[\simeq]{\Phi} & J
\end{array}$$

Then, the equivalence relation defining the J as a quotient of $\mathcal{S}_2$ is given by

$$\mathtt{A} \sim \mathtt{B} \iff \hat{\psi}_c \circ \hat{\theta}\,(\mathtt{A}) = \hat{\psi}_c \circ \hat{\theta}\,(\mathtt{B}).$$

The equation in the right-hand-side, when expressed coordinate-wise, becomes

$$\psi_c \circ \theta \circ \sigma^n\,(\mathtt{A}) = \psi_c \circ \theta \circ \sigma^n\,(\mathtt{B}) \quad \text{for all } n \in \mathbf{Z}.$$

That is,

$$\psi_c(e^{2\pi i \vartheta(\sigma^n \mathtt{A})}) = \psi_c(e^{2\pi i \vartheta(\sigma^n \mathtt{B})}) \quad \text{for all } n \in \mathbf{Z},$$

where, we recall, $\vartheta : \mathcal{S}_2 \to \mathbf{R}/\mathbf{Z}$ maps a bi-infinite sequence $\mathtt{A}$ to the point whose binary expansion is given by $\mathtt{A}_{[0,\infty)}$. Now, for the polynomial P_c, the identification of rays, (which are parameterized by $\mathbf{R}/\mathbf{Z}$), is defined precisely by

$$x \sim_c y \iff \psi_c(e^{i2\pi x}) = \psi_c(e^{i2\pi y}).$$

This proves

Lemma 11. *If $f \approx \varprojlim P_c$ and $\mathtt{A}$ and $\mathtt{B}$ are rays on the solenoid, then*

$$\mathtt{A} \overset{\psi}{\sim} \mathtt{B} \quad \Longleftrightarrow \quad \mathtt{A}_{[n,\infty)} \sim_c \mathtt{B}_{[n,\infty)} \quad \textit{for all } n \in \mathbf{Z}. \tag{3.1}$$

In other words, projecting the solenoidal rays to their circle coordinate, produces a pair of external angles identified under $\sim_c$, and this is holds for any shift of the solenoidal rays. As a consequence, we get the following corollary which confirms the assertion made after Example 3 in §3.1.

Corollary 3. *If $f \approx \varprojlim P_c$ then the graph describing the equivalence relation $\overset{\psi}{\sim}$ for f is the same as the graph describing $\sim_c$ for the polynomial P_c.*

In addition to the solenoidal planarity conditions of §2.4.1, Lemma 11 imposes some further restrictions on the of rays that can be identified under $\overset{\psi}{\sim}$. For instance, the projection to the circle of any solenoidal identification produces external angles that must satisfy the following condition (see [D]).

Lemma 12 (Non-crossing of $\sim_c$). *If $x, x', y, y' \in \mathbf{R}/\mathbf{Z}$ satisfy $x \sim_c x' \not\sim_c y \sim_c y'$, then $x < y < x'$ if, and only if, $x < y' < x'$.*

Below we consider other combinatorial properties of polynomial external rays which are relevant for obtaining the graph describing $\sim_c$ when c is real.

WORKING ASSUMPTIONS. In what follows we assume that the polynomial P_c is hyperbolic (expanding on J_c, with J_c connected), and that c is real. Then all rays land and come in complex conjugate pairs.

NOTATION AND TERMINOLOGY. In this section, the rays we consider are the external rays for the polynomial P_c. These are parameterized by $\mathbf{R}/\mathbf{Z}$. An identification of rays in $\mathbf{C}$ under $\sim_c$ will be called a planar identification. A planar identification is non-trivial if it is not produced by forward paths in the solenoid graph (figure 3.2).

The inverse image of a planar identification $\left[\begin{smallmatrix}\mathtt{A}\\ \mathtt{B}\end{smallmatrix}\right]$, denoted $\left[\begin{smallmatrix}\mathtt{A}\\ \mathtt{B}\end{smallmatrix}\right]^{-1}$, consists of the set of identifications $\left\{\left[\begin{smallmatrix}\mathtt{A}'\\ \mathtt{B}'\end{smallmatrix}\right] \,:\, \mathtt{A}' \in \sigma^{-1}(\mathtt{A}),\ \mathtt{B}' \in \sigma^{-1}(\mathtt{B})\right\}$. A planar identification has exactly one pair of inverse images given by:

$$\begin{bmatrix}\mathtt{A}\\ \mathtt{B}\end{bmatrix}^{-1} = \left\{\begin{bmatrix}\mathtt{0A}\\ \mathtt{0B}\end{bmatrix},\ \begin{bmatrix}\mathtt{1A}\\ \mathtt{1B}\end{bmatrix}\right\}, \quad \text{or} \quad \begin{bmatrix}\mathtt{A}\\ \mathtt{B}\end{bmatrix}^{-1} = \left\{\begin{bmatrix}\mathtt{0A}\\ \mathtt{1B}\end{bmatrix},\ \begin{bmatrix}\mathtt{1A}\\ \mathtt{0B}\end{bmatrix}\right\}. \tag{3.2}$$

By the landing point of an identification $\left[\begin{smallmatrix}\mathtt{A}\\ \mathtt{B}\end{smallmatrix}\right]$, we mean the common landing point of the rays $\mathtt{A}$ and $\mathtt{B}$, and we will say that an identification is real (resp. complex) if its landing point is real (resp. complex). Since c is real, a non-trivial identification is real if and only if the pair of identified planar rays are complex conjugate of each other. In terms of binary sequences this means that $\left[\begin{smallmatrix}\mathtt{A}\\ \mathtt{B}\end{smallmatrix}\right]$ is a real identification iff $\mathtt{A}$ and $\mathtt{B}$ have opposite symbols on each term: $\mathtt{A} = \overline{\mathtt{B}}$. In fact, for $c \in \mathbf{R}$, this characterization is determined by first digit of the external angles:

Proposition 13. *For $c \in \mathbf{R}$ if $\mathtt{A} \sim_c \mathtt{B}$ and $\mathtt{A}_0 \neq \mathtt{B}_0$ then $\mathtt{B} = \overline{\mathtt{A}}$, thus $\left[\begin{smallmatrix}\mathtt{A}\\ \mathtt{B}\end{smallmatrix}\right]$ is real.*

Proof. Without loss of generality, assume $\mathtt{A}_0 = \mathtt{0}, \mathtt{B}_0 = \mathtt{1}$ so that $\mathtt{A} < \mathtt{B}$. By invariance under complex conjugation, $\mathtt{A} \sim_c \mathtt{B}$ implies $\overline{\mathtt{A}} \sim_c \overline{\mathtt{B}}$. As $\overline{\mathtt{A}}_0 = \mathtt{B}_0$, if $\overline{\mathtt{A}} < \mathtt{B}$ the $\mathtt{A} > \overline{\mathtt{B}}$ and we get $\overline{\mathtt{B}} < \mathtt{A} < \overline{\mathtt{A}} < \mathtt{B}$, contradicting the non-crossing condition of Lemma 12. Similarly, non-crossing is violated if we assume $\overline{\mathtt{A}} > \mathtt{B}$ since then $\mathtt{A} < \overline{\mathtt{B}}$ and $\mathtt{A} < \overline{\mathtt{B}} < \mathtt{B} < \overline{\mathtt{A}}$. Therefore, $\overline{\mathtt{A}} = \mathtt{B}$. □

From the above proposition we can formulate a general relation between the the external angles of identified rays.

Proposition 14. *For $c \in \mathbf{R}$, if $\left[\begin{smallmatrix}\mathtt{A}\\ \mathtt{B}\end{smallmatrix}\right]$ is any non-trivial planar identification $\mathtt{A} \sim_c \mathtt{B}$, then either $\mathtt{A} = \overline{\mathtt{B}}$ or there is an $n \geq 0$ such that $\mathtt{A}_{[0,n)} = \mathtt{B}_{[0,n)}$ and $\mathtt{A}_{[n,\infty)} = \overline{\mathtt{B}}_{[n,\infty)}$.*

Proof. If $\mathtt{A}_0 \neq \mathtt{B}_0$, the result follows from the previous proposition. Assume otherwise. Since the identification is non trivial, there is a first $n > 0$ such that $\mathtt{A}_n \neq \mathtt{B}_n$. Then $\mathtt{A}_{[n,\infty)} = \overline{\mathtt{B}}_{[n,\infty)}$ by applying the previous proposition to the shifted sequences $\sigma^n\mathtt{A}$ and $\sigma^n\mathtt{B}$ which must be identified by invariance of $\sim_c$ under the shift. □

If $c \in \mathbf{R}$ the inverse images of a complex identification must also be complex. By the previous two propositions, the inverse images of $\left[\begin{smallmatrix}\mathtt{A}\\ \mathtt{B}\end{smallmatrix}\right]$ under σ^n consists of the following set of identifications

Corollary. *If $\mathtt{A} \sim_c \mathtt{B}$ and $\mathtt{A}_0 = \mathtt{B}_0$, then for any $n > 0$*

$$\begin{bmatrix}\mathtt{A}\\ \mathtt{B}\end{bmatrix}^{-n} = \left\{ \begin{bmatrix}\mathtt{wA}\\ \mathtt{wB}\end{bmatrix} : \mathtt{w} \in \{0,1\}^n \right\}. \tag{3.3}$$

A real hyperbolic component of $\mathcal{M}$ is a component of the interior of $\mathcal{M}$ intersecting the real axis. Its center corresponds to the value of c such that 0 is periodic under P_c. We now describe a method of constructing the the graph describing $\sim_c$ assuming that c is inside a real hyperbolic component of $\mathcal{M}$.

Steps to obtain the graph for real hyperbolic P_c.

Suppose for the moment that c is the center of a period-n real hyperbolic component of the Mandelbrot set. Let β be the the largest fixed point of P_c.

(a) Let $x_k = P_c^k(0),\ k = 0, \ldots, (n-1)$ and let $\mathcal{P} = \{I_n, I_{n-1}, \ldots, I_1\}$ be the partition of the interval $(-\beta, \beta) \subset \mathbf{R}$ obtained by removing $\{x_0, \ldots, x_{n-1}\}$.

(b) Thinking of $P_c|_{\mathbf{R}}$ as an unimodal map, let Γ be the graph describing the dynamics of the intervals in $\mathcal{P}$. Namely, the nodes of Γ are $I_1, \ldots, I_n$, and there is an edge (I_i, I_j) in Γ iff $P_c(I_i) \supset I_j$

(c) Next, construct a node-labeled graph $\dot{\Gamma}$ based on Γ as follows: for each node I_k of Γ there is a pair of nodes in $\dot{\Gamma}$ with opposite binary labels, I_k^{0} and I_k^{1} (where the superscript is the label). Also, for each edge (I_j, I_k) of Γ there are two edges in $\dot{\Gamma}$: either $(I_j^{\mathsf{0}}, I_k^{\mathsf{1}})$ and $(I_j^{\mathsf{1}}, I_k^{\mathsf{0}})$ if I_j lies to the left of the critical point, or $(I_j^{\mathsf{0}}, I_k^{\mathsf{0}})$ and $(I_j^{\mathsf{1}}, I_k^{\mathsf{1}})$ if I_j to the right of the critical point.

Then $\dot{\Gamma}$ describes the coding of the possible external angles that can land at points of $J_c \cap \mathbf{R}$. No additional information is needed to transform $\dot{\Gamma}$ into a graph describing the equivalence relation $\sim_c$.

(d) Let the top label of each edge be the label of its source node, and let bot be the opposite symbol. Node labels are then redundant, hence omitted. We denote by $\ddot{\Gamma}$ the resulting edge-labeled graph.

The steps leading to $\ddot{\Gamma}$ for the case of period two are illustrated in figure 3.5(a)-(d), and figure 3.6(a)-(d) shows the same for the case of period three.

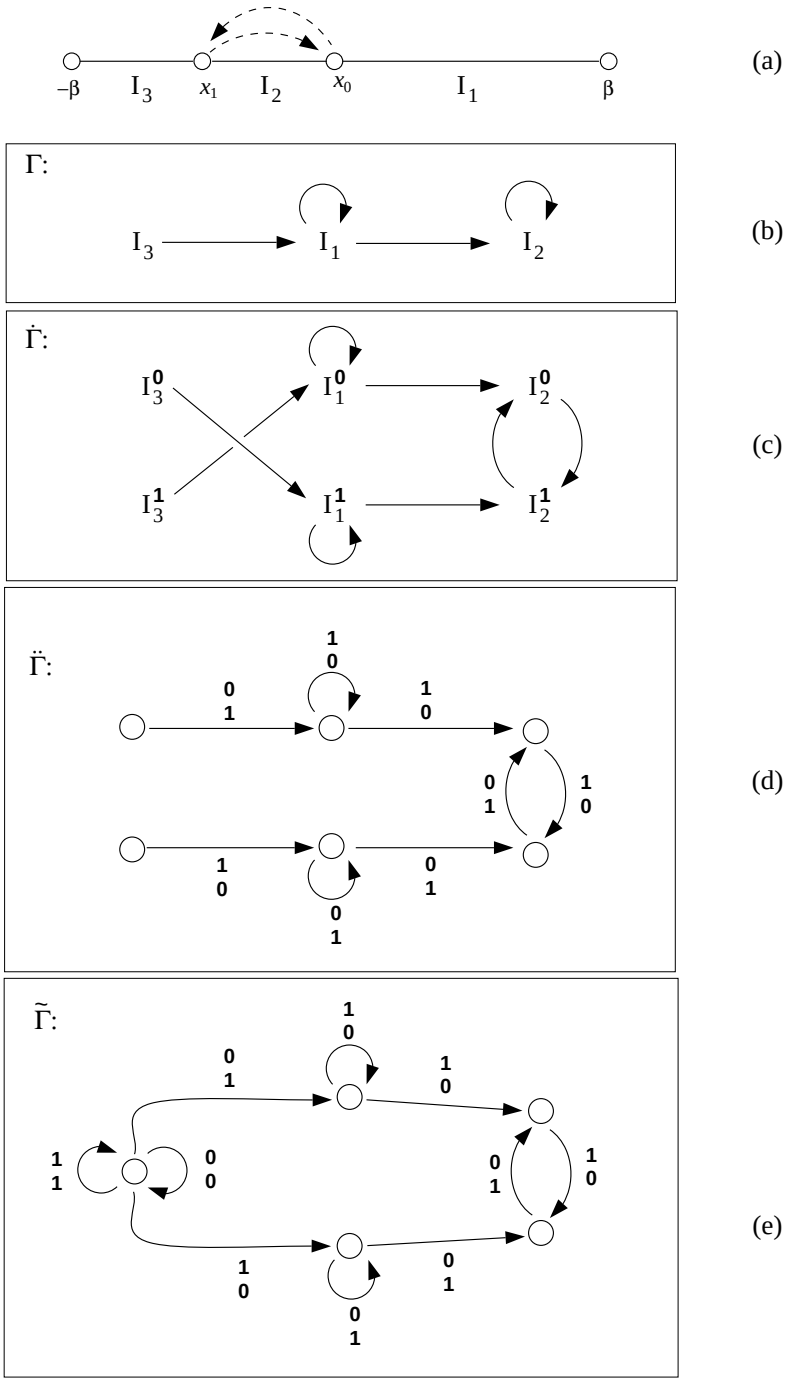

Figure 3.5:

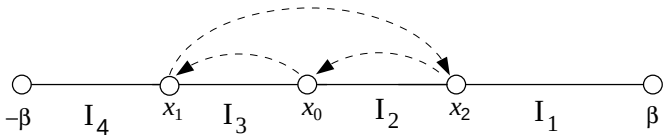

(a)

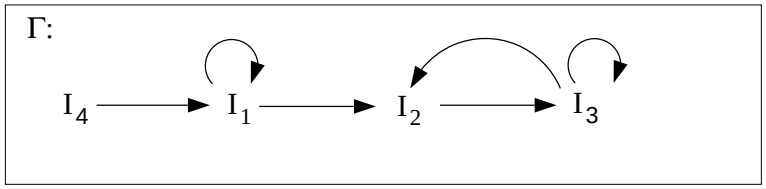

(b)

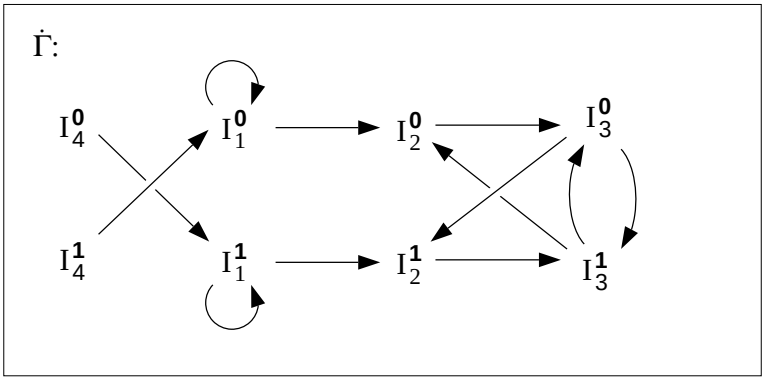

(c)

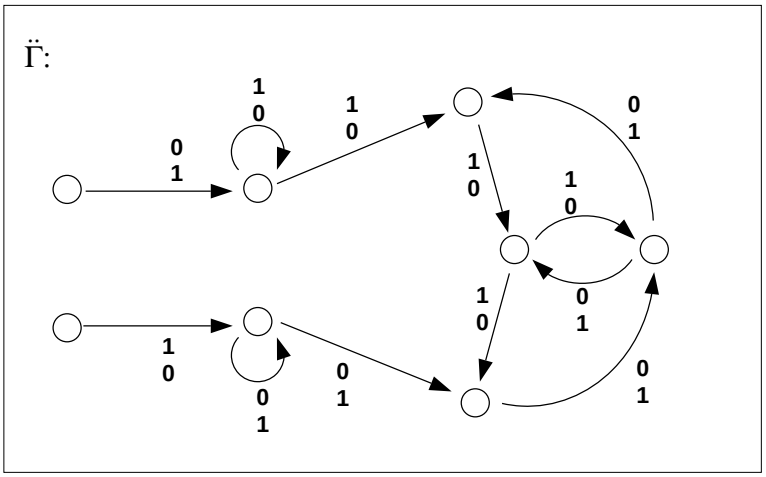

(d)

Figure 3.6:

In the graph $\ddot{\Gamma}$ constructed in step (d) there must be two nodes where no edge terminates. These correspond to the leftmost interval of $\mathcal{P}$ whose points have only complex pre-images under P_c. The last step is contained in the next proposition.

Proposition 15. *Let $\ddot{\Gamma}$ be the graph describing the real identifications of external rays under the landing map for the real hyperbolic polynomial P_c, as constructed above. Let $\tilde{\Gamma}$ be the graph obtained from $\ddot{\Gamma}$ by replacing the two non-terminal nodes by the diagonal graph. Then $\tilde{\Gamma}$ describes the equivalence relation $\sim_c$ of the pinched-disk model of J_c.*

Proof. This follows from (3.3) in Corollary 3.2 and the fact that the interval I_n has no preimages in $\mathbf{R}$. □

Figure 3.5-(e) illustrates the last step for the case of period 2, and the graph produced is the same as the one given in figure 3.3. This confirms the assertion made in Example 3 of §3.1.

Within a hyperbolic component of the Mandelbrot set all polynomials are conjugate, hence the above construction gives the graph describing $\sim_c$ for c inside a hyperbolic component of the Mandelbrot having non-empty intersection with the real axis. We expect that a similar construction can be obtained for the hyperbolic components that do not intersect the real line using as initial data the skeleton of the expanded Hubbard tree (see [D]).

3.3 Two-dimensional examples.

In this section we present bi-labeled graphs that describe equivalence relation on the solenoid which are not reducible to the equivalence relation coming from the inverse limit of quadratic polynomials on $\mathbf{C}$.

The graphs we will present have been obtained by analyzing the identification patterns of rays in the unstable manifold picture of certain specific Hénon mappings. Although it has not been proven that these maps are hyperbolic, this is strongly suggested by the qualitative features of the unstable manifold pictures and by the pictures of invariant manifolds in the real domain. We will prove that the rays identified according to these models satisfy the combinatorial constraints imposed by the planarity conditions. In the next chapter we present the computer evidence supporting our conjecture that, in fact, these graphs do describe the identifications for certain mappings.

3.3.1 A Hénon map with period-2 sink.

Figure 3.7, shows the unstable manifold picture for a certain map $f_{a,c}$ with a and c real and in the parameter region of where $f_{a,c}$ and the polynomial P_c have an attracting orbit of period two and the W^u_β-picture is symmetric with respect to complex conjugation. The value of both parameters has been increased relative to the last example of §3.1 when $f_{a,c} \approx \varprojlim P_{-1}$. The external rays in the W^u_β picture reveal that a non-trivial topological change has occurred between the parameter values for these two cases. For instance it can be observed that a fundamental

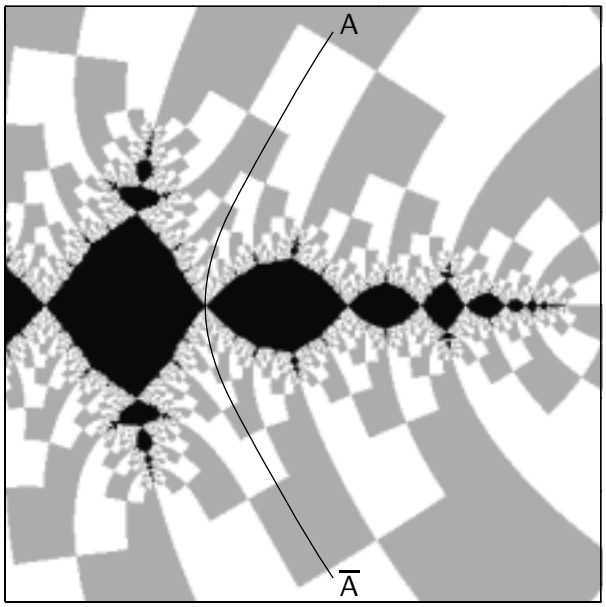

Figure 3.7: $W^u_{a,c}$ picture for $a = 0.125, c = -1.124$

domain for this mapping has three rays identified with their complex conjugate rays whereas the mapping of example 3 in §3.1 has only one (cf. figure 2.3). Specifically, it can be observed that the ray marked A in figure 3.7 has binary coding $^\infty\mathtt{0011}(\mathtt{01})^\infty$, and it is identified with the rays with coding $\overline{\mathsf{A}} = {}^\infty\mathtt{1100}(\mathtt{10})^\infty$. The computer evidence supports the following conjecture.

Conjecture 1. *For the parameters values $a = .125$ and $c = -1.24$ the ray $^\infty\mathtt{0011}(\mathtt{01})^\infty$ and its conjugate ray, $^\infty\mathtt{1100}(\mathtt{10})^\infty$, are identified under $\boldsymbol{\psi}$.*

This topological change with respect to the mapping of example 3 in §3.1 tells us the following:

Proposition 16. *If conjecture 1 holds then* $f_{a,c} \not\approx \varprojlim P_{-1}$ *for the parameter values* $a = .125$ *and* $c = -1.24$.

Proof. By the corollary to Theorem 2, if $f_{a,c} \approx \varprojlim P_{-1}$ then the graph describing $\overset{\psi}{\sim}$ for this mapping would be the same describing $\sim_c$ for $c = -1$, or the graph Γ_2 in figure 3.3. According to conjecture 1 the ray A is identified with its complex conjugate, but this identification is not produced by the graph Γ_2, which instead gives $\begin{bmatrix} {}^{\infty}0011(01)^{\infty} \\ {}^{\infty}0100(10)^{\infty} \end{bmatrix}$ for the identification corresponding to ray A. □

Computer evidence suggest that this map belongs to aregion of (real) parameter space where all maps are topologically conjugate on J.

We have obtained the graph shown in figure 3.8 as the graph that describes the quotient of the solenoid for this Hénon map. It is easy to see that the graph of figure 3.8 does encode the identifications that give rise to the the large scale features of K_β^+. For instance, in figure 3.8 we have marked some of the most evident identifications and listed the binary coding of the rays involved. Since the graph is backwards deterministic, the corresponding paths in the graph Γ_2' can be obtained starting from the two-cycle (where all forward paths that leave the solenoid subgraph terminate) and following the arrows backwards. In the next chapter we present evidence supporting the conjecture that the graph also encodes the identifications occurring at small scales.

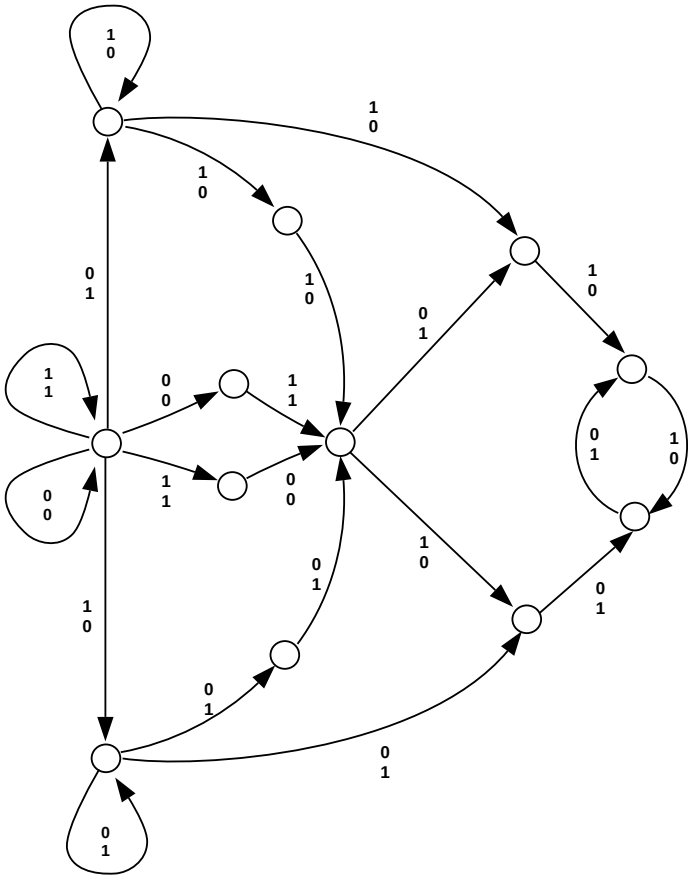

Figure 3.8: The graph Γ_2'.

$$\left[\begin{smallmatrix} A \\ A' \end{smallmatrix}\right] = \begin{bmatrix} {}^{\infty}0101.001(01)^{\infty} \\ {}^{\infty}0100.110(10)^{\infty} \end{bmatrix} \qquad \left[\begin{smallmatrix} B \\ B \end{smallmatrix}\right] = \begin{bmatrix} {}^{\infty}0100.101(01)^{\infty} \\ {}^{\infty}1011.010(10)^{\infty} \end{bmatrix}$$

$$\left[\begin{smallmatrix} C \\ C' \end{smallmatrix}\right] = \begin{bmatrix} {}^{\infty}0100.100(10)^{\infty} \\ {}^{\infty}0011.011(01)^{\infty} \end{bmatrix} \qquad \left[\begin{smallmatrix} D \\ D' \end{smallmatrix}\right] = \begin{bmatrix} {}^{\infty}0100.011(01)^{\infty} \\ {}^{\infty}0011.100(10)^{\infty} \end{bmatrix}$$

$$\left[\begin{smallmatrix} E \\ E \end{smallmatrix}\right] = \begin{bmatrix} {}^{\infty}0011.010(10)^{\infty} \\ {}^{\infty}1100.101(01)^{\infty} \end{bmatrix} \qquad \left[\begin{smallmatrix} F \\ F' \end{smallmatrix}\right] = \begin{bmatrix} {}^{\infty}0011.001(01)^{\infty} \\ {}^{\infty}0010.110(10)^{\infty} \end{bmatrix}$$

$$\left[\begin{smallmatrix} G \\ G \end{smallmatrix}\right] = \begin{bmatrix} {}^{\infty}0010.101(01)^{\infty} \\ {}^{\infty}1101.010(10)^{\infty} \end{bmatrix}$$

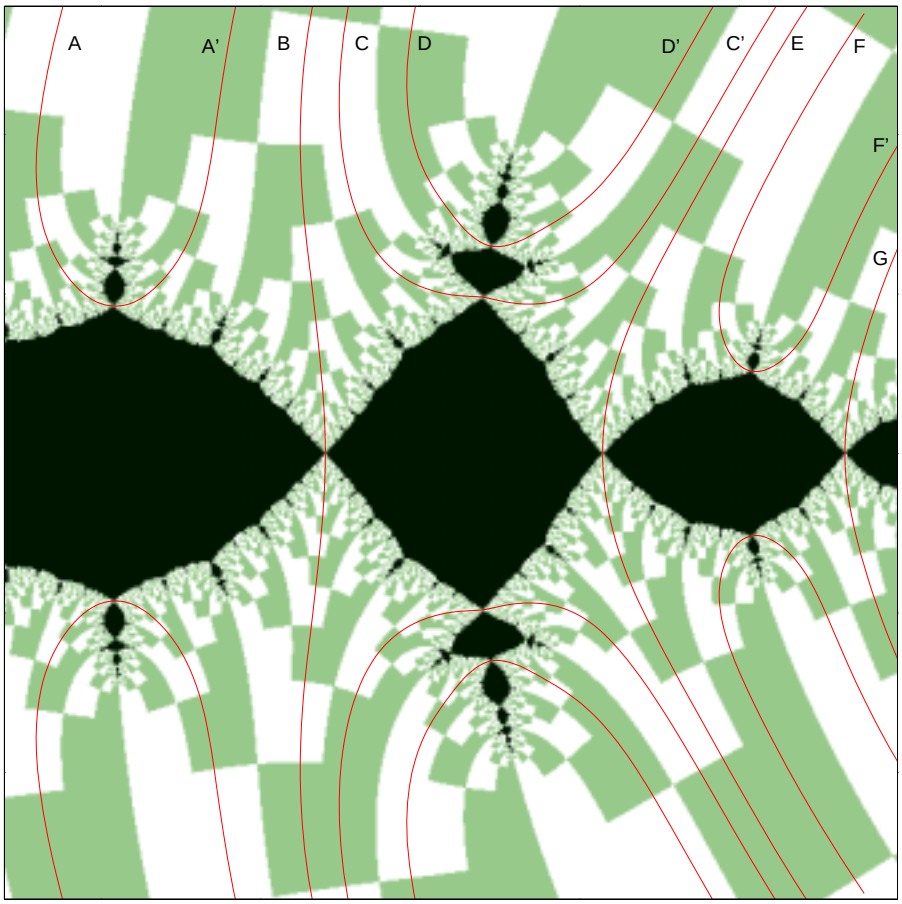

Figure 3.9:

3.3.2 A model for a map with sinks of period 1 and 3

The parameter values $a = 0.3$ and $c = -1.17$ also give rise to a Hénon mapping that appears to be hyperbolic. This is an interesting example whose study was suggested by Professor Hubbard. The map has an attracting cycle of period three as well as an attractive fixed point. Figure 3.10 shows the W^u_β picture for this map. The "round" components of $K_\beta - J$ belong to the basin of attraction of the period-three cycle, while the other components (with cusps) belong to the basin of the fixed sink. Within a fundamental domain defined by a pair of rays identified on the real axis in the W^u_β picture (and their images under multiplication by λ) there is two of each type of components of $K_\beta - J$ that intersect the real axis.

As discussed at the end of chapter 2, the real identifications arise from rays with coding ending in either $(\mathtt{011})^\infty$ or $(\mathtt{100})^\infty$. The graph we have obtained for this Hénon mapping is shown in figure 3.11 and denoted $\Gamma_{(3,1)}$. Although more complicated that the previous example, it can be readily seen that the graph $\Gamma_{(3,1)}$ encodes the identifications of the stable manifolds of the ray ${}^\infty(\mathtt{011}).(\mathtt{011})^\infty$ and ${}^\infty(\mathtt{100}).(\mathtt{100})^\infty$. In particular, the real identifications correspond to the paths in $\Gamma_{(3,1)}$ from the two 1-cycles with label $\left[\begin{smallmatrix}\mathtt{0}\\ \mathtt{1}\end{smallmatrix}\right]$ and $\left[\begin{smallmatrix}\mathtt{1}\\ \mathtt{0}\end{smallmatrix}\right]$ to the two terminal 3-cycles. These identifications have the form

$$\begin{bmatrix}\mathtt{h100}(\mathtt{100})^\infty\\ \overline{\mathtt{h}}\mathtt{011}(\mathtt{011})^\infty\end{bmatrix} \quad \text{and} \quad \begin{bmatrix}\mathtt{h100}(\mathtt{011})^\infty\\ \overline{\mathtt{h}}\mathtt{011}(\mathtt{100})^\infty\end{bmatrix}$$

where $\mathtt{h}$ is ${}^\infty\mathtt{0}$ or ${}^\infty\mathtt{1}$.

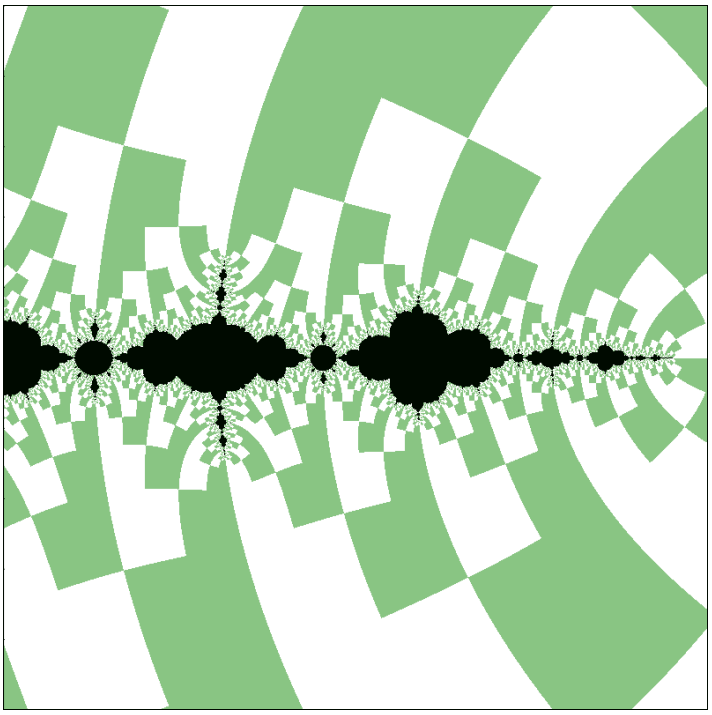

Figure 3.10: $W^u_{a,c}$ picture for $a = 0.3,\ c = -1.17$

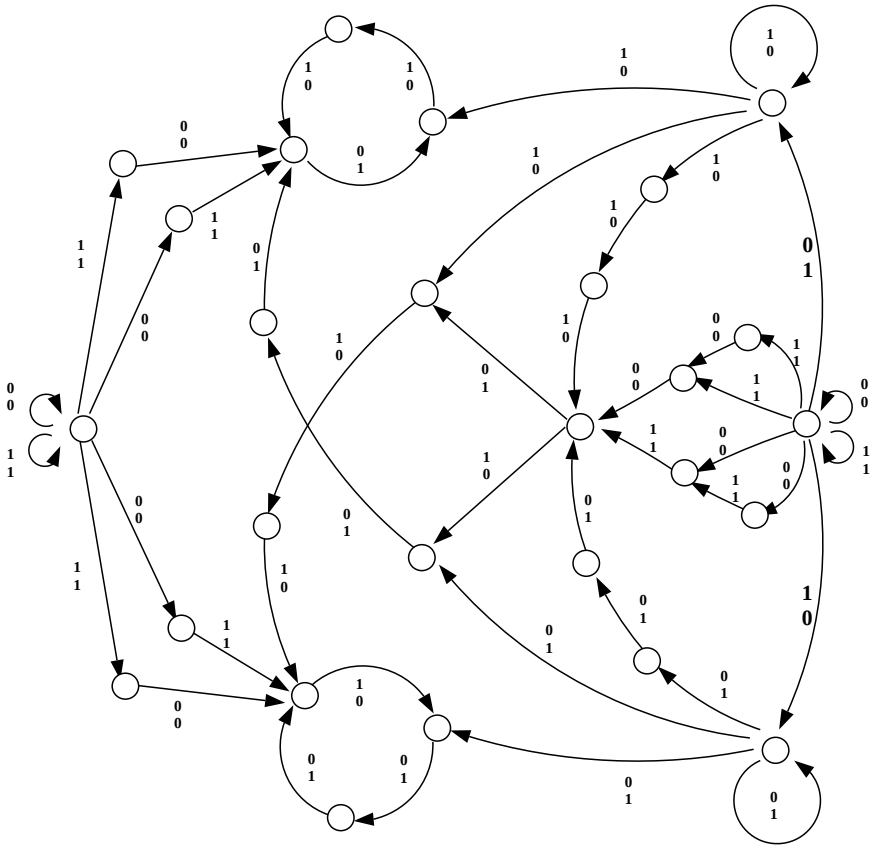

Figure 3.11: The graph $\Gamma_{(3,1)}$.

3.3.3 Verification of the planarity conditions

The rays identified under $\overset{\psi}{\sim}$ must satisfy the planarity conditions of §2.4.1 if they actually correspond to rays in the dynamics of hyperbolic maps with connected Julia set. We recall these conditions below:

- **Non-linking** If $\mathtt{A}, \mathtt{B}, \mathtt{A}', \mathtt{B}'$ are four rays in the same unstable manifold and they satisfy $\mathtt{A} \sim \mathtt{A}'$, $\mathtt{B} \sim \mathtt{B}'$, and $\mathtt{A} < \mathtt{B} < \mathtt{A}'$, then $\mathtt{A} < \mathtt{B}' < \mathtt{A}'$.

- **Orientation** Let H and H' be two distinct components of Σ_0. Suppose that $\mathtt{A}$ and $\mathtt{C}$ are rays in H and that $\mathtt{A}'$ and $\mathtt{C}'$ are rays in H' such that $\mathtt{A} \sim \mathtt{A}' \not\sim \mathtt{C} \sim \mathtt{C}'$. Then, $\mathtt{A} < \mathtt{C}$ implies $\mathtt{A}' > \mathtt{C}'$.

- **Localization** Let H and H' be two distinct components of Σ_0. Suppose that $\mathtt{A}$ and $\mathtt{C}$ are rays in H and that $\mathtt{A}'$ and $\mathtt{C}'$ are rays in H' such that $\mathtt{A} \sim \mathtt{A}' \not\sim \mathtt{C} \sim \mathtt{C}'$. Then, if $\mathtt{B} \in (\mathtt{A}, \mathtt{C}) \subset H$ and $\mathtt{A} \not\sim \mathtt{B} \sim \mathtt{B}' \not\sim \mathtt{C}$, then $\mathtt{B}' \in (\mathtt{A}, \mathtt{C}) \cup (\mathtt{A}', \mathtt{C}')$.

If a planarity condition is satisfied by all pairs of identifications produced by a graph, we say that the graph itself satisfies this planarity condition. In this section we prove the following theorems:

Theorem 4. *The graph Γ_2' satisfies the planarity conditions.*

Theorem 5. *The graph $\Gamma_{(3,1)}$ satisfies the planarity conditions.*

Remark. Proving orientation and localization is easy since these conditions are satisfied vacuously by the graphs in question. Verification of the non-linking condition is not as trivial and will require setting up notation and terminology. In particular,

the following "coloring scheme" will be useful in analyzing the combinatorics of the graphs.

TERMINOLOGY. In a bi-labeled graph Γ we will say an edge γ_0 is red if it has opposite labels, $\mathsf{top}(\gamma_0) \neq \mathsf{bot}(\gamma_0)$, otherwise we will say the edge is blue. We say that Γ is of type-R if it has the property that only red edges are reachable from red edges. Namely, Γ is of type-R if for any path γ in Γ, $\mathsf{top}(\gamma_n) \neq \mathsf{bot}(\gamma_n)$ implies $\mathsf{top}(\gamma_k) \neq \mathsf{bot}(\gamma_k)$ for all $k \geq n$. All the graphs presented in the previous section satisfy this property.

Lemma 17. *The graph Γ_2' satisfies orientation and localization.*

Proof. Both conditions apply to a pair of identifications between rays in distinct unstable manifolds. Let $\mathtt{A}$ and $\mathtt{A}'$ be the solenoidal codings of rays that belong to different unstable manifolds. It was shown in section 2.3.3 that $\mathtt{A}$ and $\mathtt{A}'$ do not agree to the left: for any $n \in \mathbf{Z}$, $\mathtt{A}_{(-\infty,n]} \neq \mathtt{A}'_{(-\infty,n]}$ Let γ be a path in Γ_2' corresponding to the identifications $\mathtt{A} \sim \mathtt{A}'$. In Γ_2' all paths producing non-trivial identification eventually end up in the 2-cycle consisting of the edges marked c and $\overline{\mathsf{c}}$ in figure 3.12. And all paths involving edges outside this two cycle end up in the solenoid sub-graph when followed backward. But a bi-infinite path that stays in the solenoid sub-graph when followed backwards always produces an identification of two rays in the same unstable manifold. Therefore, γ may not include any edges other than c and $\overline{\mathsf{c}}$, meaning that $\mathtt{A} = {}^{\infty}(\mathtt{01}).(\mathtt{01})^{\infty}$ and $\mathtt{A}' = {}^{\infty}(\mathtt{10}).(\mathtt{10})^{\infty}$, or vice versa. This shows that Γ_2' produces only one identification involving rays in distinct unstable manifolds. Since the hypothesis of the orientation and localization conditions require

two distinct such identifications, they are satisfied vacuously. □

Lemma 18. *The graph $\Gamma_{(3,1)}$ satisfies orientation and localization.*

Proof. This graph produces only three identifications of sequences that are not in the same unstable manifold:

$$^{\infty}(011).(011)^{\infty} \;\sim\; ^{\infty}(100).(100)^{\infty}$$

and its two shifts. The six rays involved in these identifications are all in distinct unstable manifolds, and therefore the hypothesis for the orientation and localization conditions are vacuously satisfied. □

Next we verify the non-linking condition for both graphs. In the proof of the non-linking condition we will use the following notation and terminology. Recall from section 3.1 that if γ is a path on a graph Γ and γ_k is the k^{th}-edge along γ then the notation $[\gamma_k]$ or $[\gamma]_k$ refers to the label of γ_k. Let $\mathtt{A}, \mathtt{B}, \mathtt{A}', \mathtt{B}'$ denote four rays belonging to the same unstable manifold. Let α and β be paths in a bi-labeled graph such that α correspond to the identifications $\mathtt{A} \overset{\psi}{\sim} \mathtt{A}'$, while β corresponds to the identification $\mathtt{B} \overset{\psi}{\sim} \mathtt{B}'$. Namely,

$$\Big[\alpha\Big]_k \equiv \begin{bmatrix} \mathtt{A}_k \\ \mathtt{A}'_k \end{bmatrix} \quad \text{and} \quad \Big[\beta\Big]_k \equiv \begin{bmatrix} \mathtt{B}_k \\ \mathtt{B}'_k \end{bmatrix}$$

and more generally,

$$\Big[\alpha\Big]_{[k,k+n]} \equiv \begin{bmatrix} \mathtt{A}_k \dots \mathtt{A}_{k+n} \\ \mathtt{A}'_k \dots \mathtt{A}'_{k+n} \end{bmatrix} \quad \text{and} \quad \Big[\beta\Big]_{[k,k+n]} \equiv \begin{bmatrix} \mathtt{B}_k \dots \mathtt{B}_{k+n} \\ \mathtt{B}'_k \dots \mathtt{B}'_{k+n} \end{bmatrix}.$$

The key idea in both theorems will be to show that the order relation $\mathtt{A} < \mathtt{B} < \mathtt{A}' < \mathtt{B}'$ is inconsistent with the assumption that paths α and β belong to the graph under

consideration. There are two ways by which symbol sequences tell us that two rays belong to the same unstable manifold, (§2.3.3). Thus, the problem breaks up naturally into two cases depending on whether $\mathtt{A}, \mathtt{B}, \mathtt{A}', \mathtt{B}'$ eventually agree to the left, or all four sequences become constant but not equal sufficiently far to the left.[1] Propositions 19 and 20 establish the general form that the binary coding of the rays must satisfy in the these two cases.

Proposition 19. *Let α and β be paths in a bi-labeled graph Γ producing the identifications $\mathtt{A} \sim \mathtt{A}'$ and $\mathtt{B} \sim \mathtt{B}'$, respectively. Suppose that $\mathtt{A}, \mathtt{B}, \mathtt{A}', \mathtt{B}'$ agree sufficiently far to the left and satisfy $\mathtt{A} < \mathtt{B} < \mathtt{A}' < \mathtt{B}'$. Set $n_0 = \max\{k \in \mathbf{Z} \,:\, \mathtt{A}_i = \mathtt{B}_i = \mathtt{A}'_i = \mathtt{B}'_i \text{ for all } i < k\}$. If Γ is of type-R, there exist integers n_1 and n_2, $n_0 < n_1 \leq n_2$, and words x and y, such that $[\alpha]_{[n_0,n_2]} \equiv \left[\begin{smallmatrix}\mathtt{A}\\ \mathtt{A}'\end{smallmatrix}\right]_{[n_0,n_2]}$ and $[\beta]_{[n_0,n_2]} \equiv \left[\begin{smallmatrix}\mathtt{B}\\ \mathtt{B}'\end{smallmatrix}\right]_{[n_0,n_2]}$ are of one of the following four form:*

$$(19.1)\qquad \begin{bmatrix}\mathtt{A}\\ \mathtt{A}'\end{bmatrix}_{[n_0,n_2]} = \begin{bmatrix} \overset{n_0}{0}\ \overset{}{\overline{x}}\ \overset{n_1}{0}\ \overline{y}\ \overset{n_2}{1} \\ 1\ x\ 1\ y\ 0 \end{bmatrix}, \qquad \begin{bmatrix}\mathtt{B}\\ \mathtt{B}'\end{bmatrix}_{[n_0,n_2]} = \begin{bmatrix} \overset{n_0}{1}\ \overset{}{x}\ \overset{n_1}{0}\ \overline{y}\ \overset{n_2}{0} \\ 1\ x\ 1\ y\ 1 \end{bmatrix}.$$

$$(19.2)\qquad \begin{bmatrix}\mathtt{A}\\ \mathtt{A}'\end{bmatrix}_{[n_0,n_2]} = \begin{bmatrix} \overset{n_0}{0}\ \overset{}{\overline{x}}\ \overset{n_1}{1}\ \overline{y}\ \overset{n_2}{0} \\ 1\ x\ 0\ y\ 1 \end{bmatrix}, \qquad \begin{bmatrix}\mathtt{B}\\ \mathtt{B}'\end{bmatrix}_{[n_0,n_2]} = \begin{bmatrix} \overset{n_0}{1}\ \overset{}{x}\ \overset{n_1}{0}\ y\ \overset{n_2}{0} \\ 1\ x\ 1\ \overline{y}\ 1 \end{bmatrix}.$$

$$(19.3)\qquad \begin{bmatrix}\mathtt{A}\\ \mathtt{A}'\end{bmatrix}_{[n_0,n_2]} = \begin{bmatrix} \overset{n_0}{0}\ \overset{}{x}\ \overset{n_1}{0}\ y\ \overset{n_2}{0} \\ 0\ x\ 1\ \overline{y}\ 1 \end{bmatrix}, \qquad \begin{bmatrix}\mathtt{B}\\ \mathtt{B}'\end{bmatrix}_{[n_0,n_2]} = \begin{bmatrix} \overset{n_0}{0}\ \overset{}{x}\ \overset{n_1}{0}\ y\ \overset{n_2}{1} \\ 1\ \overline{x}\ 1\ \overline{y}\ 0 \end{bmatrix}.$$

$$(19.4)\qquad \begin{bmatrix}\mathtt{A}\\ \mathtt{A}'\end{bmatrix}_{[n_0,n_2]} = \begin{bmatrix} \overset{n_0}{0}\ \overset{}{x}\ \overset{n_1}{0}\ \overline{y}\ \overset{n_2}{0} \\ 0\ x\ 1\ y\ 1 \end{bmatrix}, \qquad \begin{bmatrix}\mathtt{B}\\ \mathtt{B}'\end{bmatrix}_{[n_0,n_2]} = \begin{bmatrix} \overset{n_0}{0}\ \overset{}{x}\ \overset{n_1}{1}\ y\ \overset{n_2}{0} \\ 1\ \overline{x}\ 0\ \overline{y}\ 1 \end{bmatrix}.$$

[1] The second case occurs if the rays belong to the unstable manifold of the β-fixed point.

Proof. The ordering of the sequences determines seven possibilities, three of which are eliminated because they contradict the graph being of type-R, as we now explain. If exactly three of the sequences agree on the n_0-entry, let n_1 be the first index where only two of them agree, and let n_2 be the first index where the two sequences that agreed at n_1 become different. Then, there are four possibilities for the entries $n_0, \ldots, n_2$ of the sequences $\mathtt{A}, \mathtt{B}, \mathtt{A}', \mathtt{B}'$, that respect their ordering, as listed in table 3.1. On the other hand, if only two of the sequences $\mathtt{A}, \mathtt{B}, \mathtt{A}', \mathtt{B}'$ agree on the n_0-entry,

Table 3.1: Possible $[n_0, \ldots, n_2]$-block of four sequences $\mathtt{A} < \mathtt{B} < \mathtt{A}' < \mathtt{B}'$ subject to the conditions that exactly k of the sequences agree on all coordinates less than n_{4-k}, $k = 4, 3, 2$. The entries x and y denote words and $*$ is a "wild-card" (of the right length in each column) representing arbitrary entries.

		n_0		n_1		n_2
(I)	$\mathtt{A}:$	0	$*$	$*$	$*$	$*$
	$\mathtt{B}:$	1	x	0	$*$	$*$
	$\mathtt{A}':$	1	x	1	y	0
	$\mathtt{B}':$	1	x	1	y	1

		n_0		n_1		n_2
(II)	$\mathtt{A}:$	0	$*$	$*$	$*$	$*$
	$\mathtt{B}:$	1	x	0	y	0
	$\mathtt{A}':$	1	x	0	y	1
	$\mathtt{B}':$	1	x	1	$*$	$*$

		n_0		n_1		n_2
(III)	$\mathtt{A}:$	0	x	0	y	0
	$\mathtt{B}:$	0	x	0	y	1
	$\mathtt{A}':$	0	x	1	$*$	$*$
	$\mathtt{B}':$	1	$*$	$*$	$*$	$*$

		n_0		n_1		n_2
(IV)	$\mathtt{A}:$	0	x	0	$*$	$*$
	$\mathtt{B}:$	0	x	1	y	0
	$\mathtt{A}':$	0	x	1	y	1
	$\mathtt{B}':$	1	$*$	$*$	$*$	$*$

Table 3.2: Possible $[n_0, \ldots, n_2]$-block in four sequences $\mathtt{A} < \mathtt{B} < \mathtt{A}' < \mathtt{B}'$ which agree on all coordinates less than n_0 and such that no three of the sequences agree on the n_0 coordinate. The coordinates n_1 and n_2 correspond to the first distinct entry between each pair of sequences that agreed on the n_0 coordinate.

(V)						(VI)						(VII)			
	n_0		n_1		n_2		n_0		n_1		n_2		n_0		$n_1 = n_2$
$\mathtt{A}:$	0	x	0	$*$	$*$	$\mathtt{A}:$	0	x	t	y	0	$\mathtt{A}:$	0	x	0
$\mathtt{B}:$	0	x	1	$*$	$*$	$\mathtt{B}:$	0	x	t	y	1	$\mathtt{B}:$	0	x	1
$\mathtt{A}':$	1	z	t	y	0	$\mathtt{A}':$	1	z	0	$*$	$*$	$\mathtt{A}':$	1	y	0
$\mathtt{B}':$	1	z	t	y	1	$\mathtt{B}':$	1	z	1	$*$	$*$	$\mathtt{B}':$	1	y	1

necessarily $\mathtt{A}_{n_0} = \mathtt{B}_{n_0} = \mathtt{0}$ and $\mathtt{A}'_{n_0} = \mathtt{B}'_{n_0} = \mathtt{1}$ due to the ordering of the sequences. In this case, let n' be the first index where $\mathtt{A}$ and $\mathtt{B}$ become distinct, and let n'' be the first index where $\mathtt{A}'$ and $\mathtt{B}'$ become distinct. Set $n_1 = \min\{n', n''\},\ n_2 = \max\{n', n''\}$. Then, there are three possibilities for the entries $n_0, \ldots\ n_2$ of the sequences $\mathtt{A}, \mathtt{B}, \mathtt{A}', \mathtt{B}'$, as listed in table 3.2.

Now, because the graph is of type-R, the occurrence of a red edge in either of the paths α or βimplies that all subsequent edges in the path must be red as well. This determines the $*$ entries of (I)-(IV) in terms of x and y, giving (19.**1**)-(19.**4**), respectively. However, cases (V)-(VII) lead to contradictions under the hypothesis that the graph is of type-R: In (V) we have $\left[\begin{smallmatrix}\mathtt{A}\\ \mathtt{A}'\end{smallmatrix}\right]_{n_0} = \left[\begin{smallmatrix}\mathtt{0}\\ \mathtt{1}\end{smallmatrix}\right]$ and $\left[\begin{smallmatrix}\mathtt{B}\\ \mathtt{B}'\end{smallmatrix}\right]_{n_0} = \left[\begin{smallmatrix}\mathtt{0}\\ \mathtt{1}\end{smallmatrix}\right]$, hence both edges α_{n_0} and β_{n_0} are red. Since the graph is of type-R, α_{n_1} and β_{n_1} must be

red edges as well. Then, $\left[\begin{smallmatrix}\mathtt{A}\\ \mathtt{A}'\end{smallmatrix}\right]_{n_1} = \left[\begin{smallmatrix}\mathtt{0}\\ t\end{smallmatrix}\right]$ implies that $t = \mathtt{1}$, but $\left[\begin{smallmatrix}\mathtt{B}\\ \mathtt{B}'\end{smallmatrix}\right]_{n_1} = \left[\begin{smallmatrix}\mathtt{1}\\ t\end{smallmatrix}\right]$ imply that $t = \mathtt{0}$. Case-(VI) is similar: The edges α_{n_1} and β_{n_1} are red, therefore $\left[\begin{smallmatrix}\mathtt{A}\\ \mathtt{A}'\end{smallmatrix}\right]_{n_1} = \left[\begin{smallmatrix}t\\ \mathtt{0}\end{smallmatrix}\right]$ implies that $t = \mathtt{1}$ while $\left[\begin{smallmatrix}\mathtt{B}\\ \mathtt{B}'\end{smallmatrix}\right]_{n_1} = \left[\begin{smallmatrix}t\\ \mathtt{1}\end{smallmatrix}\right]$ requires $t = \mathtt{0}$. Finally, in (VII) we have $\left[\begin{smallmatrix}\mathtt{A}\\ \mathtt{A}'\end{smallmatrix}\right]_{n_0} = \left[\begin{smallmatrix}\mathtt{0}\\ \mathtt{1}\end{smallmatrix}\right]$ and $\left[\begin{smallmatrix}\mathtt{A}\\ \mathtt{A}'\end{smallmatrix}\right]_{n_1} = \left[\begin{smallmatrix}\mathtt{0}\\ \mathtt{0}\end{smallmatrix}\right]$, so that α_{n_0} is red but α_{n_1} is not, contradicting the hypothesis that the graph is of type-R. □

Proposition 20. *Let α and β be paths in a bi-labeled graph Γ producing the identifications $\mathtt{A} \sim \mathtt{A}'$ and $\mathtt{B} \sim \mathtt{B}'$, respectively, such that $A \not\sim \mathtt{B}$. Suppose that for small enough index n, $\mathtt{A}_{(-\infty,n]}$, $\mathtt{B}_{(-\infty,n]}$, $\mathtt{A}'_{(-\infty,n]}$ and $\mathtt{B}'_{(-\infty,n]}$ are constant, and that $\mathtt{A} < \mathtt{B} < \mathtt{A}' < \mathtt{B}'$. Assume furthermore that not all four sequences agree to the left. If Γ is of type-R, there exist integers n_1 and n_2, $n_1 \le n_2$, and an arbitrary word x such that $[\alpha]_{(-\infty,n_2]} \equiv \left[\begin{smallmatrix}\mathtt{A}\\ \mathtt{A}'\end{smallmatrix}\right]_{(-\infty,n_2]}$ and $[\beta]_{(-\infty,n_2]} \equiv \left[\begin{smallmatrix}\mathtt{B}\\ \mathtt{B}'\end{smallmatrix}\right]_{(-\infty,n_2]}$ are of the form given in one of the following four possibilities:*

$$(20.\mathbf{1}) \qquad \begin{bmatrix}\mathtt{A}\\ \mathtt{A}'\end{bmatrix}_{(-\infty,n_2]} = \begin{bmatrix}^{\infty}\mathtt{1} & \overset{n_1}{\mathtt{1}} & x & \overset{n_2}{\mathtt{1}}\\ ^{\infty}\mathtt{1} & \mathtt{0} & \overline{x} & \mathtt{0}\end{bmatrix}, \qquad \begin{bmatrix}\mathtt{B}\\ \mathtt{B}'\end{bmatrix}_{(-\infty,n_2]} = \begin{bmatrix}^{\infty}\mathtt{1} & \overset{n_1}{\mathtt{1}} & x & \overset{n_2}{\mathtt{0}}\\ ^{\infty}\mathtt{0} & \mathtt{0} & \overline{x} & \mathtt{1}\end{bmatrix}.$$

$$(20.\mathbf{2}) \qquad \begin{bmatrix}\mathtt{A}\\ \mathtt{A}'\end{bmatrix}_{(-\infty,n_2]} = \begin{bmatrix}^{\infty}\mathtt{1} & \overset{n_1}{\mathtt{0}} & \overline{x} & \overset{n_2}{\mathtt{1}}\\ ^{\infty}\mathtt{0} & \mathtt{1} & x & \mathtt{0}\end{bmatrix}, \qquad \begin{bmatrix}\mathtt{B}\\ \mathtt{B}'\end{bmatrix}_{(-\infty,n_2]} = \begin{bmatrix}^{\infty}\mathtt{0} & \overset{n_1}{\mathtt{0}} & \overline{x} & \overset{n_2}{\mathtt{0}}\\ ^{\infty}\mathtt{0} & \mathtt{1} & x & \mathtt{1}\end{bmatrix}.$$

$$(20.\mathbf{3}) \qquad \begin{bmatrix}\mathtt{A}\\ \mathtt{A}'\end{bmatrix}_{(-\infty,n_2]} = \begin{bmatrix}^{\infty}\mathtt{1} & \overset{n_1}{\mathtt{1}} & \overline{x} & \overset{n_2}{\mathtt{1}}\\ ^{\infty}\mathtt{1} & \mathtt{0} & x & \mathtt{0}\end{bmatrix}, \qquad \begin{bmatrix}\mathtt{B}\\ \mathtt{B}'\end{bmatrix}_{(-\infty,n_2]} = \begin{bmatrix}^{\infty}\mathtt{1} & \overset{n_1}{\mathtt{0}} & x & \overset{n_2}{\mathtt{1}}\\ ^{\infty}\mathtt{0} & \mathtt{1} & \overline{x} & \mathtt{0}\end{bmatrix}.$$

$$(20.\mathbf{4}) \qquad \begin{bmatrix}\mathtt{A}\\ \mathtt{A}'\end{bmatrix}_{(-\infty,n_2]} = \begin{bmatrix}^{\infty}\mathtt{1} & \overset{n_1}{\mathtt{1}} & \overline{x} & \overset{n_2}{\mathtt{0}}\\ ^{\infty}\mathtt{0} & \mathtt{0} & x & \mathtt{1}\end{bmatrix}, \qquad \begin{bmatrix}\mathtt{B}\\ \mathtt{B}'\end{bmatrix}_{(-\infty,n_2]} = \begin{bmatrix}^{\infty}\mathtt{0} & \overset{n_1}{\mathtt{0}} & x & \overset{n_2}{\mathtt{0}}\\ ^{\infty}\mathtt{0} & \mathtt{1} & \overline{x} & \mathtt{1}\end{bmatrix}.$$

Proof. The proof of Proposition 20 is similar to that of Proposition 19, with n_1 and n_2 defined in the same way. The ordering $\mathtt{A} < \mathtt{B} < \mathtt{A}' < \mathtt{B}'$ determines seven possibilities, three of which contradict the hypothesis that the graph is of type-R, and the other four lead to (20.**1**)-(20.**4**). □

We are now ready to verify the remaining planarity condition and complete the proof of Theorem 4.

Lemma 21. *The SFT Γ_2' satisfies the non-linking condition.*

Proof. As outlined above, we proceed by letting α and β be paths in Γ_2' producing identifications $\mathtt{A} \sim \mathtt{A}'$ and $\mathtt{B} \sim \mathtt{B}'$, respectively, where $\mathtt{A} < \mathtt{A}'$, $\mathtt{B} < \mathtt{B}'$, and $\mathtt{A} < \mathtt{B}$. We claim that the hypothesis $\mathtt{A} < \mathtt{B} < \mathtt{A}' < \mathtt{B}'$ leads to contradictions, therefore if $\mathtt{A} < \mathtt{B}$ then, in fact, $\mathtt{A} < \mathtt{B} < \mathtt{B}' < \mathtt{A}'$. There are two possibilities to consider: one where Proposition 19 applies and the other where Proposition 20 applies. resulting in eight cases to check.

Case **19.1**: $$\Big[\alpha\Big]_{[n_0,n_2]} = \begin{bmatrix} \overset{n_0}{\mathtt{0}} & \overset{n_1}{\overline{x}} & \mathtt{0} & \overline{y} & \overset{n_2}{\mathtt{1}} \\ \mathtt{1} & x & \mathtt{1} & y & \mathtt{0} \end{bmatrix}, \qquad \Big[\beta\Big]_{[n_0,n_2]} = \begin{bmatrix} \overset{n_0}{\mathtt{1}} & \overset{n_1}{x} & \mathtt{0} & \overline{y} & \overset{n_2}{\mathtt{0}} \\ \mathtt{1} & x & \mathtt{1} & y & \mathtt{1} \end{bmatrix}.$$

In this case both α_{n_0} and β_{n_1} are red edges immediately preceded by a blue edge (since, by hypothesis, $\mathtt{A}_{n_0-1} = \mathtt{A}'_{n_0-1}$). Therefore α_{n_0} and β_{n_1} must each be one of the edges a or b in figure-3.12. This implies that the subsequence $\left[\begin{smallmatrix}\overline{x}\\x\end{smallmatrix}\right]$ and $\left[\begin{smallmatrix}\overline{y}\\y\end{smallmatrix}\right]$ in (**19.1**) both begin with $\left[\begin{smallmatrix}\mathtt{11}\\\mathtt{00}\end{smallmatrix}\right]$. Consequently, the subsequence $\left[\begin{smallmatrix}\mathtt{011}\\\mathtt{100}\end{smallmatrix}\right]$ occurs at least twice in $[\alpha]$: at n_0 and at n_1. But this subsequence occurs only once among labels of forward paths which begin with edge b, hence $\alpha_{n_0} \neq \mathsf{b}$. It follows that $\alpha_{n_0} = \mathsf{a}$

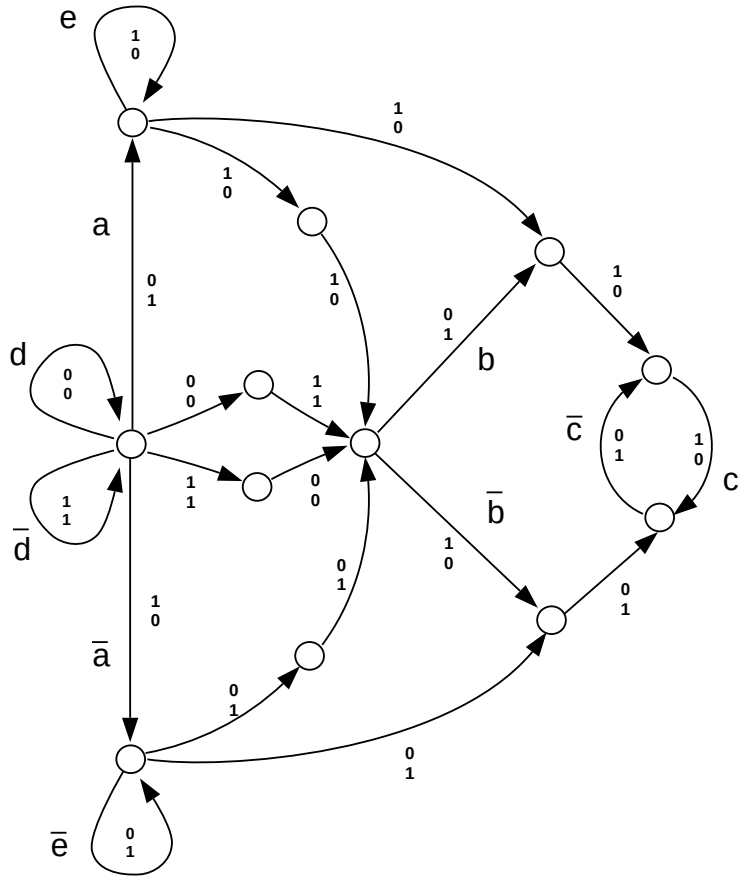

Figure 3.12: The graph Γ_2' with marked edges referenced in the proof of Lemma 21.

and $\alpha_{n_1} = \mathsf{b}$. At b the graph Γ_2' is forward deterministic, and it determines that between n_1 and n_2 $[\alpha]$ is of the form

$$\Big[\alpha\Big]_{[n_1,n_2]} = \begin{bmatrix} 0\,1\,1\,(0\,1)^k\,0\,1 \\ 1\,0\,0\,(1\,0)^k\,1\,0 \end{bmatrix} \tag{3.4}$$

for some $k \geq 0$. This specifies y in (**19.1**), giving

$$\Big[\beta\Big]_{[n_1,n_2]} = \begin{bmatrix} 0\,1\,1\,(0\,1)^k\,0\,0 \\ 1\,0\,0\,(1\,0)^k\,1\,1 \end{bmatrix}. \tag{3.5}$$

If $k = 0$ then $[\beta]_{[n_1,n_2]} = \left[\begin{smallmatrix}01100\\10011\end{smallmatrix}\right]$, and if $k > 0$ we get $[\beta]_{[n_1,n_1+5]} = \left[\begin{smallmatrix}011010\\100010\end{smallmatrix}\right]$; it follows that $\beta_{n_1} \neq \mathsf{a}$ because these subsequences do not occur on any forward path originating at edge a. Also, the fact that Γ_2' is forward deterministic at b implies that $\beta_{n_1} \neq \mathsf{b}$ since $\alpha_{n_1} = \mathsf{b}$ but $[\alpha]$ and $[\beta]$ differ at n_2 which is to the right of n_1. This contradicts $\beta_{n_1} \in \{\mathsf{a}, \mathsf{b}\}$.

Case **19.2**: $\Big[\alpha\Big]_{[n_0,n_2]} = \begin{bmatrix} \overset{n_0}{0} & \overset{n_1}{\overline{x}} & \overset{}{1} & \overline{y} & 0 \\ 1 & x & 0 & y & 1 \end{bmatrix}$, $\Big[\beta\Big]_{[n_0,n_2]} = \begin{bmatrix} \overset{n_0}{1} & \overset{n_1}{x} & \overset{}{0} & y & 0 \\ 1 & x & 1 & \overline{y} & 1 \end{bmatrix}$.

By arguing as in the previous case, we first conclude that α_{n_0}, $\beta_{n_1} \in \{\mathsf{a}, \mathsf{b}\}$, and therefore the undetermined words $\overline{x}$ and y in (**19.2**) both begin with at least two 1's. Then, $[\alpha]_{[n_0,n_0+3]} = \left[\begin{smallmatrix}011\\100\end{smallmatrix}\right]$ and $[\alpha]_{[n_1,n_1+3]} = \left[\begin{smallmatrix}100\\011\end{smallmatrix}\right]$, which leads to the conclusion that α_{n_0} must be a and that α_{n_1} is $\overline{\mathsf{b}}$. The graph Γ_2' is forward deterministic at $\overline{\mathsf{b}}$, specifying that

$$\Big[\alpha\Big]_{[n_1,n_2]} = \begin{bmatrix} 1\,0\,0\,(1\,0)^k\,1\,0 \\ 0\,1\,1\,(0\,1)^k\,0\,1 \end{bmatrix} \tag{3.6}$$

with $k \geq 0$. By (**19.2**), we then get

$$\Big[\beta\Big]_{[n_1,n_2]} = \begin{bmatrix} 0\,1\,1\,(0\,1)^k\,0\,0 \\ 1\,0\,0\,(1\,0)^k\,1\,1 \end{bmatrix}. \tag{3.7}$$

It follows that $\beta_{n_1} \neq \mathsf{b}$ since the subsequence $\left[\begin{smallmatrix}00\\11\end{smallmatrix}\right]$ does not occur on the forward path that begins at b. But equation (3.7) is the same as equation (3.5) which ruled out $\beta_{n_1} = \mathsf{a}$. Hence $\beta_{n_1} \notin \{\mathsf{a}, \mathsf{b}\}$, giving a contradiction.

Cases **19.3** & **19.4**: The analysis of (19.**3**) is exactly as case (19.**1**) with the roles of $[\alpha]$ and $[\beta]$ interchanged –the difference between $\left[\begin{smallmatrix}\mathsf{B}\\\mathsf{B}'\end{smallmatrix}\right]_{[n_0,n_1)}$ in (**19.1**) and $\left[\begin{smallmatrix}\mathsf{A}\\\mathsf{A}'\end{smallmatrix}\right]_{[n_0,n_1)}$ in (**19.3**) does not affect the argument. Similarly, case (19.**4**) follows from case (19.**2**)

with $[\alpha]$ and $[\beta]$ interchanged.

Case **20.1**: $\Big[\alpha\Big]_{(-\infty,n_2]} = \begin{bmatrix} \overset{}{\overset{\infty}{\infty}}\mathsf{1} & \overset{n_1}{\mathsf{1}} & x & \overset{n_2}{\mathsf{1}} \\ \infty\mathsf{1} & \mathsf{0} & \overline{x} & \mathsf{0} \end{bmatrix}, \quad \Big[\beta\Big]_{(-\infty,n_2]} = \begin{bmatrix} \overset{}{\overset{\infty}{\infty}}\mathsf{1} & \overset{n_1}{\mathsf{1}} & x & \overset{n_2}{\mathsf{0}} \\ \infty\mathsf{0} & \mathsf{0} & \overline{x} & \mathsf{1} \end{bmatrix}.$

Observe in figure-3.12 that the only paths which produce the constant left-infinite sequence $\left[\begin{smallmatrix}\infty\mathsf{0}\\ \infty\mathsf{1}\end{smallmatrix}\right]$ are those that remain in edge e when followed backwards. Hence $\beta_k = \mathsf{e}$ for all $k < n$ for some $n \leq n_1$. Also, it must be that $\alpha_{n_1} = \overline{\mathsf{a}}$ because no other edge in Γ_2' has label $\left[\begin{smallmatrix}\mathsf{1}\\ \mathsf{0}\end{smallmatrix}\right]$ and can be preceded exclusively by edges with label $\left[\begin{smallmatrix}\mathsf{1}\\ \mathsf{1}\end{smallmatrix}\right]$. It follows that the word x in (**20.1**) begins with at least two $\mathsf{0}$'s. Then, $\beta_{[n_1,n_1+2]} = \left[\begin{smallmatrix}\mathsf{100}\\ \mathsf{011}\end{smallmatrix}\right]$ and this determines that $\beta_{n_1} = \overline{\mathsf{b}}$, because $\overline{\mathsf{b}}$ is the only edge in Γ_2' where the subsequence $\left[\begin{smallmatrix}\mathsf{100}\\ \mathsf{011}\end{smallmatrix}\right]$ occurs for forward paths that originate from edge e. At $\overline{\mathsf{b}}$ the graph is forward deterministic, giving

$$\Big[\beta\Big]_{[n_1,n_2]} = \begin{bmatrix} \mathsf{1\,0\,0\,(1\,0)}^k\,\mathsf{1\,0} \\ \mathsf{0\,1\,1\,(0\,1)}^k\,\mathsf{0\,1} \end{bmatrix} \tag{3.8}$$

with $k \geq 0$. This specifies x in (**20.1**), to yield

$$\Big[\alpha\Big]_{[n_1,n_2]} = \begin{bmatrix} \mathsf{1\,0\,0\,(1\,0)}^k\,\mathsf{1\,1} \\ \mathsf{0\,1\,1\,(0\,1)}^k\,\mathsf{0\,0} \end{bmatrix} \tag{3.9}$$

Now, if $k = 0$ in 3.9 then $\alpha_{n_1} \neq \overline{\mathsf{a}}$ as the subsequence $\left[\begin{smallmatrix}\mathsf{10011}\\ \mathsf{01100}\end{smallmatrix}\right]$ does not occur on labels of any path that begins with $\overline{\mathsf{a}}$. And if $k > 0$, then $[\alpha]_{[n_1,n_1+5]} = \left[\begin{smallmatrix}\mathsf{100101}\\ \mathsf{011010}\end{smallmatrix}\right]$ which also does not occur after edge $\overline{\mathsf{a}}$. This contradicts $\alpha_{n_1} = \overline{\mathsf{a}}$.

Case **20.2**: $\Big[\alpha\Big]_{(-\infty,n_2]} = \begin{bmatrix} \overset{}{\overset{\infty}{\infty}}\mathsf{1} & \overset{n_1}{\mathsf{0}} & \overline{x} & \overset{n_2}{\mathsf{1}} \\ \infty\mathsf{0} & \mathsf{1} & x & \mathsf{0} \end{bmatrix}, \quad \Big[\beta\Big]_{(-\infty,n_2]} = \begin{bmatrix} \overset{}{\overset{\infty}{\infty}}\mathsf{0} & \overset{n_1}{\mathsf{0}} & \overline{x} & \overset{n_2}{\mathsf{0}} \\ \infty\mathsf{0} & \mathsf{1} & x & \mathsf{1} \end{bmatrix}.$

From $[\beta]_{(-\infty,n_1]} = \left[\begin{smallmatrix}\infty\mathsf{00}\\ \infty\mathsf{01}\end{smallmatrix}\right]$ it follows that $\beta_{n_1} = \mathsf{a}$. Therefore $\left[\begin{smallmatrix}\overline{x}\\ x\end{smallmatrix}\right]$ begins with $\left[\begin{smallmatrix}\mathsf{11}\\ \mathsf{00}\end{smallmatrix}\right]$. Then, from $[\alpha]_{(-\infty,n_1+2]} = \left[\begin{smallmatrix}\infty\mathsf{1011}\\ \infty\mathsf{0100}\end{smallmatrix}\right]$ we conclude $\alpha_{n_1} = \mathsf{b}$. At b the graph Γ_2' is forward

deterministic, hence the labels of $\alpha_{[n_1,n_2]}$ specify x. Then, (**20.2**) gives

$$\Big[\beta\Big]_{[n_1,n_2]} = \begin{bmatrix} \mathsf{0\,1\,1\,(0\,1)^k\,0\,0} \\ \mathsf{1\,0\,0\,(1\,0)^k\,1\,1} \end{bmatrix}.$$

But this is equation (3.5) which leads to $\beta_{n_1} \neq \mathsf{a}$, giving a contradiction.

Case **20.3**: $\Big[\alpha\Big]_{(-\infty,n_2]} = \begin{bmatrix} {}^{\infty}\mathsf{1}\ \overset{n_1}{\mathsf{1}}\ \overline{x}\ \overset{n_2}{\mathsf{1}} \\ {}^{\infty}\mathsf{1\ 0}\ x\ \mathsf{0} \end{bmatrix}$, $\Big[\beta\Big]_{(-\infty,n_2]} = \begin{bmatrix} {}^{\infty}\mathsf{1}\ \overset{n_1}{\mathsf{0}}\ x\ \overset{n_2}{\mathsf{1}} \\ {}^{\infty}\mathsf{0\ 1}\ \overline{x}\ \mathsf{0} \end{bmatrix}$.

From the form of $[\alpha]_{(-\infty,n_1]}$ it follows that $\alpha = \overline{\mathsf{a}}$. Therefore $\left[\begin{smallmatrix}\overline{x}\\ x\end{smallmatrix}\right]$ begins with $\left[\begin{smallmatrix}\mathsf{00}\\ \mathsf{11}\end{smallmatrix}\right]$. Then, from $[\beta]_{(-\infty,n_1+2]} = \left[\begin{smallmatrix}\infty\mathsf{1011}\\ \infty\mathsf{0100}\end{smallmatrix}\right]$ we conclude $\beta_{n_1} = \mathsf{b}$. At b the graph Γ_2' is forward deterministic, therefore the labels of $\beta_{[n_1,n_2]}$ specify x and we get

$$\Big[\alpha\Big]_{[n_1,n_2]} = \begin{bmatrix} \mathsf{1\,0\,0\,(1\,0)^k\,1\,1} \\ \mathsf{0\,1\,1\,(0\,1)^k\,0\,0} \end{bmatrix}$$

according (**20.3**). But this is the same as equation (3.9) which contradicted $\alpha_{n_1} = \overline{\mathsf{a}}$.

Case **20.4**: $\Big[\alpha\Big]_{(-\infty,n_2]} = \begin{bmatrix} {}^{\infty}\mathsf{1}\ \overset{n_1}{\mathsf{1}}\ \overline{x}\ \overset{n_2}{\mathsf{0}} \\ {}^{\infty}\mathsf{0\ 0}\ x\ \mathsf{1} \end{bmatrix}$, $\Big[\beta\Big]_{(-\infty,n_2]} = \begin{bmatrix} {}^{\infty}\mathsf{0}\ \overset{n_1}{\mathsf{0}}\ x\ \overset{n_2}{\mathsf{0}} \\ {}^{\infty}\mathsf{0\ 1}\ \overline{x}\ \mathsf{1} \end{bmatrix}$.

Exactly as in (**20.2**), it follows that $\beta = \mathsf{a}$ and that $\left[\begin{smallmatrix}x\\ \overline{x}\end{smallmatrix}\right]$ begins with $\left[\begin{smallmatrix}\mathsf{11}\\ \mathsf{00}\end{smallmatrix}\right]$. Then, from $[\alpha]_{(-\infty,n_1+2]} = \left[\begin{smallmatrix}\infty\mathsf{1100}\\ \infty\mathsf{0011}\end{smallmatrix}\right]$ we conclude $\alpha_{n_1} = \overline{\mathsf{b}}$. At $\overline{\mathsf{b}}$ Γ_2' is forward deterministic and specifies x to give that $[\beta]_{[n_1,n_2]}$ is given by the left-hand-side of equation (3.5), which rules out $\beta_{n_1} = \mathsf{a}$, giving a contradiction. □

The next lemma completes the proof of Theorem 5.

Lemma 22. *The graph $\Gamma_{(3,1)}$ satisfies the non-linking condition.*

Proof. The proof is similar to that of the Γ_2' graph. We show that the eight possibilities allowed by propositions 19 and 20 lead to contradictions. We will make use of the observation that in $\Gamma_{(3,1)}$ only the three edges marked a,b, and c in figure 3.13 have labels top=0, bot=1, and are immediately preceded by a blue node. Namely,

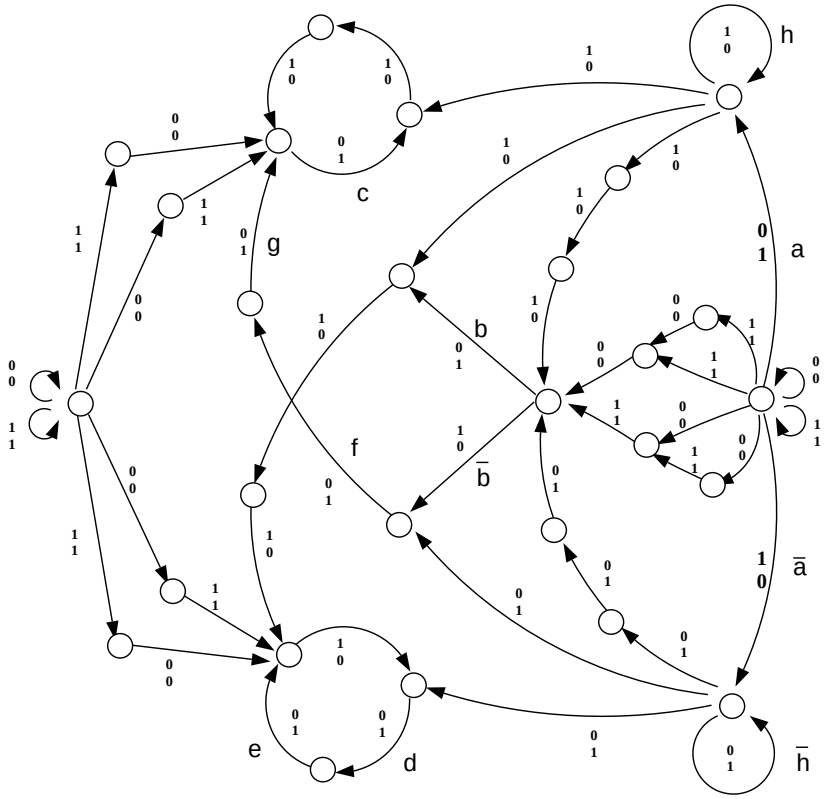

Figure 3.13: The graph $\Gamma_{(3,1)}$ with marked edges referenced in the proof of Lemma 22.

for any path γ in $\Gamma_{(3,1)}$ we have

$$[\gamma]_{[k-1,\,k]} \in \{\, \left[\begin{smallmatrix}0&0\\0&1\end{smallmatrix}\right],\ \left[\begin{smallmatrix}1&0\\1&1\end{smallmatrix}\right] \,\} \quad \text{implies} \quad \gamma_k \in \{\mathsf{a},\mathsf{b},\mathsf{c}\}. \tag{3.10}$$

In addition, it can also be checked by inspection that if $\gamma_m \in \{\mathsf{a},\mathsf{b},\mathsf{c}\}$ and $[\gamma]_n = \left[\begin{smallmatrix}0\\1\end{smallmatrix}\right]$ for $n > m$ then the following holds:

$$\left.\begin{array}{lcl} \gamma_m = \mathsf{a} & \Longrightarrow & \gamma_n \in \{\mathsf{b},\mathsf{c},\mathsf{d},\mathsf{e},\mathsf{f},\mathsf{g}\} \\ \gamma_m = \mathsf{b} & \Longrightarrow & \gamma_n \in \{\mathsf{d},\mathsf{e}\} \\ \gamma_m = \mathsf{c} & \Longrightarrow & \gamma_n = \mathsf{c}. \end{array}\right\} \tag{3.11}$$

We rule out the cases given in Proposition 19 by showing that their are incompatible with the above facts about $\Gamma_{(3,1)}$.

Case **19.1**:
$$\Big[\alpha\Big]_{[n_0,n_2]} = \overset{\scriptstyle n_0\quad n_1\quad n_2}{\begin{bmatrix} 0 & \overline{x} & 0 & \overline{y} & 1 \\ 1 & x & 1 & y & 0 \end{bmatrix}}, \qquad \Big[\beta\Big]_{[n_0,n_2]} = \overset{\scriptstyle n_0\quad n_1\quad n_2}{\begin{bmatrix} 1 & x & 0 & \overline{y} & 0 \\ 1 & x & 1 & y & 1 \end{bmatrix}}.$$

By (3.10),

$$\alpha_{n_0},\, \beta_{n_1} \in \{\mathsf{a},\mathsf{b},\mathsf{c}\}, \tag{3.12}$$

and by (3.11),

$$\alpha_{n_1} \in \{\mathsf{b},\mathsf{c},\mathsf{d},\mathsf{e},\mathsf{f},\mathsf{g}\}. \tag{3.13}$$

We will show that (3.12) can not hold for β_{n_1} if β is a path in $\Gamma_{(3,1)}$.

First, suppose that β_{n_1} is the edge a. Then

$$\begin{bmatrix}\overline{y}\\ y\end{bmatrix} = \begin{bmatrix}111\cdots\\ 000\cdots\end{bmatrix} \tag{3.14}$$

and by (**19.1**) we get

$$\Big[\alpha\Big]_{[n_1,\, n_1+3]} = \begin{bmatrix} \mathsf{0111}\cdots \\ \mathsf{1000}\cdots \end{bmatrix}.$$

Now, the subsequence $\left[\begin{smallmatrix}\mathsf{0111}\\ \mathsf{1000}\end{smallmatrix}\right]$ does not occur after any of the edges $\mathsf{c}, \mathsf{d}, \mathsf{e}, \mathsf{f}$ or g. Hence $\alpha_{n_1} \notin \{\mathsf{c}, \mathsf{d}, \mathsf{e}, \mathsf{f}, \mathsf{g}\}$and (3.13) imply that $\alpha_{n_1} = \mathsf{b}$. After edge b the graph $\Gamma_{(3,1)}$ is forward deterministic, and $\alpha_{n_1} = \mathsf{b}$ together with (3.14) and $[\alpha_{n_2}] = \left[\begin{smallmatrix}\mathsf{0}\\ \mathsf{1}\end{smallmatrix}\right]$ imply that

$$\Big[\alpha\Big]_{[n_1,\, n_2]} = \begin{bmatrix} \mathsf{011100}(\mathsf{100})^k\mathsf{1} \\ \mathsf{100011}(\mathsf{011})^k\mathsf{0} \end{bmatrix}, \qquad k \geq 0.$$

Then, by (**19.1**) we get that

$$\Big[\beta\Big]_{[n_1,\, n_2]} = \begin{bmatrix} \mathsf{011100}(\mathsf{100})^k\mathsf{0} \\ \mathsf{100011}(\mathsf{011})^k\mathsf{1} \end{bmatrix},$$

This contradicts $\beta_{n_1} = \mathsf{a}$ since the sequence $\left[\begin{smallmatrix}\mathsf{011100}\\ \mathsf{100011}\end{smallmatrix}\right]$ does not occurs after edge a.

Second, suppose that β_{n_1} is the edge b. Then the graph $\Gamma_{(3,1)}$ specifies that

$$\Big[\beta\Big]_{[n_1,\, n_2]} = \begin{bmatrix} \mathsf{011100}(\mathsf{100})^k\mathsf{10}^t\mathsf{0} \\ \mathsf{100011}(\mathsf{011})^k\mathsf{01}^t\mathsf{1} \end{bmatrix}, \qquad k \geq 0,\ t \in \{0, 1\},$$

and then, by (**19.1**) we get

$$\Big[\alpha\Big]_{[n_1,\, n_2]} = \begin{bmatrix} \mathsf{011100}(\mathsf{100})^k\mathsf{10}^t\mathsf{1} \\ \mathsf{100011}(\mathsf{011})^k\mathsf{01}^t\mathsf{0} \end{bmatrix}, \qquad k \geq 0,\ t \in \{0, 1\}.$$

This is inconsistent with $\alpha_{n_1} \in \{\mathsf{b}, \mathsf{c}, \mathsf{d}, \mathsf{e}, \mathsf{f}, \mathsf{g}\}$, as can be checked by inspection. Hence $\beta_{n_1} = \mathsf{b}$ violates (3.13).

Finally, suppose that β_{n_1} is the edge c. Then, as $[\beta_{n_2}] = \left[\begin{smallmatrix}\mathsf{0}\\ \mathsf{1}\end{smallmatrix}\right]$, we have

$$\Big[\beta\Big]_{[n_1,\, n_2]} = \begin{bmatrix} \mathsf{011}(\mathsf{011})^k\mathsf{0} \\ \mathsf{100}(\mathsf{100})^k\mathsf{1} \end{bmatrix}, \qquad k \geq 0.$$

Then, by (**19.1**),

$$\Big[\alpha\Big]_{[n_1,\, n_2]} = \begin{bmatrix} \mathsf{011}(\mathsf{011})^k\mathsf{1} \\ \mathsf{100}(\mathsf{100})^k\mathsf{0} \end{bmatrix}, \qquad k \geq 0.$$

The sequence $\left[\begin{smallmatrix}\mathsf{0110}\\ \mathsf{1001}\end{smallmatrix}\right]$ does not occur on labels of forward paths originating at any of these edges $\mathsf{b}, \mathsf{d}, \mathsf{e}, \mathsf{f}$ or $\mathsf{g}\}$, therefore $k > 0$ implies that $\alpha_{n_1} \notin \{\mathsf{b}, \mathsf{d}, \mathsf{e}, \mathsf{f}, \mathsf{g}\}$. In addition, the fact that Γ_2' is forward deterministic at c implies that $\alpha_{n_1} \neq \mathsf{c}$ since $\beta_{n_1} = \mathsf{c}$ but $[\alpha]$ and $[\beta]$ differ at n_2 which is to the right of n_1. Thus $k > 0$ contradicts (3.13). We check that $k = 0$ is also inconsistent with $\beta_{n_1} = \mathsf{c}$. If $k = 0$ then $[\alpha]_{[n_1, n_2]} = \left[\begin{smallmatrix}\mathsf{0111}\\ \mathsf{1000}\end{smallmatrix}\right]$, therefore $\alpha_{n_1} \notin \{\mathsf{d}, \mathsf{e}, \mathsf{f}, \mathsf{g}\}$. It follows that $\alpha_{n_1} = \mathsf{b}$ and $\alpha_{n_0} = \mathsf{a}$. In $\Gamma_{(3,1)}$, all paths between a and b consist of edges with label $\left[\begin{smallmatrix}\mathsf{1}\\ \mathsf{0}\end{smallmatrix}\right]$; in fact, $[\alpha]_{(n_1, n_2)} \equiv \left[\begin{smallmatrix}\overline{x}\\ x\end{smallmatrix}\right] = \left[\begin{smallmatrix}\mathsf{1}^m\\ \mathsf{0}^m\end{smallmatrix}\right]$ for some $m > 3$. Then, (**19.1**) implies that $[\beta]_{n_1-1}$ and $[\beta]_{n_1-2}$ are blue edges with the same pair of labels, but this is inconsistent with $\beta_{n_1} = \mathsf{c}$. This completes the proof that (**19.1**) is inconsistent with $\beta_{n_1} \in \{\mathsf{a}, \mathsf{b}, \mathsf{c}\}$, in contradiction with (3.12).

Case **19.2**:
$$\left[\alpha\right]_{[n_0,n_2]} = \begin{array}{c}\overset{n_0\quad n_1\quad n_2}{\left[\begin{smallmatrix}\mathsf{0}\ \overline{x}\ \mathsf{1}\ \overline{y}\ \mathsf{0}\\ \mathsf{1}\ x\ \mathsf{0}\ y\ \mathsf{1}\end{smallmatrix}\right]}\end{array}, \qquad \left[\beta\right]_{[n_0,n_2]} = \begin{array}{c}\overset{n_0\quad n_1\quad n_2}{\left[\begin{smallmatrix}\mathsf{1}\ x\ \mathsf{0}\ y\ \mathsf{0}\\ \mathsf{1}\ x\ \mathsf{1}\ \overline{y}\ \mathsf{1}\end{smallmatrix}\right]}\end{array}.$$

Note that equations (3.12) and (3.13) still apply in this case. Again, we show that the three choices for β_{n_1} lead to contradictions. If $\beta_{n_1} = \mathsf{a}$ then $\left[\begin{smallmatrix}y\\ \overline{y}\end{smallmatrix}\right] = \left[\begin{smallmatrix}\mathsf{111}\\ \mathsf{000}\end{smallmatrix}\right]$ which implies $[\alpha]_{[n_1, n_1+3]} = \left[\begin{smallmatrix}\mathsf{1000}\cdots\\ \mathsf{0111}\cdots\end{smallmatrix}\right]$. This leads to the conclusion that $\alpha_{n_1} = \overline{b}$, and then $\alpha_{n_0} = \mathsf{a}$. At $\overline{\mathsf{b}}$, the graph $\Gamma_{(3,1)}$ is forward deterministic, and it determines

$$\left[\alpha\right]_{[n_1, n_2]} = \begin{bmatrix}\mathsf{100011(011)}^k\mathsf{0}\\ \mathsf{011100(100)}^k\mathsf{1}\end{bmatrix}, \qquad k \geq 0,$$

Then, (**19.2**) gives

$$\left[\beta\right]_{[n_1, n_2]} = \begin{bmatrix}\mathsf{011100(100)}^k\mathsf{0}\\ \mathsf{100011(011)}^k\mathsf{1}\end{bmatrix}, \qquad k \geq 0.$$

But this contradicts $\beta_{n_1} = \mathsf{a}$ as the subsequence $\left[\begin{smallmatrix}\mathsf{011100}\\ \mathsf{100011}\end{smallmatrix}\right]$ never occurs after edge a.

Next we consider $\beta_{n_1} = \mathsf{b}$. In this case there are two possibilities for $[\beta]_{[n_1,\,n_2]}$:

$$\begin{bmatrix}\mathtt{0111(001)}^k\mathtt{0}\\ \mathtt{1000(110)}^k\mathtt{1}\end{bmatrix} \qquad \text{or} \qquad \begin{bmatrix}\mathtt{01110(010)}^k\mathtt{0}\\ \mathtt{10001(101)}^k\mathtt{1}\end{bmatrix},$$

according to whether $\beta_{n_2} = \mathsf{e}$ or $\beta_{n_2} = \mathsf{d}$. The resulting symbols sequence for $[\alpha]_{[n_1,\,n_2]}$ according to (**19.2**) are

$$\begin{bmatrix}\mathtt{1000(110)}^k\mathtt{0}\\ \mathtt{0111(001)}^k\mathtt{1}\end{bmatrix} \qquad \text{or} \qquad \begin{bmatrix}\mathtt{10001(101)}^k\mathtt{0}\\ \mathtt{01110(010)}^k\mathtt{1}\end{bmatrix},$$

respectively. Both of these lead to the conclusion that α_{n_0} is neither b nor c: the subsequence $[\begin{smallmatrix}\mathtt{1000}\\ \mathtt{0111}\end{smallmatrix}]$ does not occur after these edges. By (3.12), $\alpha_{n_0} = \mathsf{a}$. Then $\alpha_{n_1} = \overline{\mathsf{b}}$ as $\overline{\mathsf{b}}$ is the only edge of $\Gamma_{(3,1)}$ where the subsequence $[\begin{smallmatrix}\mathtt{1000}\\ \mathtt{0111}\end{smallmatrix}]$ occurs after edge a. But according to $\Gamma_{(3,1)}$, $\beta_{n_1} = \mathsf{b}$ and $\alpha_{n_1} = \overline{b}$ imply that $\beta_{[n_1,\infty)}$ and $\alpha_{[n_1,\infty)}$ have opposite labels, which is not the case since $[\beta]_{n_2} = [\alpha]_{n_2}$. Thus, $\beta_{n_1} \neq \mathsf{b}$ either.

The last possibility according to (3.12) is that $\beta_{n_1} = \mathsf{c}$. Then, the graph $\Gamma_{(3,1)}$ implies that

$$\Big[\beta\Big]_{[n_1,\,n_2]} = \begin{bmatrix}\mathtt{011(011)}^k\mathtt{0}\\ \mathtt{100(100)}^k\mathtt{1}\end{bmatrix}, \qquad k \geq 0,$$

and by (**19.2**) we get

$$\Big[\alpha\Big]_{[n_1,\,n_2]} = \begin{bmatrix}\mathtt{100(100)}^k\mathtt{0}\\ \mathtt{011(011)}^k\mathtt{1}\end{bmatrix} \qquad k \geq 0.$$

Now, $k > 0$ implies that $\alpha_{n_1} \notin \{\mathsf{b},\mathsf{c},\mathsf{d},\mathsf{e},\mathsf{f},\mathsf{g}\}$, as the sequence $[\begin{smallmatrix}\mathtt{1001}\\ \mathtt{0110}\end{smallmatrix}]$ does not occur on labels of forward paths originating at any of these edges. Thus, $k > 0$ violates (3.13). If $k = 0$ we have $[\alpha]_{[n_1,\,n_2]} = [\begin{smallmatrix}\mathtt{1000}\\ \mathtt{0111}\end{smallmatrix}]$, implying $\alpha_{n_1} \notin \{\mathsf{d},\mathsf{e},\mathsf{f},\mathsf{g}\}$. It follows that $\alpha_{n_0} = \mathsf{a}$ and $\alpha_{n_1} = \overline{\mathsf{b}}$. In $\Gamma_{(3,1)}$, all paths between a and $\overline{\mathsf{b}}$ consist of edges with label $[\begin{smallmatrix}\mathtt{1}\\ \mathtt{0}\end{smallmatrix}]$ and, in fact, $[\alpha]_{(n_1,\,n_2)} \equiv [\begin{smallmatrix}\overline{x}\\ x\end{smallmatrix}] = [\begin{smallmatrix}\mathtt{1}^m\\ \mathtt{0}^m\end{smallmatrix}]$ for some $m > 3$. Then, (**19.2**) implies

$[\beta]_{n_1-1} = [\beta]_{n_1-2}$, which is inconsistent with $\beta_{n_1} = \mathsf{c}$. We conclude that if (**19.2**) holds then $\beta_{n_1} \notin \{\mathsf{a}, \mathsf{b}, \mathsf{c}\}$, in contradiction with (3.12).

Cases **19.3** & **19.4**: As in the proof of the previous lemma, cases **19.3** & **19.4** follow from the analysis of cases **19.1** & **19.2**, respectively.

Case **20.1**: $\Big[\alpha\Big]_{(-\infty,n_2]} = \begin{bmatrix} & & & & n_1 & n_2 \\ \infty & \mathsf{1} & \mathsf{1} & x & \mathsf{1} & \\ \infty & \mathsf{1} & \mathsf{0} & \overline{x} & \mathsf{0} & \end{bmatrix}$, $\Big[\beta\Big]_{(-\infty,n_2]} = \begin{bmatrix} & & & & n_1 & n_2 \\ \infty & \mathsf{1} & \mathsf{1} & x & \mathsf{0} & \\ \infty & \mathsf{0} & \mathsf{0} & \overline{x} & \mathsf{1} & \end{bmatrix}$.

Observe in figure-3.13 that the only paths which produce the constant left-infinite sequence $\left[\begin{smallmatrix}\infty\mathsf{0}\\ \infty\mathsf{1}\end{smallmatrix}\right]$ are those that remain in edge h when followed backwards. Hence $\beta_k = \mathsf{h}$ for all $k < n$ for some $n \leq n_1$. Also, it must be that $\alpha_{n_1} = \overline{\mathsf{a}}$ because no other edge in Γ_2' has label $\left[\begin{smallmatrix}\mathsf{1}\\ \mathsf{0}\end{smallmatrix}\right]$ and can be preceded exclusively by edges with label $\left[\begin{smallmatrix}\mathsf{1}\\ \mathsf{1}\end{smallmatrix}\right]$. It follows that $\left[\begin{smallmatrix}x\\ \overline{x}\end{smallmatrix}\right]$ in (**20.1**) begins with $\left[\begin{smallmatrix}\mathsf{000}\cdots\\ \mathsf{111}\cdots\end{smallmatrix}\right]$ and therefore $\beta_{[n_1,n_1+3]} = \left[\begin{smallmatrix}\mathsf{1000}\\ \mathsf{0111}\end{smallmatrix}\right]$. From this we must conclude that $\beta_{n_1} = \overline{\mathsf{b}}$, because $\overline{\mathsf{b}}$ is the only edge in $\Gamma_{(3,1)}$ where the subsequence $\left[\begin{smallmatrix}\mathsf{1000}\\ \mathsf{0111}\end{smallmatrix}\right]$ occurs for forward paths that originate from edge h. At $\overline{\mathsf{b}}$ the graph is forward deterministic, giving

$$\Big[\beta\Big]_{[n_1,n_2]} = \begin{bmatrix} \mathsf{1\,0\,0\,0\,(1\,1\,0)^k\,1\,1\,0} \\ \mathsf{0\,1\,1\,1\,(0\,0\,1)^k\,0\,0\,1} \end{bmatrix} \tag{3.15}$$

for $k \geq 0$. This specifies x in (**20.1**), to yield

$$\Big[\alpha\Big]_{[n_1,n_2]} = \begin{bmatrix} \mathsf{1\,0\,0\,0\,(1\,1\,0)^k\,1\,1\,1} \\ \mathsf{0\,1\,1\,1\,(0\,0\,1)^k\,0\,0\,0} \end{bmatrix} \tag{3.16}$$

However, the subsequence $\left[\begin{smallmatrix}\mathsf{100011}\\ \mathsf{011100}\end{smallmatrix}\right]$ does not occur on labels of any forward path originating at $\overline{\mathsf{a}}$ in $\Gamma_{(3,1)}$; this contradicts $\alpha_{n_1} = \overline{\mathsf{a}}$.

Case **20.2**: $\Big[\alpha\Big]_{(-\infty,n_2]} = \begin{bmatrix} \overset{\infty}{\infty}\mathtt{1}\ \overset{n_1}{\mathtt{0}}\ \overset{}{\overline{x}}\ \overset{n_2}{\mathtt{1}} \\ \infty\mathtt{0}\ \mathtt{1}\ x\ \mathtt{0} \end{bmatrix}, \qquad \Big[\beta\Big]_{(-\infty,n_2]} = \begin{bmatrix} \overset{\infty}{\infty}\mathtt{0}\ \overset{n_1}{\mathtt{0}}\ \overset{}{\overline{x}}\ \overset{n_2}{\mathtt{0}} \\ \infty\mathtt{0}\ \mathtt{1}\ x\ \mathtt{1} \end{bmatrix}.$

From $[\beta]_{(-\infty,n_1]} = \left[\begin{smallmatrix}\infty\mathtt{00}\\ \infty\mathtt{01}\end{smallmatrix}\right]$ it follows that $\beta_{n_1} = \mathsf{a}$. Therefore $\left[\begin{smallmatrix}\overline{x}\\ x\end{smallmatrix}\right]$ begins with $\left[\begin{smallmatrix}\mathtt{111}\\ \mathtt{000}\end{smallmatrix}\right]$. Then, from $[\alpha]_{(-\infty,n_1+2]} = \left[\begin{smallmatrix}\infty\mathtt{10111}\\ \infty\mathtt{01000}\end{smallmatrix}\right]$ we conclude $\alpha_{n_1} = \mathsf{b}$. At b the graph $\Gamma_{(3,1)}$ is forward deterministic, hence the labels of $\alpha_{[n_1,n_2]}$ specify x. Then, (**20.2**) implies

$$\Big[\beta\Big]_{[n_1,n_2]} = \begin{bmatrix} \mathtt{0\,1\,1\,1\,(0\,0\,1)^k\,0\,0\,0} \\ \mathtt{1\,0\,0\,0\,(1\,1\,0)^k\,1\,1\,1} \end{bmatrix}. \tag{3.17}$$

However, the subsequence $\left[\begin{smallmatrix}\mathtt{011100}\\ \mathtt{100011}\end{smallmatrix}\right]$ does not occur on labels of any forward path originating at a in $\Gamma_{(3,1)}$; this contradicts $\beta_{n_1} = \mathsf{a}$.

Case **20.3**: $\Big[\alpha\Big]_{(-\infty,n_2]} = \begin{bmatrix} \overset{\infty}{\infty}\mathtt{1}\ \overset{n_1}{\mathtt{1}}\ \overset{}{\overline{x}}\ \overset{n_2}{\mathtt{1}} \\ \infty\mathtt{1}\ \mathtt{0}\ x\ \mathtt{0} \end{bmatrix}, \qquad \Big[\beta\Big]_{(-\infty,n_2]} = \begin{bmatrix} \overset{\infty}{\infty}\mathtt{1}\ \overset{n_1}{\mathtt{0}}\ \overset{}{x}\ \overset{n_2}{\mathtt{1}} \\ \infty\mathtt{0}\ \mathtt{1}\ \overline{x}\ \mathtt{0} \end{bmatrix}.$

From $[\alpha]_{(-\infty,n_1]} = \left[\begin{smallmatrix}\infty\mathtt{11}\\ \infty\mathtt{10}\end{smallmatrix}\right]$ it follows that $\alpha_{n_1} = \mathsf{a}$. Therefore $\left[\begin{smallmatrix}\overline{x}\\ x\end{smallmatrix}\right]$ begins with $\left[\begin{smallmatrix}\mathtt{000}\\ \mathtt{111}\end{smallmatrix}\right]$ hence $[\beta]_{(-\infty,n_1+2]} = \left[\begin{smallmatrix}\infty\mathtt{10111}\\ \infty\mathtt{01000}\end{smallmatrix}\right]$, which leads to the conclusion that $\beta_{n_1} = \mathsf{b}$. At b the graph $\Gamma_{(3,1)}$ is forward deterministic, giving

$$\Big[\beta\Big]_{[n_1,n_2]} = \begin{bmatrix} \mathtt{0\,1\,1\,1\,(0\,0\,1)^k\,0\,0\,1} \\ \mathtt{1\,0\,0\,0\,(1\,1\,0)^k\,1\,1\,0} \end{bmatrix} \tag{3.18}$$

for $k \geq 0$. This specifies x in (**20.3**), resulting in

$$\Big[\alpha\Big]_{[n_1,n_2]} = \begin{bmatrix} \mathtt{1\,0\,0\,0\,(1\,0\,0)^k\,1\,1\,1} \\ \mathtt{0\,1\,1\,1\,(0\,1\,1)^k\,0\,0\,0} \end{bmatrix} \tag{3.19}$$

But this is equation (3.16), which contradicts $\alpha_{n_1} = \overline{\mathsf{a}}$.

Case **20.4**: $\Big[\alpha\Big]_{(-\infty,n_2]} = \begin{bmatrix} \overset{\infty}{\infty}\mathtt{1}\ \overset{n_1}{\mathtt{1}}\ \overset{}{\overline{x}}\ \overset{n_2}{\mathtt{0}} \\ \infty\mathtt{0}\ \mathtt{0}\ x\ \mathtt{1} \end{bmatrix}, \qquad \Big[\beta\Big]_{(-\infty,n_2]} = \begin{bmatrix} \overset{\infty}{\infty}\mathtt{0}\ \overset{n_1}{\mathtt{0}}\ \overset{}{x}\ \overset{n_2}{\mathtt{0}} \\ \infty\mathtt{0}\ \mathtt{1}\ \overline{x}\ \mathtt{1} \end{bmatrix}.$

From $[\beta]_{(-\infty,n_1]} = [\,{}^{\infty}_{\infty}{}^{\mathsf{00}}_{\mathsf{01}}\,]$ it follows that $\beta_{n_1} = \mathsf{a}$. Therefore $[\,{}^{\overline{x}}_{x}\,]$ begins with $[\,{}^{\mathsf{111}}_{\mathsf{000}}\,]$. Then $[\alpha]_{(-\infty,n_1+2]} = [\,{}^{\infty}_{\infty}{}^{\mathsf{11000}}_{\mathsf{00111}}\,]$ which leads to $\alpha_{n_1} = \overline{\mathsf{b}}$. At $\overline{\mathsf{b}}$ the graph $\Gamma_{(3,1)}$ is forward deterministic, hence the labels of $\alpha_{[n_1,n_2]}$ specify x in (**20.2**) to give

$$\Big[\beta\Big]_{[n_1,n_2]} = \begin{bmatrix} \mathsf{0\,1\,1\,1\,(0\,0\,1)^k\,0\,0\,0} \\ \mathsf{1\,0\,0\,0\,(1\,1\,0)^k\,1\,1\,1} \end{bmatrix}.$$

This is equation (3.17), which contradicts $\beta_{n_1} = \mathsf{a}$. □

Chapter 4

On the Combinatorial Structure of a Region of Real Parameter Space

4.1 Introduction.

In this section we take a experimental approach to examining the combinatorics of Hénon mappings. More specifically, we examine how the unstable manifold pictures at the β-fixed point of $f_{a,c}$ vary with the mapping, as a way of detecting by inspection changes in the identifications of external rays.

Recall that for a given Hénon mapping, the unstable manifold picture at p, or W^u_p picture, refers to the image of the partition of $\mathbf{C}$ into $\phi_p^{-1}(K_p^+)$ and its complement, $\phi_p^{-1}(U_p^+)$, where where ϕ_p is the natural parameterization of $W^u(p)$. In this chapter p will always be the fixed point with largest eigenvalues, which we call the β-fixed point. The discussion will involve mappings at various parameter values so we will

also use the notation $W^u_{a,c}$ to refer to the W^u_β picture of the mapping $f_{a,c}$.

The experiment will consist of "scanning" parameter space by observing how $W^u_{a,c}$ changes as parameter values are incremented along a line joining two points in parameter space.

We want to apply these experiments in a systematic way to gain intuition about the structure of parameter space. A strategy we find natural to start with is to consider first Hénon mappings which are perturbations of a hyperbolic quadratic polynomial P_c since then we know from that the set K^+_β in the W^u_β picture will "look" as the the filled Julia set of P_c at the β-fixed point of the polynomial. More specifically, we know from section §3.2 that the graph describing the identifications of the external rays for these mappings is the same as the graph describing the identifications of rays for P_c, and we can construct it explicitly at least for c in a real hyperbolic component of $\mathcal{M}$. In addition, the structural stability of these mappings ensures that if the initial changes in the parameters are small enough then the initial changes in the W^u_β picture will be qualitative only, not topological. Thus, the landing point of the rays will vary continuously with the parameters, at least for small enough changes in the initial parameter values. Determining what "small enough" should be for a particular mapping forms part of the experiment, since for any given c inside a hyperbolic component of the Mandelbrot set, it is not known how large can we take $|a|$ and still have $f_{a,c} \approx \varprojlim P_c$. One of our objectives, therefore, will be to address this question experimentally, using stability of the W^u_β pictures as an in indication of hyperbolicity.

We expect that the largest hyperbolic components of $\mathcal{M}$ will yield the more

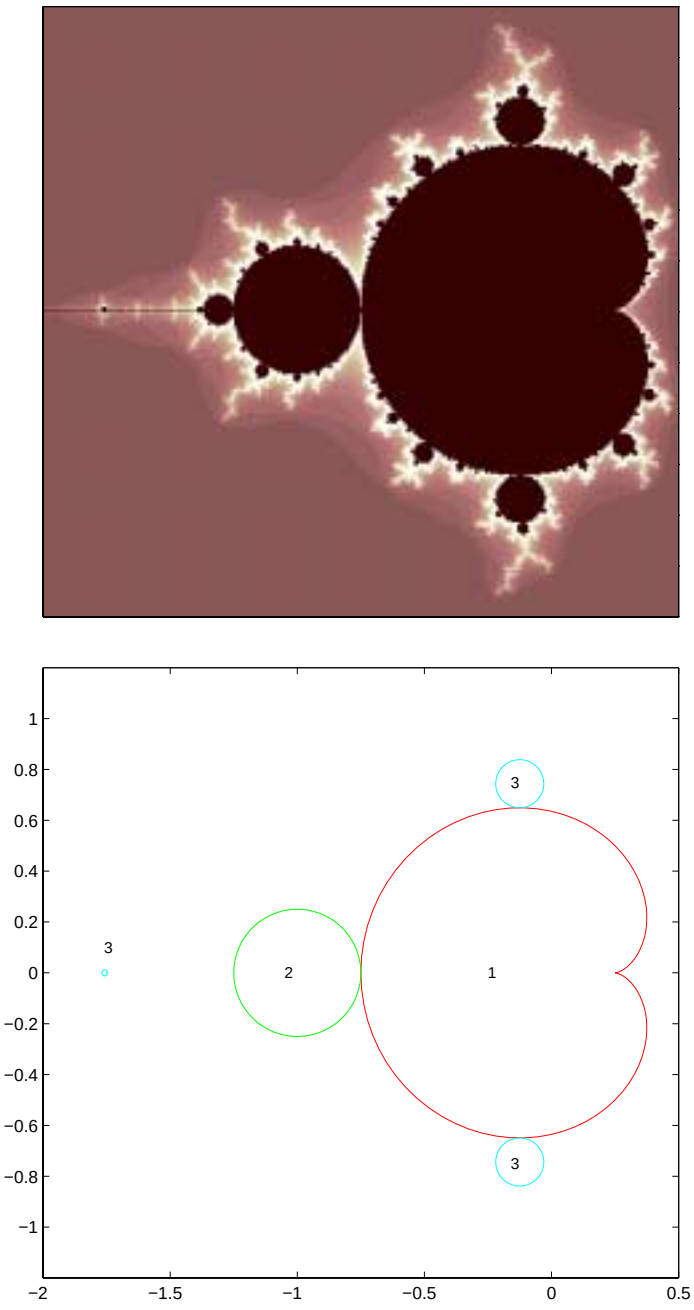

Figure 4.1: $\mathcal{M}$ and its hyperbolic components of period 1, 2 and 3.

stable Hénon mappings $f_{0,c}$, and we want to start with mappings having the simplest combinatorics. Thus, we will focus on the hyperbolic components of low period. The hyperbolic components of the Mandelbrot set can be characterized as the set of parameter values for which the polynomial P_c has a sink of a specific period, also called the period-n sink locus. Figure 4.1 shows the sink loci up to period three. The sink loci for P_c coincide with the sink-loci for the Hénon map $f_{a,c}$ in the plane $\{a = 0\}$. For small, non-zero, values of a the sink loci of $f_{a,c}$ in the plane $\{a = \text{constant}\}$ appear to form "deformed" Mandelbrot sets, as shown in figure 4.2. In particular the main cardioid and its attached components seem to persists for $0 < a < .3$, but the period-three "island" located near $c = -1.75$ in the plane $\{a = 0\}$, drifts to the right and intersects the other loci as the value of a increases. This sink locus lies at the center of the period-2 locus in the plane $\{a = 0.2\}$ and just inside the fixed-sink locus in the plane $\{a = 0.3\}$. Other so called satellite components of $\mathcal{M}$ also drift as the value of a is increased, and they intersect other components at different $\{a =\text{const}\}$ planes; but components in the "main body" of $\mathcal{M}$ appear to maintain their relative position [1]. Parameter values that belong to more than one sink locus are particularly interesting because they provide examples of mappings whose dynamics must be distinct from those of polynomials in the plane, which have at most one sink. Figure 4.3 shows how these sink loci intersect in parameter space with $c \in \mathbf{C}$ and $a \in \mathbf{R}$, and figure 4.4 shows the restriction of these loci to $\mathbf{R}^2$.

[1] Although not shown in figure 4.2 we have also observed this behavior for the components of period four.

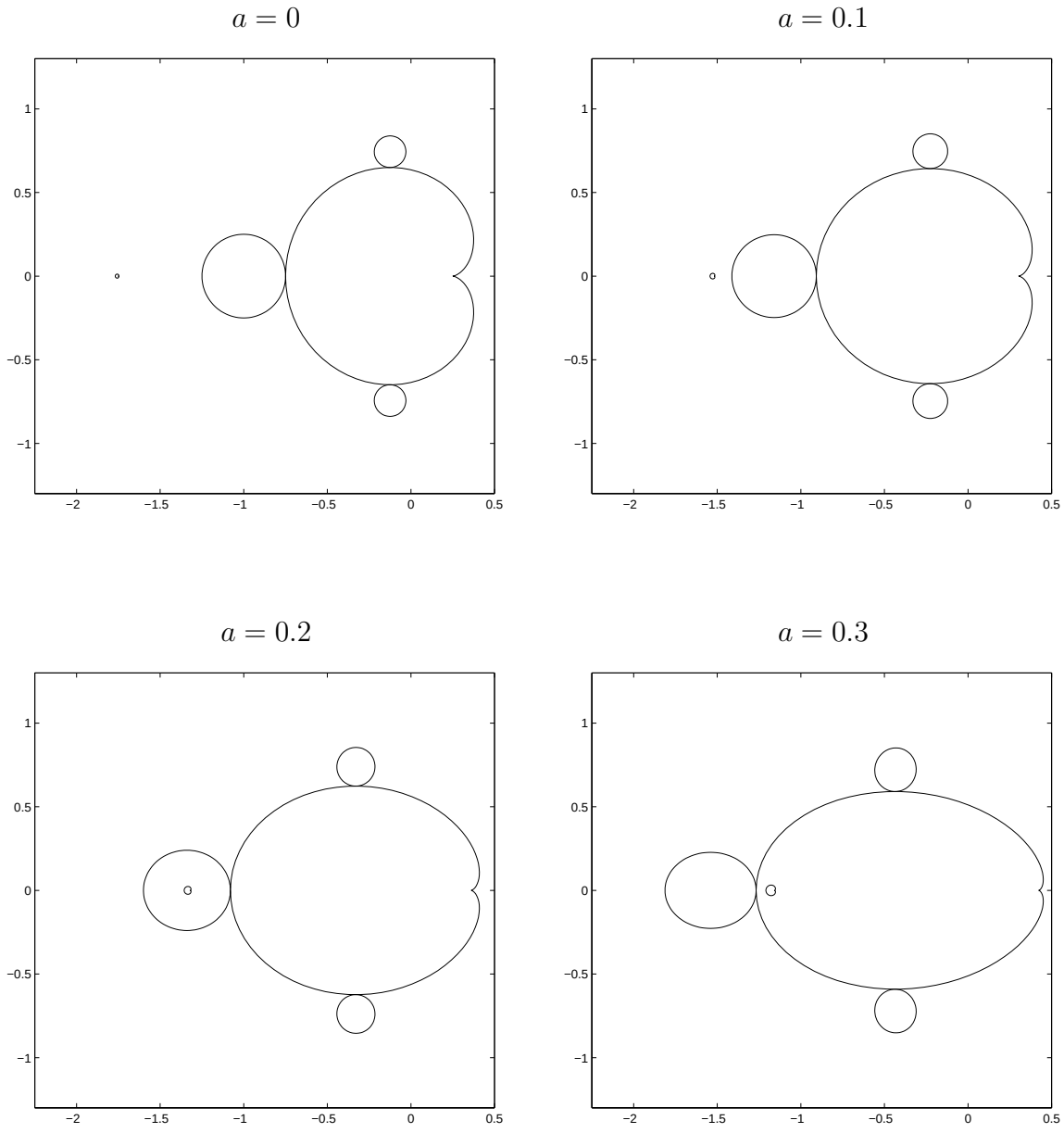

Figure 4.2: Sink loci of $f_{a,c}$ in c-plane for small values of a.

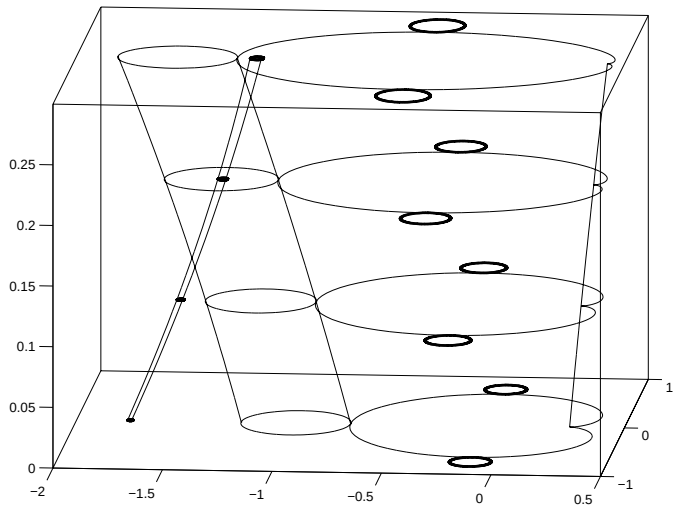

Figure 4.3: Sink loci in $\mathbf{C} \times \mathbf{R}$.

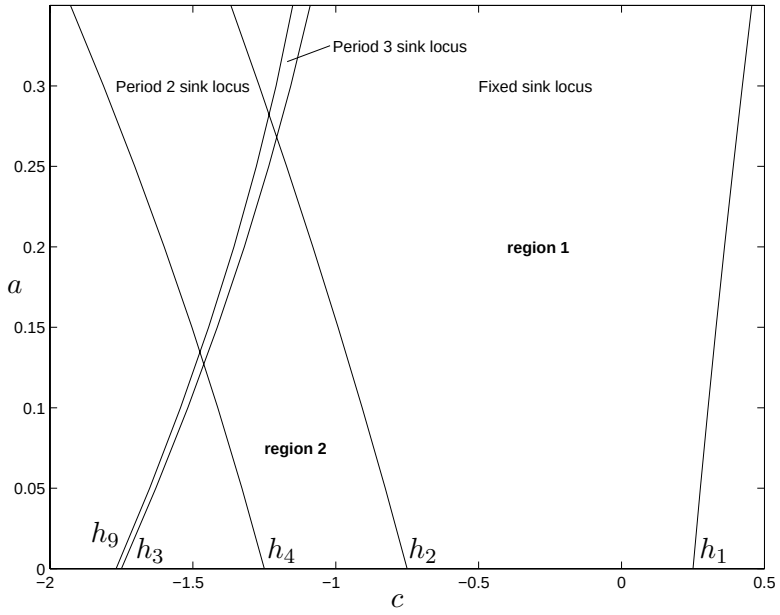

Figure 4.4: Sink loci in $\mathbf{R} \times \mathbf{R}$.

The boundaries between the sink loci in $\mathbf{R}^2$ are curves whose endpoints at the level $a = 0$ are root-points of hyperbolic components of the Mandelbrot set, hence parabolic bifurcation points [DH, Br]. Let these root-points be denoted by r_i where the subscript indicates the period of the hyperbolic component. In figure 4.4 we have labeled as h_i the curve ending at r_i. Hence, the fixed-sink locus in $\mathbf{R}^2$ is bounded by h_1 and h_2, the period-two sink locus by h_2 and h_4, and the period-3 locus is the thin strip between h_3 and h_9.

When $f_{a,c} \approx \varprojlim P_{c'}$ the picture of K^+_β has the same topology as the picture of the filled-in Julia set of the polynomial $P_{c'}$ at its β-fixed point. Thus, for each value of c between r_2 and r_1 there is some ε such that for $a < \varepsilon$ the W^u_β picture of $f_{a,c}$ is topological the same as that of P_0: without any identifications of external rays. Similarly, for each $c \in (r_4, r_2)$ there is a small enough $|a|$ such that $f_{a,c} \approx \varprojlim P_{-1}$ and rays are in W^u_β are identified as given by the graph Γ_2 of Example-3, section §3.1. On the other hand, the intersection of the period-3 sink locus with the period-2 sink locus (or with the fixed-sink locus) consists of parameters where $f_{a,c} \not\approx \varprojlim P$ for any polynomial P. This makes the region inside the period-2 locus and below h_3 an interesting window in parameter space in which to concentrate out experiments in order to answer, for instance, whether or not the polynomial combinatorics from the level $a = 0$ extend to h_3. We have labeled this region as Region 2 in figure 4.4, and Region 1 will be the adjacent region inside the fixed-sink locus and below h_3, where we begin exploring the same question.

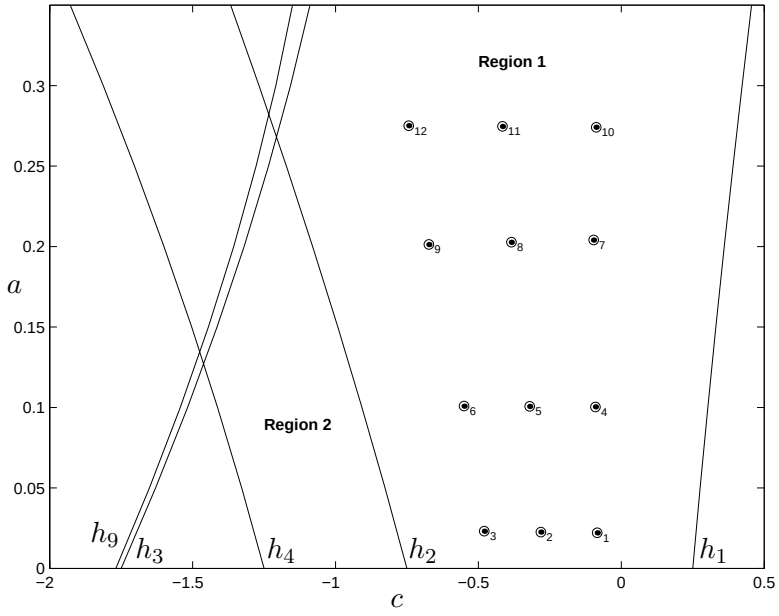

Figure 4.5: Some selected parameter values in Region 1.

4.1.1 Scanning Parameter Space.

Figure 4.5 show four sample scans with twelve selected parameter values (circled) distributed throughout region-1. The resulting W^u_β picture at each of the twelve selected points is shown in figure 4.6. Each of these images indicates that $K^+_\beta - J$ is a single component; distinct rays are not identified under the landing map. We have conducted numerous other scans through this region all of which produce pictures with the same trivial combinatorics. Closer to h_2 and h_3 the cusps in K^+_β become more pronounced, but we still find that no identifications take place inside Region 1. This suggests the following statement which we call a conjecture since it is based on empirical evidence.

Conjecture 2. *For parameter values* (a, c) *inside the fixed sink-locus in* $\mathbf{R}^2$ *below*

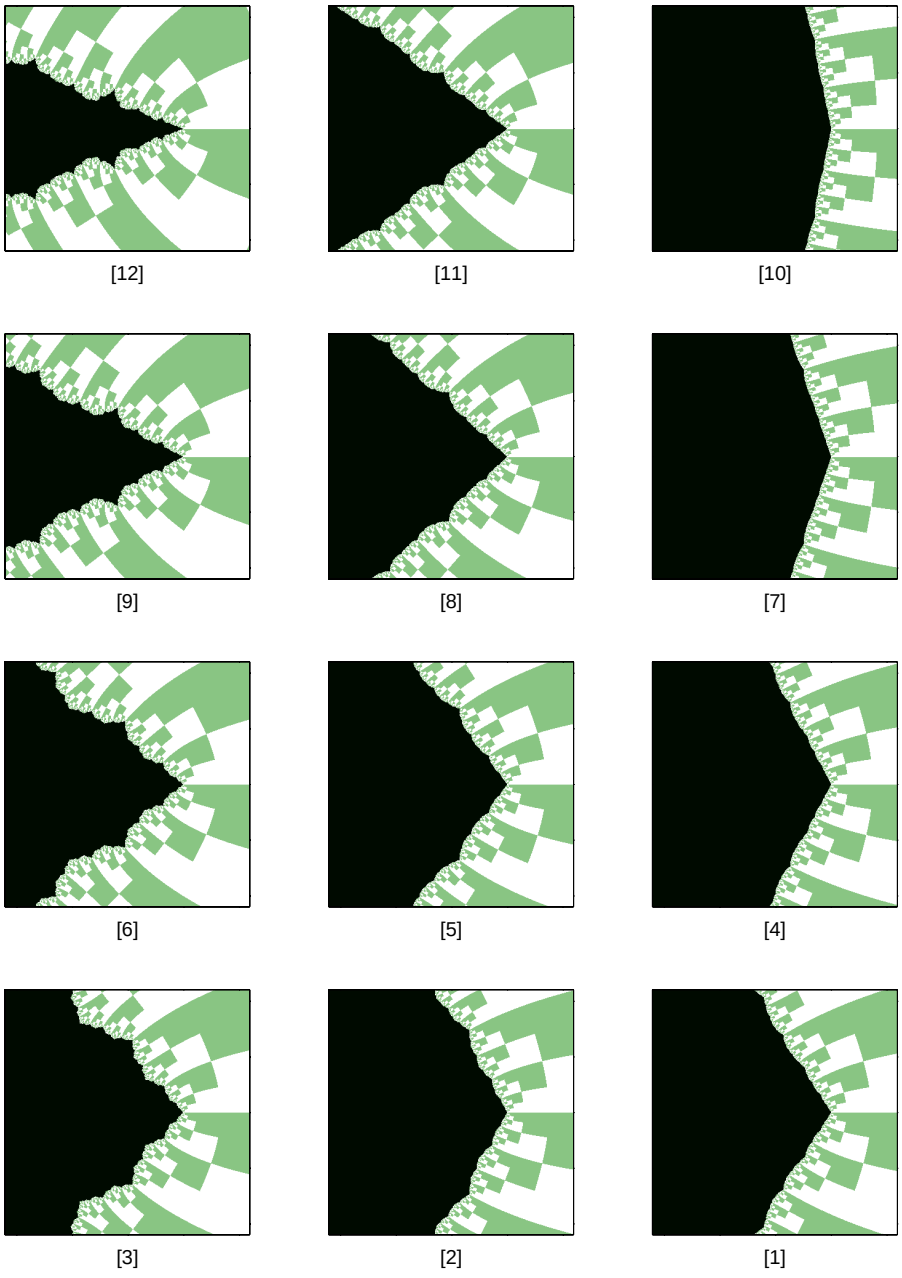

Figure 4.6: W^u_β pictures for parameter values of figure 4.5

h_3 and with $0 \leq a \leq 0.35$, the Hénon map satisfies $f_{a,c} \approx \varprojlim P_0$.

REMARK. Implicit in this conjecture is the statement that no other sink-locus intersects the fixed sink locus in this region.

We now consider the same experiments in Region 2. We will be referring to the parameter values shown in figure 4.7, and to their corresponding W^u_β pictures shown in figure 4.8.

As it was the case in Region 1, we find that within Region 2 the combinatorics determined by the one-dimensional map P_c appear to survive for small values a independently of c.

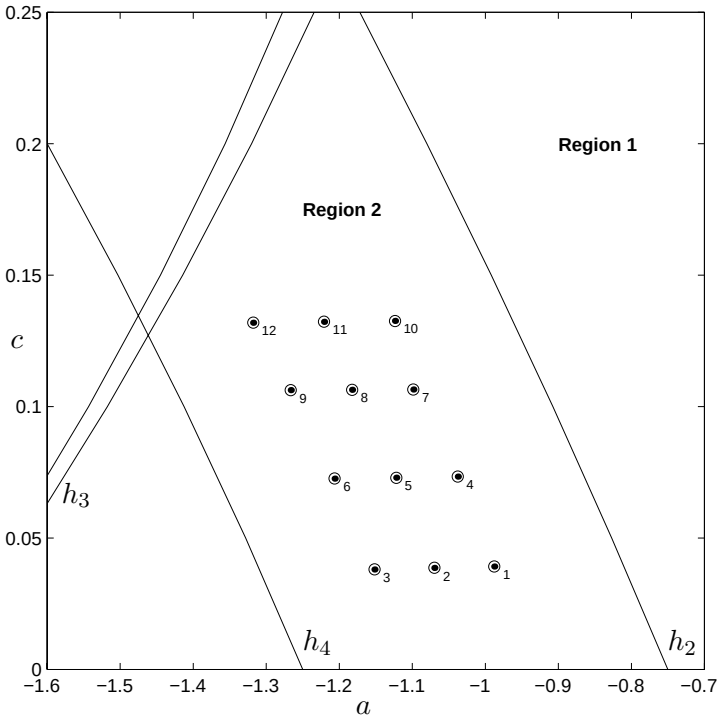

Figure 4.7: Selected parameter values through Region 2.1

Conjecture 3. *For parameter values* (a, c) *inside the period-two sink locus in* $\mathbf{R}^2$ *and such that* $0 \leq a \leq 0.05$*, the Hénon map satisfies* $f_{a,c} \approx \varprojlim P_{-1}$.

This is illustrated in two bottom rows of the array in figure 4.8 (compare with figure 3.4). In fact, the W^u_β pictures in a scan of Region 2 at $a = 0.01$ and those at the polynomial level $a = 0$ seem identical. However, near the middle part of Region 2 the W^u_β pictures reveal topological changes: at least two identifications are different for a near 0.14, say, than they are for $a < 0.5$ (this is emphasized in figure 4.8 by the rays drawn in the W^u_β pictures numbered 2 and 11). Specifically, $\mathsf{A} = {}^\infty\mathtt{0011}(\mathtt{01})^\infty$ and $\mathsf{B} = {}^\infty\mathtt{0100}(\mathtt{10})^\infty$ are identified with each other for small values of a, as are their complex conjugate pairs, $\overline{\mathsf{A}} = {}^\infty\mathtt{1011}(\mathtt{01})^\infty$ and $\overline{\mathsf{B}} = {}^\infty\mathtt{1100}(\mathtt{10})^\infty$. But when a has reached the value 0.14 these four rays have changed partners and each ray has become identified with its respective conjugate ray. Figure 4.8-8 is suggestive of how the rays in the identifications $\mathsf{A} \sim \mathsf{B}$ and $\overline{\mathsf{A}} \sim \overline{\mathsf{B}}$ change partners as parameters are varied (say from $a = 0.05$ towards h_3, for concreteness): the landing points of the two identifications approach the real axis in the W^u_β picture in a continuous manner with increasing a, (giving the appearance of squeezing the component of K^+ containing the landing points at its boundary). As a is increased further the the four rays appear to meet on the real axis pinching K^+, and then the previously identified rays drift apart along $\mathbf{R} \subset W^u_\beta$, now identified with their conjugate rays. This process is shown in the sequence of W^u_β pictures in figure 4.9 corresponding to nine parameter values between those of figure 4.8-5 and 4.8-11. Figure 4.10 shows the approximate location in parameter space where the bifurcation occurs.

A parameter value at which a pair of identified rays switch partners will be called

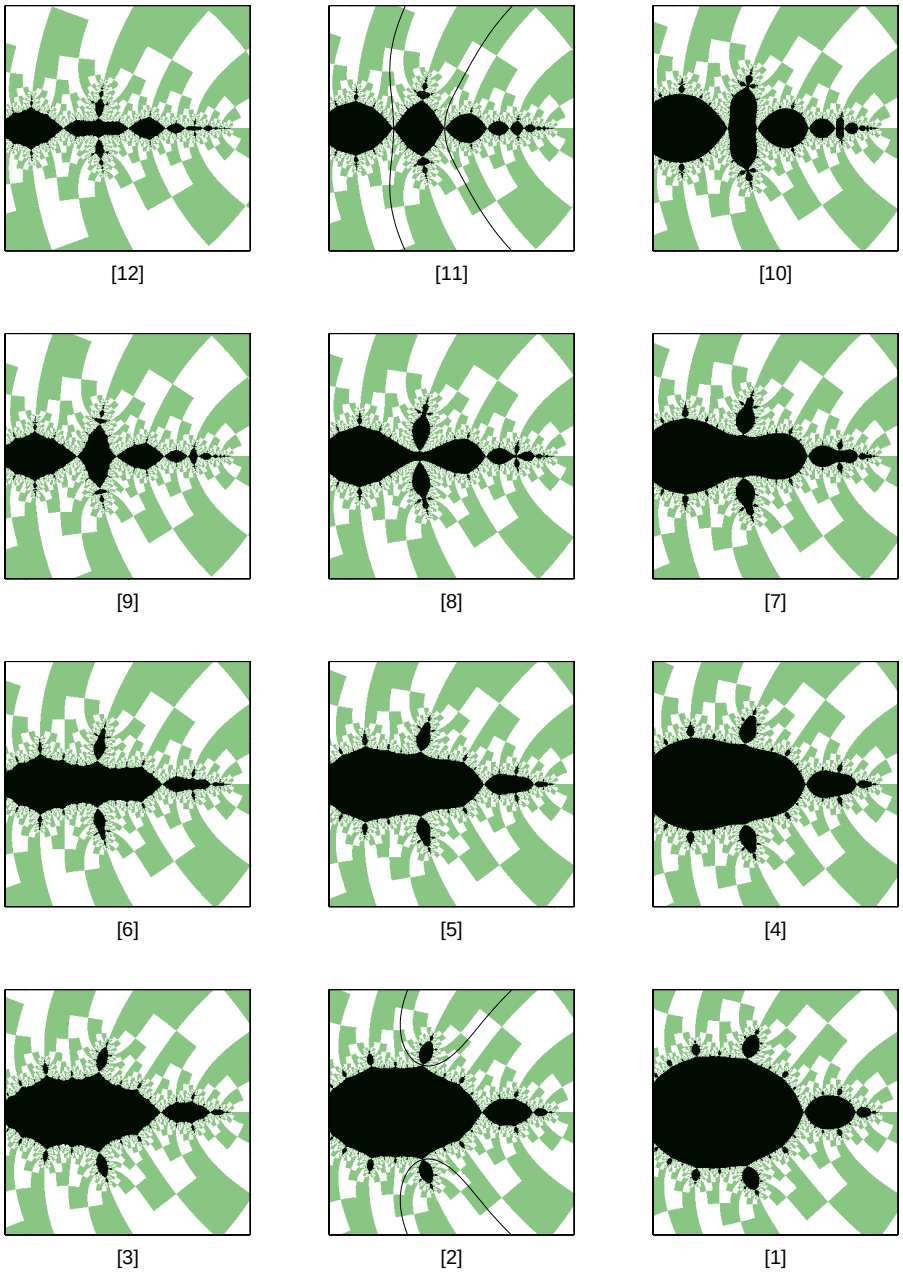

Figure 4.8: W^u_β pictures for the parameters of figure 4.7.

a "bifurcation point" in parameter space.

The bifurcation illustrated in figures 4.9 appears as the first prominent change in the identifications of external rays when the parameters are varied within Region 2 from $a = 0$ towards h_3. At parameter values close to those where this bifurcation occurs we also observe other pairs of identified rays which approach each other and appear to meet and change partners at the small-scale limbs of $K_\beta^+ - J$. Figure 4.11 shows an example.

We will say a bifurcation is real or complex according to whether or not it involves pairs of complex conjugate rays. Thus, the bifurcation of figure 4.10 is a real bifurcation but that of figure 4.11 is complex. The rays corresponding to a real bifurcation meet on $\mathbf{R}$ in the W_β^u-picture. At end of §2.5 we pointed out that rays landing on $\mathbf{R}$ in the W_β^u-picture for $c = -1$ and $a = .01$ correspond to point where $W^u(\beta)$ and $W^s(p')$ intersect in $\mathbf{R}^2$, with p' being the other fixed point of f. Thus the real bifurcation corresponds to a tangency of these unstable manifolds in $\mathbf{R}^2$.

When f is hyperbolic $\boldsymbol{\psi}$ is injective on stable manifolds (§2.4.1). Thus, at parameter values corresponding to a real bifurcation $f_{a,c}$ is not hyperbolic. It is interesting to ask whether the four rays changing partners in a complex bifurcation actually meet. In 4.4 we discuss a specific case when they do not.

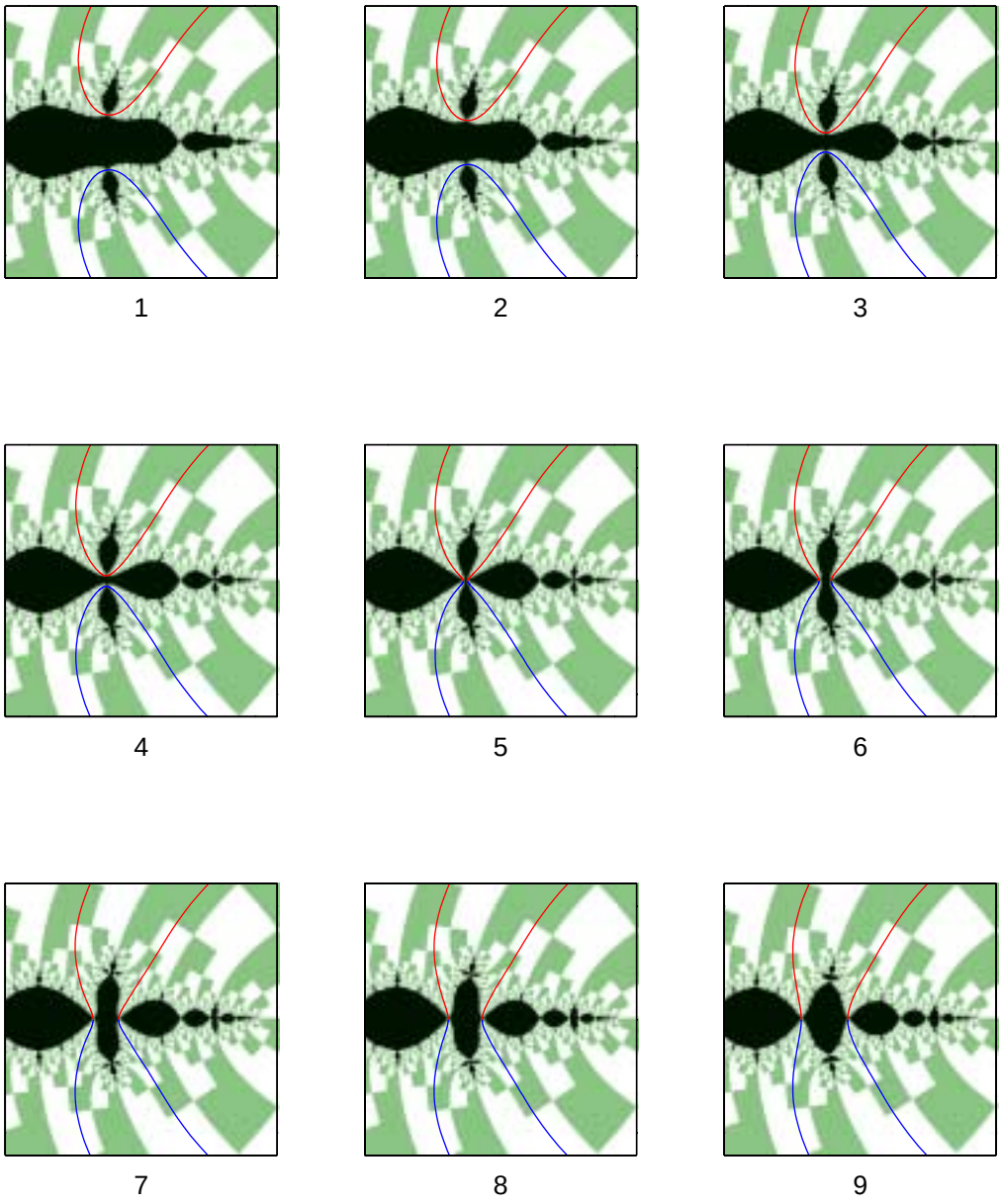

Figure 4.9: Sequence of W^u_β pictures illustrating how two pairs of identified rays change partners.

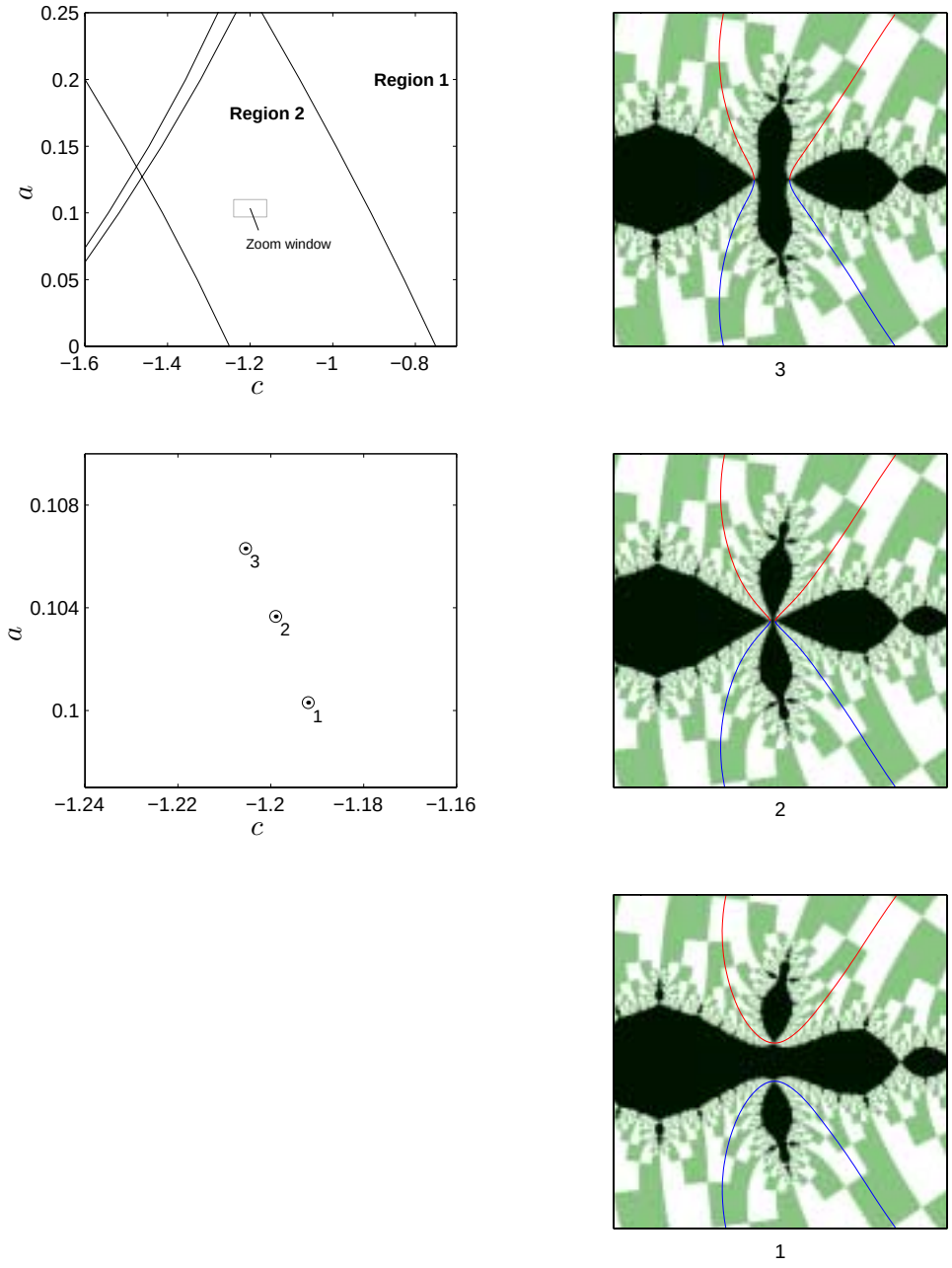

Figure 4.10: Parameter values near the first bifurcation in Region 2.

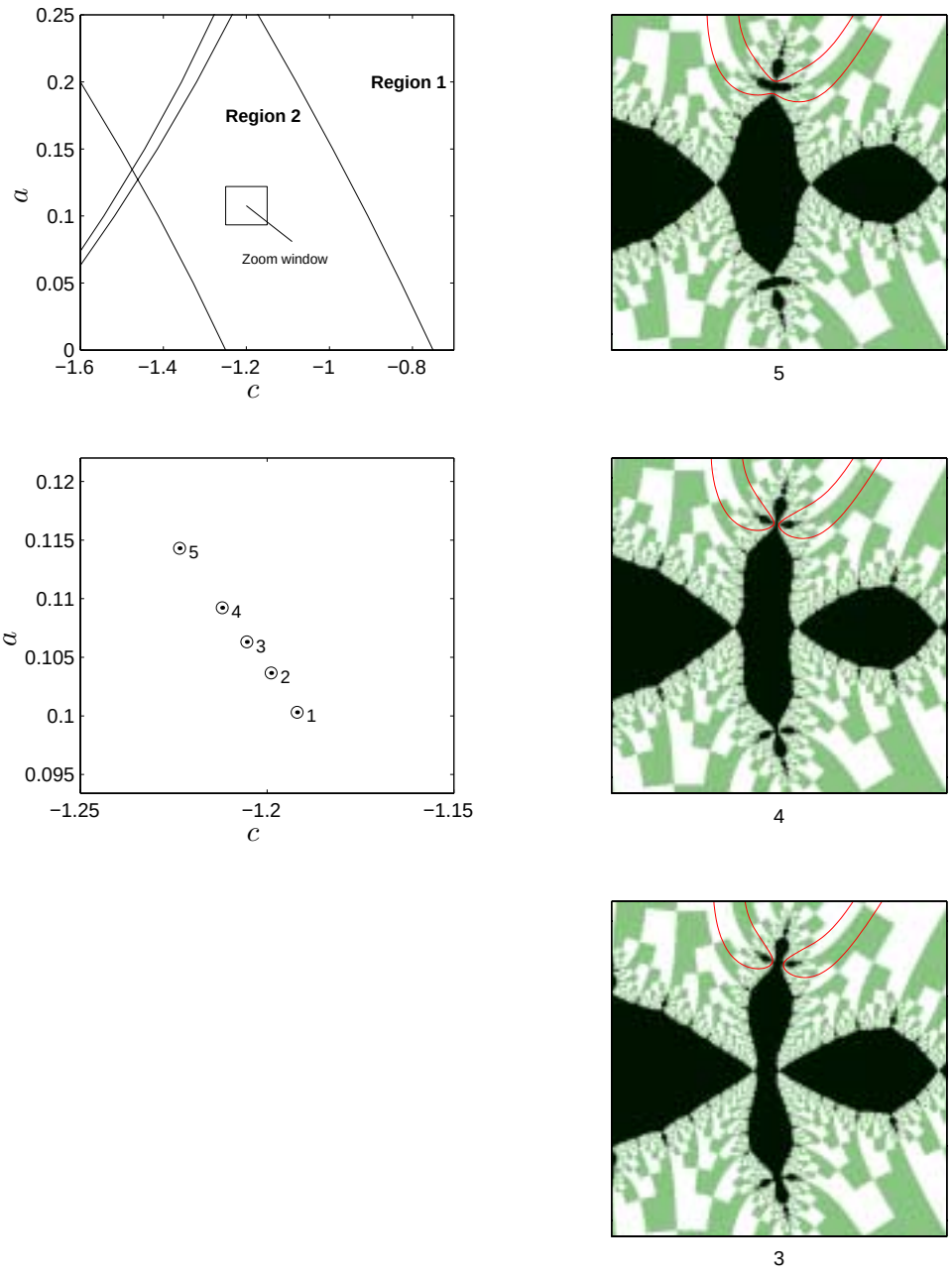

Figure 4.11: A second bifurcations in Region 2 (cf. figure 4.10). Since the rays do not meet on $\mathbf{R}$ we call this a complex bifurcation.

Since the real bifurcations correspond to tangencies we expect these bifurcation points in parameter space will have co-dimension one. In fact, even these observational experiments reveal that the parameter values corresponding to the bifurcation of figure 4.9 lie on a "line" that cuts through Region 2. However, these type of experiments only produce a rough approximation to the location of the bifurcation points, and it is impractical to use this method to locate many such points since obtaining each W^u_β picture is computationally intensive. In the next section we address the problem of how to locate these bifurcations more accurately and efficiently.

4.2 Locating bifurcations in parameter space.

The experiments of the previous section revealed that there are parameter values in Region 2 at which pairs of identified rays change partners, and suggested that these bifurcation points could have co-dimension one, forming curves in $\mathbf{R}^2$. In this section we will move from observations of unstable manifold pictures to a computational way of finding these bifurcations in parameter space.

Let I be a line segment in parameter space containing only one bifurcation point (a_*, c_*) for a bifurcation involving the identifications $\{\mathsf{A} \sim \mathsf{B},\ \mathsf{A}' \sim \mathsf{B}'\}$ changing to $\{\mathsf{A} \sim \mathsf{A}',\ \mathsf{B}' \sim \mathsf{B}'\}$. Using a binary-search algorithm on I one obtains a sequence of points converging to (a_*, c_*). In order for the computer to perform this search automatically it needs to be able to determine whether the rays are identified as $\mathsf{A} \sim \mathsf{A}'$ and $\mathsf{B} \sim \mathsf{B}'$, or as $\mathsf{A} \sim \mathsf{B}$ and $\mathsf{A}' \sim \mathsf{B}'$ at parameter values near (a_*, c_*).

The problem of distinguishing between the two possibilities can be solved by the

computer if given parameter value it can determine the landing point of each ray. We have implemented a program that accomplishes this last task, in effect enabling the computer to check with high precision whether or not two rays are identified for specific parameter values (see appendix). With this tool we can use the computer to locate, up to a specified accuracy, curves of bifurcation points in real parameter space by using a simple binary-search algorithm in the plane.

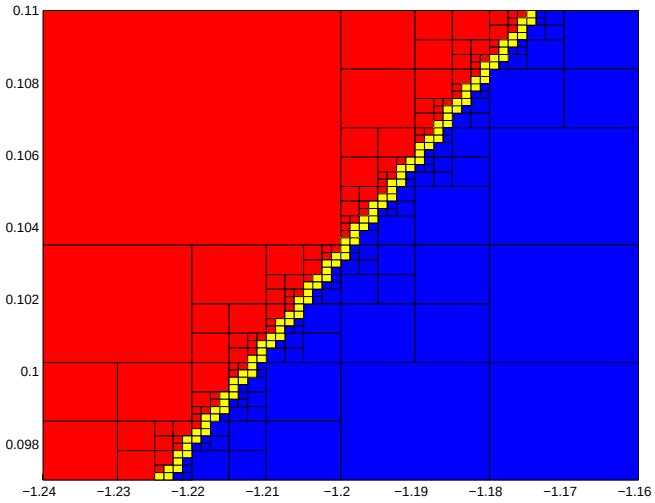

Figure 4.12:

Given a neighborhood B_δ of a bifurcation point (a_*, c_*) the computer can produce an ε-neighborhood of the bifurcation curve inside B_δ, in principle, by sampling a fine grid over the neighborhood (say with cells of diagonal length less than $\varepsilon/2$), and forming a list of grid cells selected according to the following "four-corners" test: if the identifications involved are the same for the parameter values at the four corners of the cell, then conclude that the cell contains no bifurcation points, otherwise add the cell to the list. This works if ε is small enough so that the

curve intersects the side of each cell at most once. If B_δ itself is a small window in parameter space where the curve just "cuts through" without too much turning, then a two-dimensional binary search algorithm can be used to produce the desired list: recursively subdivide the window into four by connecting the midpoints of each edge; the the recursion terminates if a window does not contain a bifurcation point according to the four-corners test, in which case it is discarded, or it has become smaller in size than the allowed tolerance, in which case it is added to the list. For example, figure 4.12 illustrates some intermediate steps of this procedure as used to obtain a neighborhood of the bifurcations shown in figure 4.10, starting with the small zoom-window in that same figure; showing in blue are the boxes where the computer found $\{\mathsf{A} \sim \mathsf{B},\ \overline{\mathsf{A}} \sim \overline{\mathsf{B}}\}$, in red those where $\{\mathsf{A} \sim \overline{\mathsf{A}},\ \mathsf{B} \sim \overline{\mathsf{B}}\}$, and in yellow the cells containing the bifurcation curve. After a initial segment of the bifurcation curve has been found to the desired accuracy, the computer can extend the curve by placing an adjacent test-window at the endpoints and repeating the search. Besides providing control on the accuracy with which we know the curve, one advantage of this method is that it does not make many assumptions about the global shape of the curve its trying to locate: if needed, the local curvature of the found part of the curve can be estimated and the size of the adjacent B_δ can be adjusted accordingly before extending the curve. In addition, processing of the curve as computed at a tolerance ε can be used to guide the search at a smaller tolerance without subdividing every ε-cell (for instance when the curvature is small relative to the length).

Figure 4.13 shows the curve of figure 4.12 computed with a smaller tolerance

and continued to the level $\{a = 0\}$. The line extends all the way to h_2, but our algorithm for computing the landing point of rays slows down at near this curve so we the curve is not completely drawn.

This bifurcation curve, which we label ρ_0, correspond to the the first bifurcation detected by the experiments of the previous section.

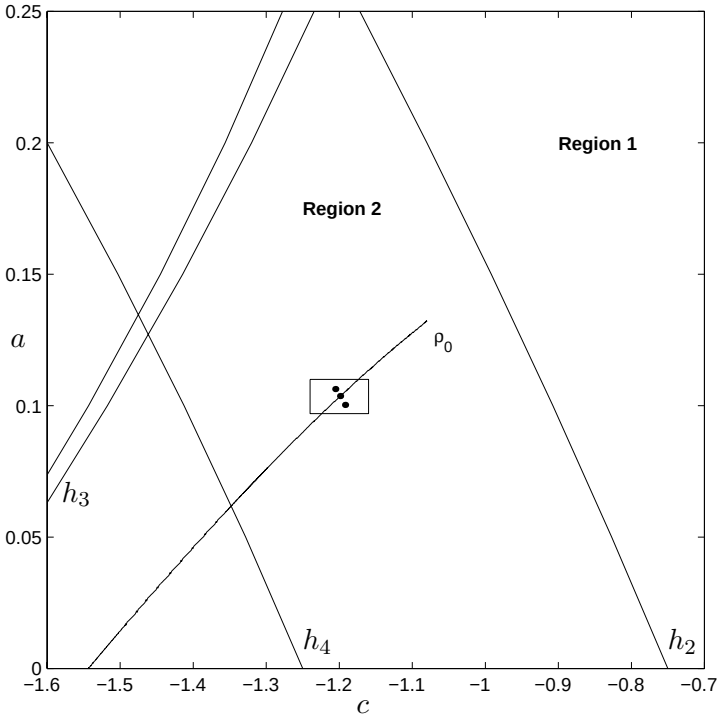

Figure 4.13: The bifurcation curve ρ_0.

4.2.1 Some specific bifurcation curves in Region 2.

The experiments of section §4.1.1 allow us to find specific pairs of identified rays that change partners by observing the W^u_β picture at varying parameter values. The method of section §4.2 gives us the ability to locate such bifurcations in parameter space independently of the W^u_β picture. Combining these techniques we have obtained several bifurcation curves Region 2. Below we describe the pair of rays we have associated with three bifurcations that are relevant for understanding the combinatorial structure of the lower part of Region 2.[2]

First, we have computed the curve ρ_0 of figure 4.13 as the set of parameter values where the rays identified as

$$\begin{bmatrix} {}^{\infty}001(10)^{\infty} \\ {}^{\infty}010(01)^{\infty} \end{bmatrix} \quad \text{and} \quad \begin{bmatrix} {}^{\infty}101(10)^{\infty} \\ {}^{\infty}110(01)^{\infty} \end{bmatrix}$$

change partners to become

$$\begin{bmatrix} {}^{\infty}001(10)^{\infty} \\ {}^{\infty}110(01)^{\infty} \end{bmatrix} \quad \text{and} \quad \begin{bmatrix} {}^{\infty}101(10)^{\infty} \\ {}^{\infty}010(01)^{\infty} \end{bmatrix}.$$

recall from the end of section 4.1.1 that this is the first noticeable topological change in the W^u_β pictures as parameter values are varied in Region 2 from $a = 0$ towards h_3. This can be seen in figures 4.10 and 4.9. At parameter values near those where this real bifurcation occurs we also found complex bifurcations. The most noticeable of these complex bifurcations is shown in figure 4.11; it occurs at a point in parameter space just above ρ_0 (the curve ρ_0 passes close to the point labeled 2 in figure 4.11).

[2]Other lines are shown in figure A.26 in the Appendix.

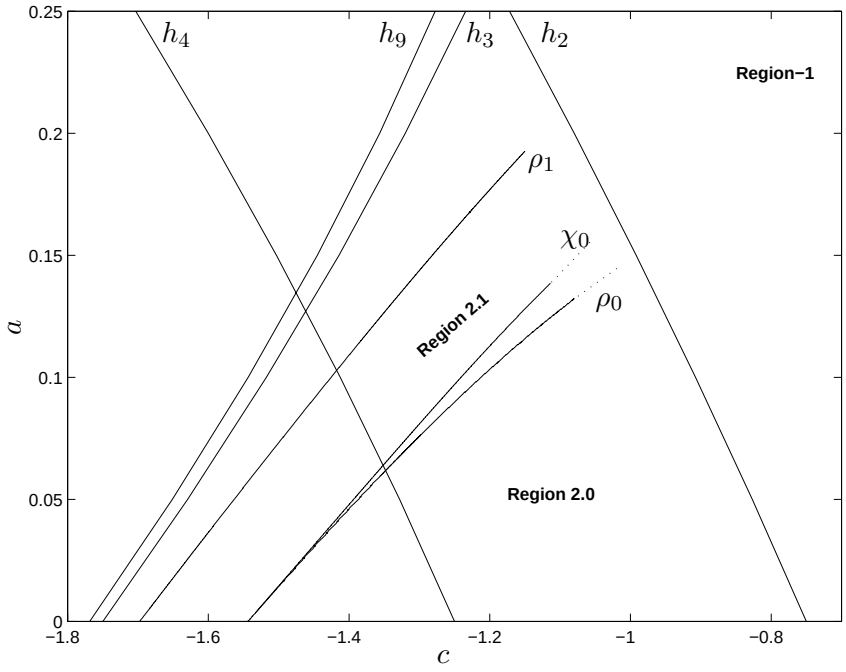

Figure 4.14:

This complex bifurcation corresponds to the identifications

$$\begin{bmatrix} ^{\infty}001101(10)^{\infty} \\ ^{\infty}001110(01)^{\infty} \end{bmatrix} \quad \text{and} \quad \begin{bmatrix} ^{\infty}010001(10)^{\infty} \\ ^{\infty}010010(01)^{\infty} \end{bmatrix}$$

changing to

$$\begin{bmatrix} ^{\infty}001101(10)^{\infty} \\ ^{\infty}010010(01)^{\infty} \end{bmatrix} \quad \text{and} \quad \begin{bmatrix} ^{\infty}010001(10)^{\infty} \\ ^{\infty}001110(01)^{\infty} \end{bmatrix}.$$

The curve for this bifurcation will be called χ_0. We find that χ_0 lies above ρ_0 throughout region two, although the two curves appear tangent near $\{a = 0\}$, as shown in figure 4.14. Above χ_0 in the same figure there is a third bifurcation curve labeled ρ_1. The curve ρ_1 corresponds to parameters where the identifications

$$\begin{bmatrix} ^{\infty}001101(10)^{\infty} \\ ^{\infty}010010(01)^{\infty} \end{bmatrix} \quad \text{and} \quad \begin{bmatrix} ^{\infty}101101(10)^{\infty} \\ ^{\infty}110010(01)^{\infty} \end{bmatrix}$$

change to

$$\begin{bmatrix} {}^{\infty}001101(10)^{\infty} \\ {}^{\infty}110010(01)^{\infty} \end{bmatrix} \quad \text{and} \quad \begin{bmatrix} {}^{\infty}101101(10)^{\infty} \\ {}^{\infty}010010(01)^{\infty} \end{bmatrix}.$$

This is not one of the complex bifurcations that occur for parameter values near ρ_0. In fact this another real bifurcation: the resulting pair of identification involve conjugate rays. The results of our computer experiments in this region of parameter space can be summarized in the following statement which because of its empirical nature we call a conjecture.

Conjecture 4. *Let ρ_0, ρ_1, and χ_0 be the curves defined in terms of the bifurcations described in the previous paragraph.*

1. *There are no bifurcations below ρ_0 in Region 2.*

2. *There are no bifurcations between χ_0 and ρ_1 in Region 2.*

This conjecture also says that the complex bifurcations occurring at parameter values near ρ_0 actually occur for parameter values between ρ_0 and χ_0. Looking at the W^u_β picture in detail we find that some of these complex bifurcations occur very close to ρ_0 in parameter space. Perhaps some coincide with the main bifurcation that occurs for parameter values in ρ_0, but our experiments indicate that none occur at parameters below ρ_0 or above χ_0.

According to Conjecture 4, the curve ρ_0 provides a more concrete answer than Conjecture 3 to the problem of determining the part of Region 2 above $a = 0$ where $f_{a,c} \approx \varprojlim P_{-1}$.

We will denote the part of Region 2 below ρ_0 as Region 2.0 and the part of Region 2 between χ_0 and ρ_1 as Region 2.1.

Next we consider two complementary and related questions motivated by Conjecture 4. One is to describe all the bifurcations that occur between ρ_0 and χ_0. The other is to describe all the identifications for parameters values in Region 2.1. We begin with the second question, since knowledge of the identifications in Region 2.1 and in Region 2.0 can be used to predict bifurcations that must occur between these two regions.

4.2.2 Describing all identifications in a stable region.

We have used external rays to locate bifurcations in parameter space. In this section we use rays to provide computational evidence that a single graph describes all the identifications of external rays for mappings in this region.

The graph Γ_2' was presented in figure 3.8 where we proved that it satisfies the planarity conditions. We constructed this graph by considering the identifications of rays in the $W^u_{a,c}$ picture with $(c, a) = (-1.24, 0.125)$, which lies between χ_0 and ρ_1 in parameter space. We conjecture that Γ_2' is the graph encoding all the identifications for this map as well as for any mapping in Region 2.1.

Both of these conjectures have been submitted to computer verification. To test the graph at a specific parameter value we let the computer generate a large number of paired sequences given by paths in the graph, and then the computer checks whether or not both rays in each pair lands at the same point (to machine accuracy). For instance, we can consider all possible paths of length N between the diagonal subgraph and the terminal 2-cycle in the graph. These constitute identifications of the form $\left[\begin{smallmatrix} \mathsf{h}\,\mathsf{u}\,\mathsf{w} \\ \mathsf{h}\,\mathsf{v}\,\overline{\mathsf{w}} \end{smallmatrix}\right]$ where h is $^\infty\mathtt{0}$ or $^\infty\mathtt{1}$, w is $(\mathtt{01})^\infty$ or $(\mathtt{10})^\infty$ depending on the

node chosen in the 2-cycle, and v and w are words of length N. These sequences all belong to the unstable manifold of the fixed point, therefore the corresponding rays can be seen in the W^u_β picture (after shifting if necessary). Paths between either of the other two nodes of the solenoid subgraph and the terminal 2-cycle give the real identifications in W^u_β. Figure 4.16 shows some of 256 pairs of sequences generated from the graph, all of which were verified as valid identifications (a smaller subset of twice as many verified identifications is shown near the center of the figure). In practice the symmetries of the graph can be taken into account to avoid computing duplicate sequences.

We have applied the same computer test at other parameters in Region 2.1 (figure 4.15). In each test the computer checked about 1000 pairs of sequences and all pairs resulted in identified rays.

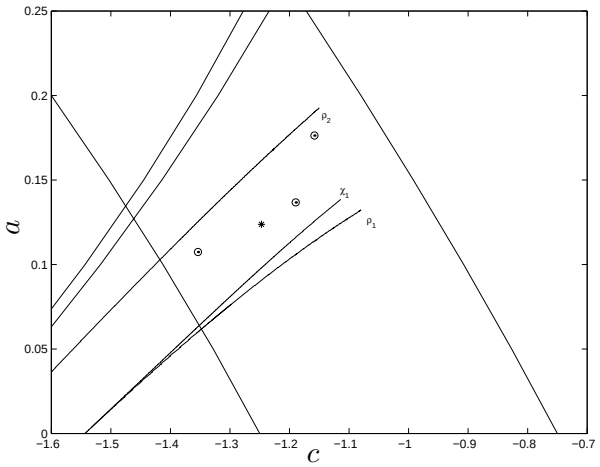

Figure 4.15: Points in Region 2.1 where we the computer has tested the graph Γ_2. The asterisk indicates $(c, a) = (-1.24, 0.125)$.

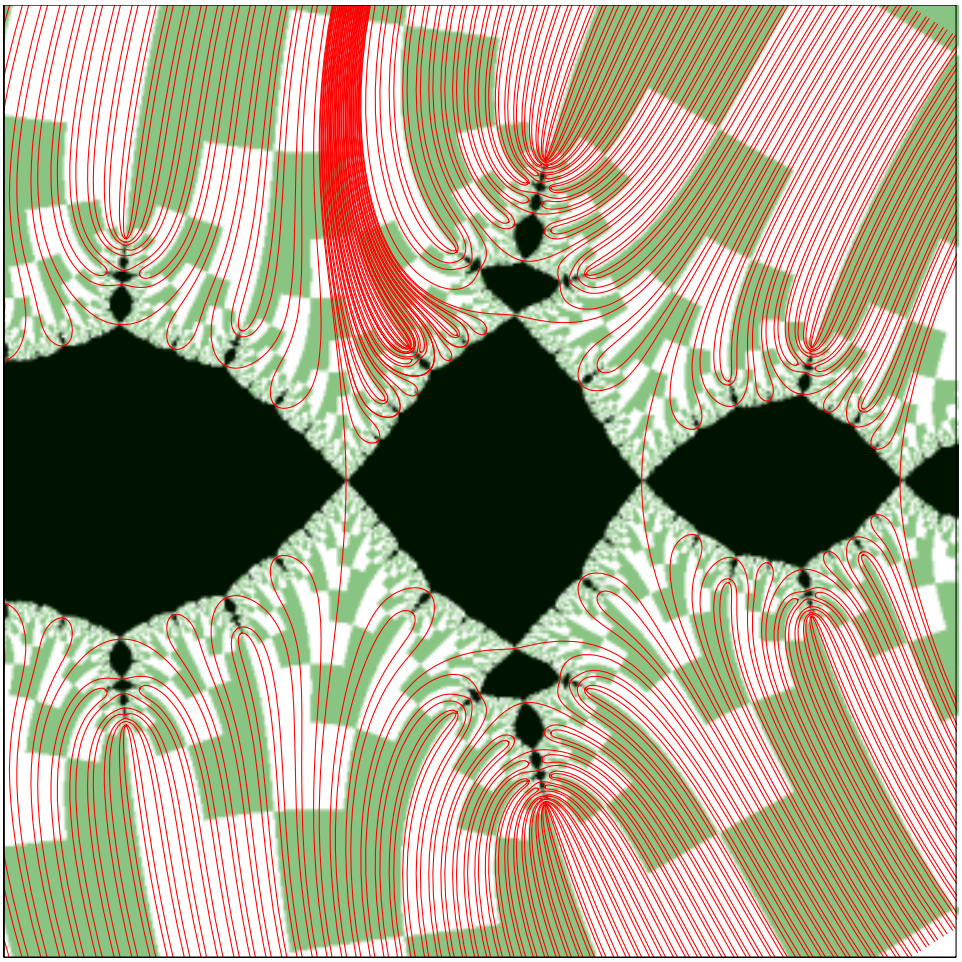

Figure 4.16: A sample of the rays generated in pairs by the computer from the graph Γ_2' of figure 3.8. Rays on each pair were tested by the computer to have the same landing point.

Testing the graph $\Gamma_{(3,1)}$.

We used the same computer test to check the identifications produced by the graph $\Gamma_{(3,1)}$ of section §3.3.2. Recall that we computed this graph for the mapping with parameters $a_0 = 0.3$ and $c_0 = -1.17$. Figures 4.17 shows 504 rays corresponding to pairs of sequences obtained from paths in the graph $\Gamma_{(3,1)}$, and verified by the computer as being pairwise identified at the parameter values a_0 and c_0. Different colors are used by the computer when drawing the rays to emphasize the fact that it is testing rays in pairs. Figure 4.18 is a close-up of the region near the center of the picture in figure 4.17.

We also have carried out a few preliminary experiments of the type discussed in section §4.1.1, and these indicate that bifurcations do not occur for parameter values in a neighborhood of (c_0, a_0). See figures 4.19 and 4.20.

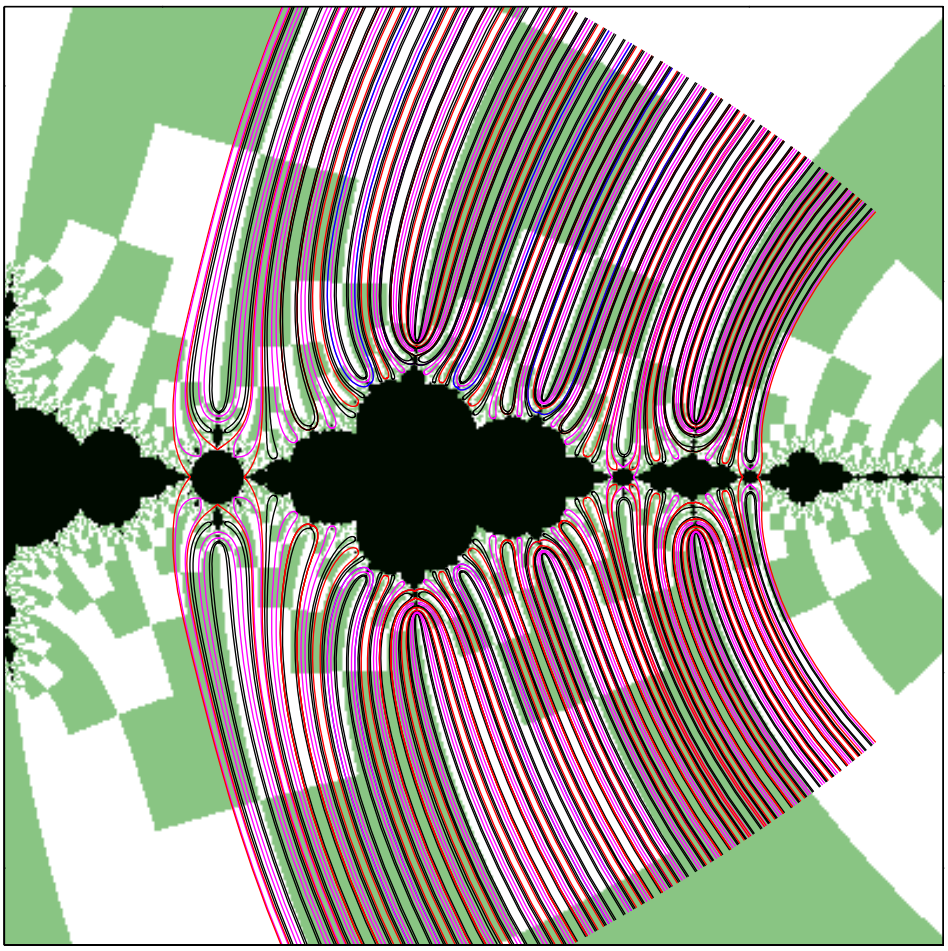

Figure 4.17: 252 pairs of rays generated by the computer from the graph $\Gamma_{(3,1)}$ of figure 3.11. The landing point of each pair was verified by the computer to be the same (to machine accuracy).

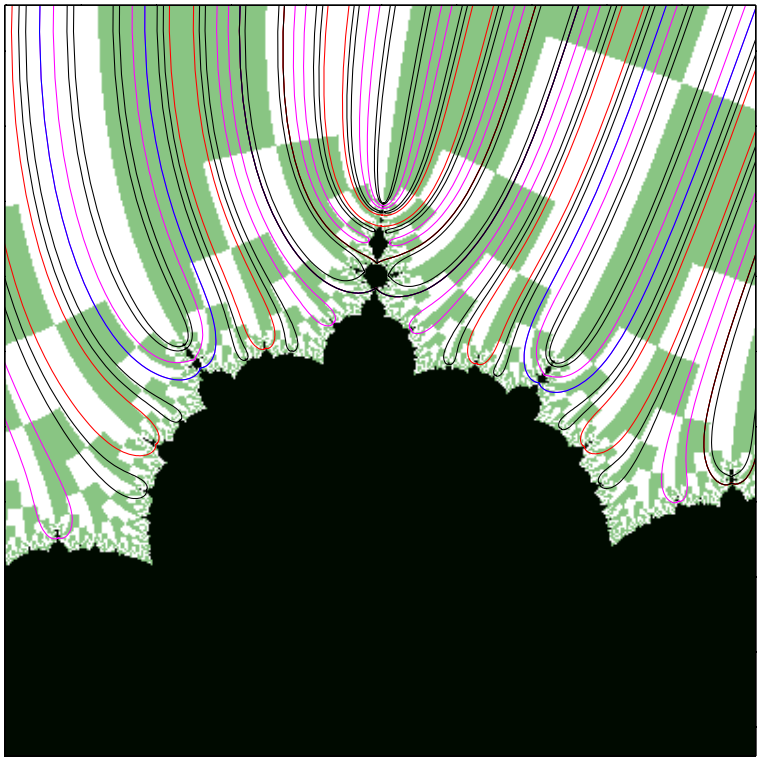

Figure 4.18: Close up of figure 4.17.

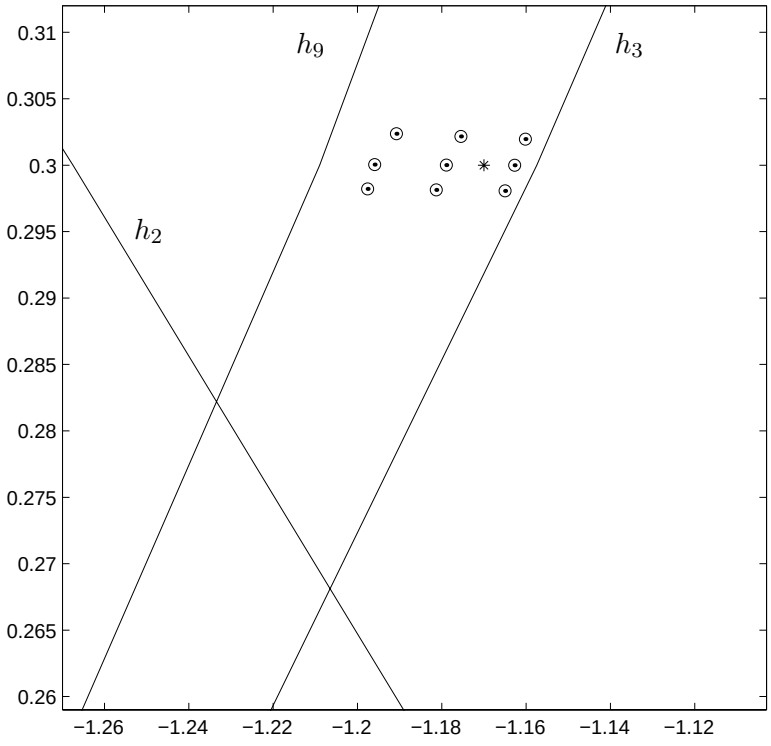

Figure 4.19: A neighborhood of the point the point $(c_0, a_0) = (-1.17, 0.3)$ in parameter space. The asterisk indicates (c_0, a_0). The $W^u_{a,c}$ pictures for the nine neighboring points appear stable (see figure 4.20).

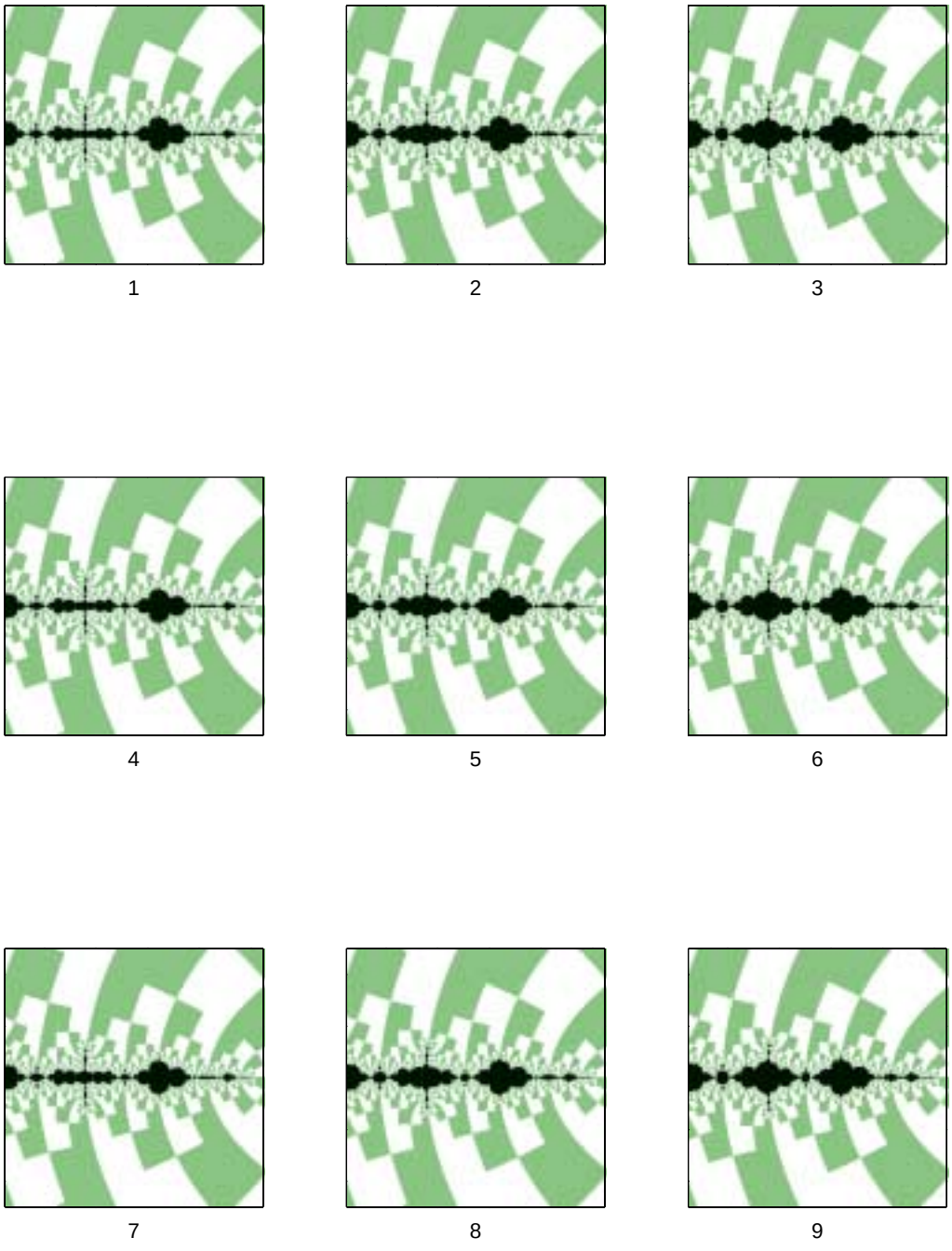

Figure 4.20: W^u_β pictures for the parameter values of figure 4.19.

4.3 Bifurcations predicted by the models.

Knowing the graphs that give the identifications in Region 2.0 and Region 2.1 enable us to obtain a combinatorial description of the bifurcations that occur for parameter values between these two regions.

Note that the graphs Γ_2 and Γ_2' both describe the same set of rays with non-trivial identifications, namely both graphs specify identifications between rays in $W^s((\mathtt{01})^\infty)$ with rays in $W^s((\mathtt{10})^\infty)$. We will exploit the idea that if the the two graphs give different "partners" for a given ray, then the ray must have changed partners at least once as parameters vary between the regions described by each of the graphs.

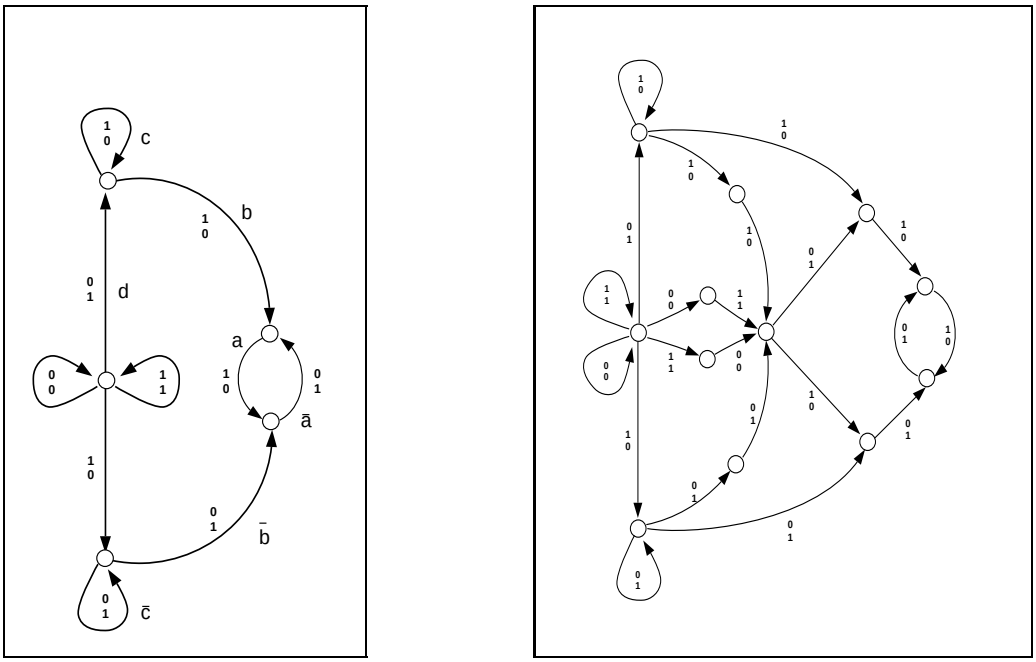

Figure 4.21: The graphs Γ_2 (left) and Γ_2' (right).

The proposed set of bifurcations will be obtained as an application of the following theorem.

Theorem 6. *Let $\mathcal{X}$ denote the set of non-trivial identifications described by the graph Γ_2. Let $\mathcal{X}'$ denote the set of non-trivial identifications described by the graph Γ_2'. There exist four families of rays*

$$P(\mathsf{h}, n),\ Q(\mathsf{h}, n),\ R(\mathsf{h}, n),\ S(\mathsf{h}, n), \qquad \mathsf{h} \in \mathcal{S}_2^-,\ n \in \mathbf{N},$$

and, in addition, other four rays $P(0), Q(0), R(0), S(0)$, such that for fixed h and $n \in \{\mathbf{N} \cup 0\}$ these rays satisfy

$$\left[\begin{smallmatrix} P \\ Q \end{smallmatrix}\right],\ \left[\begin{smallmatrix} R \\ S \end{smallmatrix}\right] \in \mathcal{X} \quad \textit{and} \quad \left[\begin{smallmatrix} P \\ S \end{smallmatrix}\right],\ \left[\begin{smallmatrix} R \\ Q \end{smallmatrix}\right] \in \mathcal{X}'.$$

The collection of all these partner switches, $\left\{\left[\begin{smallmatrix} P \\ Q \end{smallmatrix}\right], \left[\begin{smallmatrix} R \\ S \end{smallmatrix}\right]\right\}$ to $\left\{\left[\begin{smallmatrix} P \\ S \end{smallmatrix}\right], \left[\begin{smallmatrix} R \\ Q \end{smallmatrix}\right]\right\}$ for $\mathsf{h} \in \mathcal{S}_2^-$ and $n \in \{\mathbf{N} \cup 0\}$, constitutes the smallest set of combinatorial changes necessary to change $\mathcal{X}$ into $\mathcal{X}'$.

We will prove theorem 6 and compute the families $P(\mathsf{h}, n), \ldots,\ S(\mathsf{h}, n)$ and the four rays $P(0)$, ... ,$S(0)$ in §4.3.1.

Under the assumption that the graphs Γ_2 and Γ_2' describe the identifications in Region 2.1 and Region 2.0, respectively, we obtain a description of the bifurcations occurring between these two regions.

Proposition 23. *Assume that the identifications in region 2.0 are given by the graph Γ_2 and the identifications in region 2.1 are given by the graph Γ_2'. Suppose all changes in the combinatorics between the two regions occur through bifurcations*

where two pairs of identified rays change partners. If rays change partners at most once between these regions, then the set of all bifurcations between Region 2.0 and Region 2.1 is given by the collection of partner exchanges predicted by Theorem 6, with

$$\begin{aligned} P(\mathsf{h},n) &= \mathsf{h}01^n110(01)^\infty \\ Q(\mathsf{h},n) &= \mathsf{h}01^n101(10)^\infty \\ R(\mathsf{h},n) &= \mathsf{h}10^n010(01)^\infty \\ S(\mathsf{h},n) &= \mathsf{h}10^n001(10)^\infty \end{aligned}$$

$\mathsf{h} \in \mathcal{S}_2^-,\ n \in \mathbf{N},$ *and*

$$\begin{aligned} P(0) &= {}^\infty 110(01)^\infty \\ Q(0) &= {}^\infty 101(10)^\infty \\ R(0) &= {}^\infty 010(01)^\infty \\ S(0) &= {}^\infty 001(10)^\infty \end{aligned}$$

where rays are identified as $\left[\begin{smallmatrix} P \\ Q \end{smallmatrix}\right]$, $\left[\begin{smallmatrix} R \\ S \end{smallmatrix}\right]$ *in Region 2.0 and as* $\left[\begin{smallmatrix} P \\ S \end{smallmatrix}\right]$, $\left[\begin{smallmatrix} R \\ Q \end{smallmatrix}\right]$ *in Region 2.1.*

Proof. The proof will follow from that of Theorem 6. □

4.3.1 Computing $P(\mathsf{h},\mathsf{n})$, ... ,$S(\mathsf{h},\mathsf{n})$, and $P(0)$, ... ,$S(0)$.

To simplify the notation we will drop the subscript 2 in the notation Γ_2 and Γ_2' and we will refer to these graphs as Γ and Γ' respectively. Accordingly, Region 2.0 and Region 2.1 will be referred to as the Γ-region and the Γ'-region, respectively.

We let $\mathcal{X}$ stand for the set of non-trivial identifications given by Γ, modulo symmetry and shifting. That is to say, the following identifications are treated as one and the same element in $\mathcal{X}$

$$\begin{bmatrix} s \\ t \end{bmatrix} \equiv \begin{bmatrix} t \\ s \end{bmatrix} \equiv \begin{bmatrix} \sigma^n s \\ \sigma^n t \end{bmatrix},\ n \in \mathbf{Z}. \tag{4.1}$$

We call $\mathcal{X}$ the language[3] of Γ. The language of Γ' is defined similarly and denoted $\mathcal{X}'$. For a bi-infinite sequence A such that $\left[\begin{smallmatrix} A \\ B \end{smallmatrix}\right] \in \mathcal{X}$ we define the sequence ΓA to be B; namely ΓA stands for the "partner" of A as given by the graph Γ. Similarly, for $\left[\begin{smallmatrix} A \\ C \end{smallmatrix}\right] \in \mathcal{X}'$ we define $\Gamma' A$ to be C, so that $\Gamma' A$ is the "partner" of A according to the graph Γ'. Thus, $\left[\begin{smallmatrix} A \\ \Gamma A \end{smallmatrix}\right] \in \mathcal{X}$ and $\left[\begin{smallmatrix} A \\ \Gamma' A \end{smallmatrix}\right] \in \mathcal{X}'$ by definition.

If $\Gamma A \neq \Gamma' A$, then the pair of rays in the identifications $\left[\begin{smallmatrix} A \\ \Gamma A \end{smallmatrix}\right] \in \mathcal{X}$ must change partners as parameter values are varied from the Γ-region to the Γ'-region; similarly, the rays identified as $\left[\begin{smallmatrix} A \\ \Gamma' A \end{smallmatrix}\right] \in \mathcal{X}'$ must change partner when parameters change values in the other direction. Therefore, the sets $\mathcal{X} - \mathcal{X}'$ and $\mathcal{X}' - \mathcal{X}$ consists of identifications that undergo bifurcations.

Lemma 24. *Assume that between the Γ-region and the Γ'-region each ray is involved in at most one bifurcation. Then, the following holds:*

1. *If $\left[\begin{smallmatrix} A \\ B \end{smallmatrix}\right] \in \mathcal{X} - \mathcal{X}'$ then $\left[\begin{smallmatrix} \Gamma' A \\ \Gamma' B \end{smallmatrix}\right]$ also belongs to $\mathcal{X} - \mathcal{X}'$.*

2. *If $\left[\begin{smallmatrix} A \\ B \end{smallmatrix}\right] \in \mathcal{X} - \mathcal{X}'$ then between the Γ-region and the Γ'-region the rays in the identification $\left[\begin{smallmatrix} A \\ B \end{smallmatrix}\right]$ change partners with the rays in the identification $\left[\begin{smallmatrix} \Gamma' A \\ \Gamma' B \end{smallmatrix}\right]$.*

Proof. Let $\left[\begin{smallmatrix} A \\ B \end{smallmatrix}\right] \in \mathcal{X} - \mathcal{X}'$. Then A has a different partner under Γ than under Γ', so by hypothesis there is exactly one bifurcation involving a second pair of rays identified under Γ which change partners with $[A, B]$ as parameter values are varied from the Γ-region to the Γ'-region. Thus, there exist $\left[\begin{smallmatrix} A' \\ B' \end{smallmatrix}\right] \in \mathcal{X} - \mathcal{X}'$, such that $\left[\begin{smallmatrix} A \\ A' \end{smallmatrix}\right] \in \mathcal{X}'$ and $\left[\begin{smallmatrix} B \\ B' \end{smallmatrix}\right] \in \mathcal{X}'$. But then, $A' = \Gamma' A$ and $B' = \Gamma' B$. □

[3]This differs somewhat from the Computer Science terminology where the language of a directed labeled graph also include finite words.

In general, knowing that $\left[\begin{smallmatrix} A \\ B \end{smallmatrix}\right]$ and $\left[\begin{smallmatrix} \Gamma' A \\ \Gamma' B \end{smallmatrix}\right]$ are both in $\mathcal{X} - \mathcal{X}'$ is not enough to conclude that there is a bifurcation involving all four rays, since there could be intermediate bifurcations leading to $\left[\begin{smallmatrix} A \\ \Gamma' A \end{smallmatrix}\right]$ and $\left[\begin{smallmatrix} B \\ \Gamma' B \end{smallmatrix}\right]$. Also, the set $\mathcal{X} \cap \mathcal{X}'$ is not, a priori, the set of stable identifications since a pair of rays identified in the Γ-region could break-up and then reunite again before reaching the Γ'-region. But according to our computer experiments it seems to be the case that rays bifurcate only once between Region 2.0 and Region 2.1. Additionally, all bifurcation lines appear to be disjoint (see 4.3.2). This justifies the hypothesis in Lemma 24 and in Proposition 23.

Corollary 7. *The smallest set of pairs of identifications whose rays exchange partners in order for* $\mathcal{X}$ *to become* $\mathcal{X}'$ *is given by*

$$\left\{ \left\{ \left[\begin{smallmatrix} A \\ B \end{smallmatrix}\right], \left[\begin{smallmatrix} \Gamma' B \\ \Gamma' A \end{smallmatrix}\right] \right\} : \left[\begin{smallmatrix} A \\ B \end{smallmatrix}\right] \in \mathcal{X} - \mathcal{X}' \right\}. \tag{4.2}$$

If rays change partners at most once, this is also the set of identifications corresponding to all bifurcations between the Γ*-region and the* Γ'*-region.*

Expressing this set of identifications in terms of binary sequences is a way of predicting specific bifurcations from the combinatorial data encoded in the two graphs. The following lemma list the language of Γ as determined by this method.

Lemma 25. $\mathcal{X} = X_0 \cup X_1 \cup \{X(\mathsf{h}, n) \,:\, \mathsf{h} \in \mathcal{S}_2,\, n \in \mathbf{N}\}$ *where*

$$X_0 = \begin{bmatrix} {}^{\infty}(\mathtt{01}).(\mathtt{01}^{\infty}) \\ {}^{\infty}(\mathtt{10}).(\mathtt{10}^{\infty}) \end{bmatrix} = \begin{bmatrix} {}^{\infty}(\mathtt{10}).(\mathtt{10}^{\infty}) \\ {}^{\infty}(\mathtt{01}).(\mathtt{01}^{\infty}) \end{bmatrix}, \tag{4.3}$$

$$X_1 = \begin{bmatrix} {}^{\infty}\mathtt{1}(\mathtt{10})^{\infty} \\ {}^{\infty}\mathtt{0}(\mathtt{01})^{\infty} \end{bmatrix} = \begin{bmatrix} {}^{\infty}\mathtt{1}(\mathtt{01})^{\infty} \\ {}^{\infty}\mathtt{0}(\mathtt{10})^{\infty} \end{bmatrix}, \quad \textit{and} \tag{4.4}$$

$$X(\mathsf{h}, n) = \begin{bmatrix} \mathsf{h}\mathtt{10}^n(\mathtt{01})^{\infty} \\ \mathsf{h}\mathtt{01}^n(\mathtt{10})^{\infty} \end{bmatrix}. \tag{4.5}$$

Proof. An explicit description of $\mathcal{X}$ can be obtained by following backwards-paths in Γ from its terminal 2-cycle and then using (4.1) to eliminate redundancies (cf. §3.1, example 3). □

Proposition 26. *The set $\mathcal{X} - \mathcal{X}'$ consists of the identifications $A(\mathsf{h}) \sim B(\mathsf{h})$ and $C(\mathsf{h}) \sim D(\mathsf{h})$, with arbitrary $\mathsf{h} \in \mathcal{S}_2^-$, where*

$$\begin{aligned} A(\mathsf{h}) &= \mathsf{h}\mathtt{1110}(\mathtt{01})^{\infty} \\ B(\mathsf{h}) &= \mathsf{h}\mathtt{1101}(\mathtt{10})^{\infty} \\ C(\mathsf{h}) &= \mathsf{h}\mathtt{0010}(\mathtt{01})^{\infty} \\ D(\mathsf{h}) &= \mathsf{h}\mathtt{0001}(\mathtt{10})^{\infty} \end{aligned}$$

Proof. The graph Γ' is also backwards deterministic; following the sequences of $\mathcal{X}$, (4.3) to (4.5), backwards from the terminal 2-cycle in Γ' we find that both X_0 and X_1 belong to $\mathcal{X}'$. Also $X(\mathsf{h}, n) \in \mathcal{X}'$ for $n > 1$, while for $n = 1$ we get $X(\mathsf{h}, n) \in \mathcal{X}'$ if and only if $\mathsf{h}_{-2} \neq \mathsf{h}_{-1}$. Thus, $X(\mathsf{h}, n) \in \mathcal{X} - \mathcal{X}'$ if and only if $n = 1$ and $\mathsf{h} = \mathsf{k}\mathtt{11}$ or $\mathsf{h} = \mathsf{k}\mathtt{00}$, with $\mathsf{k} \in \mathcal{S}_2^-$ arbitrary. The rays as listed in the statement of the proposition correspond to writing $\begin{bmatrix} A(\mathsf{h}) \\ B(\mathsf{h}) \end{bmatrix} = X(\mathsf{h}\mathtt{11}, 1)$ and $\begin{bmatrix} C(\mathsf{h}) \\ D(\mathsf{h}) \end{bmatrix} = X(\mathsf{h}\mathtt{00}, 1)$. □

To apply Corollary 7 to the result of Proposition 26 we will need to find the partners of rays $A(\mathsf{h}), \ldots, D(\mathsf{h})$ under Γ'. We begin with a special case.

Lemma 27. *Let $A(\mathsf{h}), \ldots, D(\mathsf{h})$ be as in Proposition 26. Then,*

$$\begin{aligned} \Gamma' A(^\infty\mathtt{1}) &= D(^\infty\mathtt{0}) \\ \Gamma' B(^\infty\mathtt{1}) &= C(^\infty\mathtt{0}) \end{aligned}$$

Proof. By inspection of the graph Γ'. □

According to Lemma 24 and Lemma 27 the rays

$$\begin{aligned} A(^\infty\mathtt{1}) &= {}^\infty\mathtt{11110}(\mathtt{01})^\infty \\ B(^\infty\mathtt{1}) &= {}^\infty\mathtt{11101}(\mathtt{10})^\infty \\ C(^\infty\mathtt{0}) &= {}^\infty\mathtt{00010}(\mathtt{01})^\infty \\ D(^\infty\mathtt{0}) &= {}^\infty\mathtt{00001}(\mathtt{10})^\infty \end{aligned}$$

correspond to a bifurcation in which $A(^\infty\mathtt{1}) \sim B(^\infty\mathtt{1})$ and $C(^\infty\mathtt{0}) \sim D(^\infty\mathtt{0})$ change partners and become identified as $A(^\infty\mathtt{1}) \sim D(^\infty\mathtt{0})$ and $C(^\infty\mathtt{0}) \sim B(^\infty\mathtt{1})$. We recognize these rays as those that defined the bifurcation line ρ_0 in section §4.2.1.

In Lemma 27 we found $\Gamma' A(\mathsf{h})$ and $\Gamma' B(\mathsf{h})$ for $\mathsf{h} = {}^\infty\mathtt{1}$. If the sequence h is not of this form it can be written as $\mathsf{h} = \mathsf{k}\mathtt{01}^n$, with $n \geq 0$ and $\mathsf{k} \in \mathcal{S}_2^-$ arbitrary. Then, the rays $\Gamma' A(\mathsf{h})$ and $\Gamma' B(\mathsf{h})$ for $\mathsf{h} \neq {}^\infty\mathtt{1}$ are as given in the next Lemma.

Lemma 28. *Let $A(\mathsf{h}), \ldots, D(\mathsf{h})$ be as in Proposition 26. Then, for $n \geq 0$*

$$\begin{aligned} \Gamma' A(\mathsf{h}\mathtt{01}^n) &= D(\mathsf{h}\mathtt{10}^n) \\ \Gamma' B(\mathsf{h}\mathtt{01}^n) &= C(\mathsf{h}\mathtt{10}^n) \end{aligned}$$

Proof. By inspection of the graph Γ'. □

According to Lemma 24 and Lemma 28, the rays

$$\begin{aligned} A(\mathsf{h}\mathtt{01}^n) &= \mathsf{h}\mathtt{01}^n\mathtt{1110}(\mathtt{01})^\infty \\ B(\mathsf{h}\mathtt{01}^n) &= \mathsf{h}\mathtt{01}^n\mathtt{1101}(\mathtt{10})^\infty \\ C(\mathsf{h}\mathtt{10}^n) &= \mathsf{h}\mathtt{10}^n\mathtt{0010}(\mathtt{01})^\infty \\ D(\mathsf{h}\mathtt{10}^n) &= \mathsf{h}\mathtt{10}^n\mathtt{0001}(\mathtt{10})^\infty \end{aligned}$$

for fixed $n \geq 0$, correspond to a bifurcation in which rays identified as $A(\mathtt{h01}^n) \sim B(\mathtt{h01}^n)$ and $C(\mathtt{h10}^n) \sim D(\mathtt{h10}^n)$ change partners to become identified as $A(\mathtt{h01}^n) \sim D(\mathtt{h10}^n)$ and $C(\mathtt{h10}^n) \sim B(\mathtt{h01}^n)$.

Proof of **Theorem 6**. Corollary 7 gives the smallest set of combinatorial changes needed to change $\mathcal{X}$ into $\mathcal{X}'$ since each identification that must change changes only once. Using Proposition 26 we obtained one such combinatorial change after Lemma 27, which involved the rays $A(\,^\infty\mathtt{1})$, $B(\,^\infty\mathtt{1})$, $C(\,^\infty\mathtt{0})$, and $D(\,^\infty\mathtt{0})$. The remaining changes involved the rays $A(\mathtt{h01}^n)$ to $D(\mathtt{h10}^n)$ for $\mathtt{h} \in \mathcal{S}_2^-$ arbitrary, as given in the paragraph following Lemma 28. The four rays $P(0), \ldots, S(0)$ in the statement of Theorem 6 correspond to $A(\,^\infty\mathtt{1}), \ldots, D(\,^\infty\mathtt{0})$, and the rays $P(\mathtt{h}, n{+}1), \ldots, S(\mathtt{h}, n{+}1)$ are given by $A(\mathtt{h}, n), \ldots, D(\mathtt{h}, n)$ for $n \geq 0$. □

4.3.2 A Cantor fan of bifurcation lines.

As noted after Lemma 27, the bifurcation involving the rays $P(0), \ldots, S(0)$ corresponds to the curve ρ_0. To test other bifurcations predicted by Proposition 23 we consider $P(\mathtt{h}, n), \ldots, S(\mathtt{h}, n)$ when $\mathtt{h}$ is eventually constant; then the rays that change partners belong to $W^u(\underline{\mathtt{0}}\,)$ and can be seen in the W^u_β picture. Let $\mathtt{h} = \,^\infty\mathtt{0}w$ for some for some fixed, non-empty, word w and consider the countable families

given by

$$\begin{aligned} P_n &= P({}^{\infty}\mathtt{0}.w, n) \\ Q_n &= Q({}^{\infty}\mathtt{0}.w, n) \\ R_n &= R({}^{\infty}\mathtt{0}.w, n) \\ S_n &= S({}^{\infty}\mathtt{0}.w, n) \end{aligned}$$

where P, Q, R, and S are as in Proposition 23. Namely,

$$\begin{aligned} P_n &= {}^{\infty}\mathtt{0}.w\mathtt{01}^n\mathtt{101}(\mathtt{10})^{\infty} \\ Q_n &= {}^{\infty}\mathtt{0}.w\mathtt{01}^n\mathtt{110}(\mathtt{01})^{\infty} \\ R_n &= {}^{\infty}\mathtt{0}.w\mathtt{10}^n\mathtt{001}(\mathtt{10})^{\infty} \\ S_n &= {}^{\infty}\mathtt{0}.w\mathtt{10}^n\mathtt{010}(\mathtt{01})^{\infty}. \end{aligned}$$

According to Proposition 23, these four families of rays correspond to a sequence of bifurcations indexed by n. We will denote this sequence of bifurcations by $\mathcal{Y}_w(n)$. For example, figure 4.22 shows the first 3 bifurcations in $\mathcal{Y}_w(n)$ when $w = \mathtt{0}$.

We note that $\mathcal{Y}_w(n)$ is a nested sequence in the sense that

$$P_n < Q_n < P_m < Q_m < R_m < S_m < R_n < S_n$$

for $n < m$. Therefore each bifurcation in $\mathcal{Y}_w(n)$ could occur at distinct parameter values while respecting the non-linking condition (§3.3.3).

To compute some specific rays lets choose the simplest possible non-empty word: $w = \mathtt{0}$. Then, the first bifurcation in the sequence $\mathcal{Y}_{\mathtt{0}}(n)$ corresponds to the rays identified as

$$\begin{bmatrix} P_0 \\ Q_0 \end{bmatrix} = \begin{bmatrix} {}^{\infty}\mathtt{0.001101}(\mathtt{10})^{\infty} \\ {}^{\infty}\mathtt{0.001110}(\mathtt{01})^{\infty} \end{bmatrix} \quad \text{and} \quad \begin{bmatrix} R_0 \\ S_0 \end{bmatrix} = \begin{bmatrix} {}^{\infty}\mathtt{0.010001}(\mathtt{10})^{\infty} \\ {}^{\infty}\mathtt{0.010010}(\mathtt{01})^{\infty} \end{bmatrix},$$

changing partners to become

$$\begin{bmatrix} P_0 \\ S_0 \end{bmatrix} = \begin{bmatrix} {}^{\infty}\mathtt{0.001101(10)}^{\infty} \\ {}^{\infty}\mathtt{0.010010(01)}^{\infty} \end{bmatrix} \quad \text{and} \quad \begin{bmatrix} R_0 \\ Q_0 \end{bmatrix} = \begin{bmatrix} {}^{\infty}\mathtt{0.001101(10)}^{\infty} \\ {}^{\infty}\mathtt{0.010010(01)}^{\infty} \end{bmatrix}.$$

This is the combinatorial change that defined the curve χ_0.

In our computer experiments we found that the bifurcations $\mathcal{Y}_{\mathtt{0}}(n)$ for $n = 0, 1,$ and 2, occur on distinct curves in parameter space. We let χ_n denote the curve for the bifurcation $\mathcal{Y}_{\mathtt{0}}(n)$. Figure 4.23 shows χ_n for $n = 0, 1, 2$. These curves are located consecutively closer to ρ_0, suggesting that the sequence of bifurcations corresponds to a fan of bifurcation curves which converge to ρ_0.

Figure 4.22 also illustrate how the rays in $\mathcal{Y}_{\mathtt{0}}(n)$ accumulate on the tip of the most visible limb of $K^+ \cap W^u_\beta$ in the fundamental domain. More generally, for any given w the sequence P_n, Q_n converge to $T_w = {}^{\infty}\mathtt{0}.w\mathtt{01}^{\infty}$ from below as n increases, while R_n and S_n converge to T_w from above as n increases. Stated informally, each ray T_w lands at the tip of a limb of the W^u_β picture, on a point that locally "looks like" a neighborhood of the fixed point, and $\mathcal{Y}_w(n)$ forms a sequence of bifurcations involving rays that land on that limb, consecutively closer to the tip. [4]. Our computer experiments have revealed that other choices of w yield different "fans" of bifurcations curves approaching ρ_0, and it appears that each of the curves χ_i is itself a "fan", suggesting that these bifurcation curves have a Cantor set structure.

[4] More specifically, if $q \in W^u(p) \cap W^s(p')$ then a neighborhoods of K^+_p at q is homeomorphic to a neighborhood of $K^+_{p'}$ at p', (see [BS7])

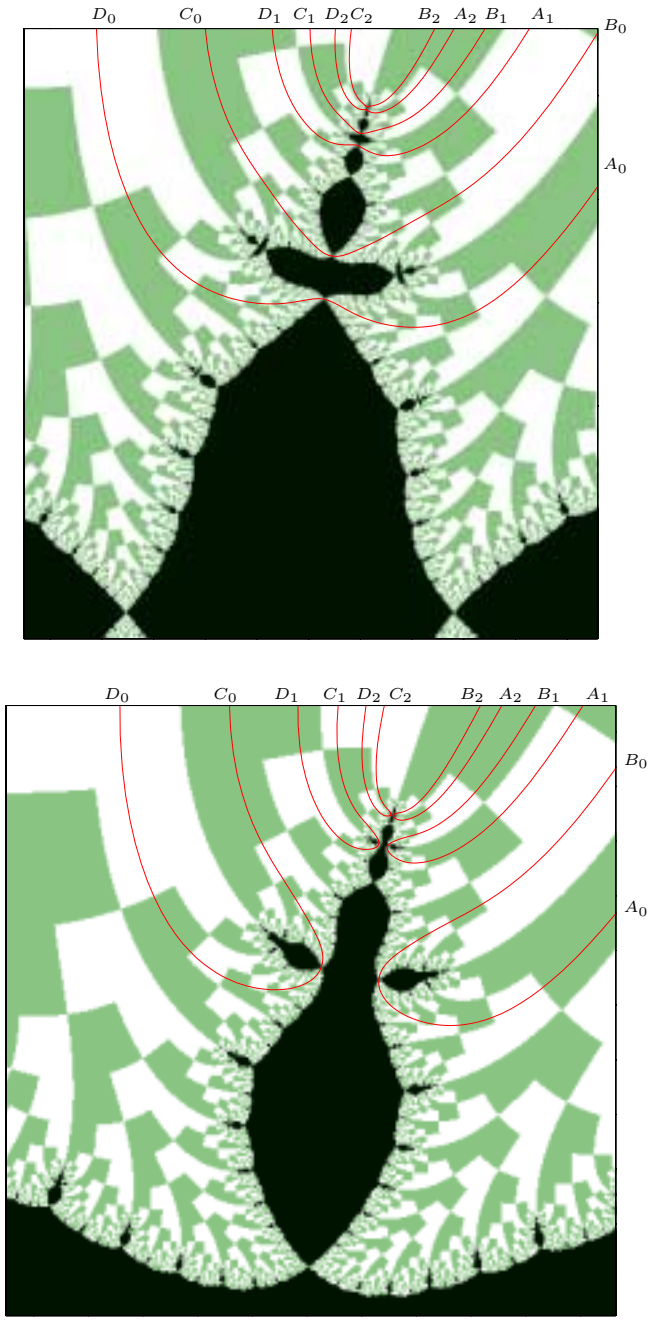

Figure 4.22: The bifurcations $\mathcal{Y}_0(k)$ corresponding to the curves χ_k, $k = 0$, 1, and 2 (see figure 4.23). Top: rays as identified in Region 2.1 (cf. figure 4.11-5). Bottom: rays as identified in Region 2.0 (cf. figure 4.10-1).

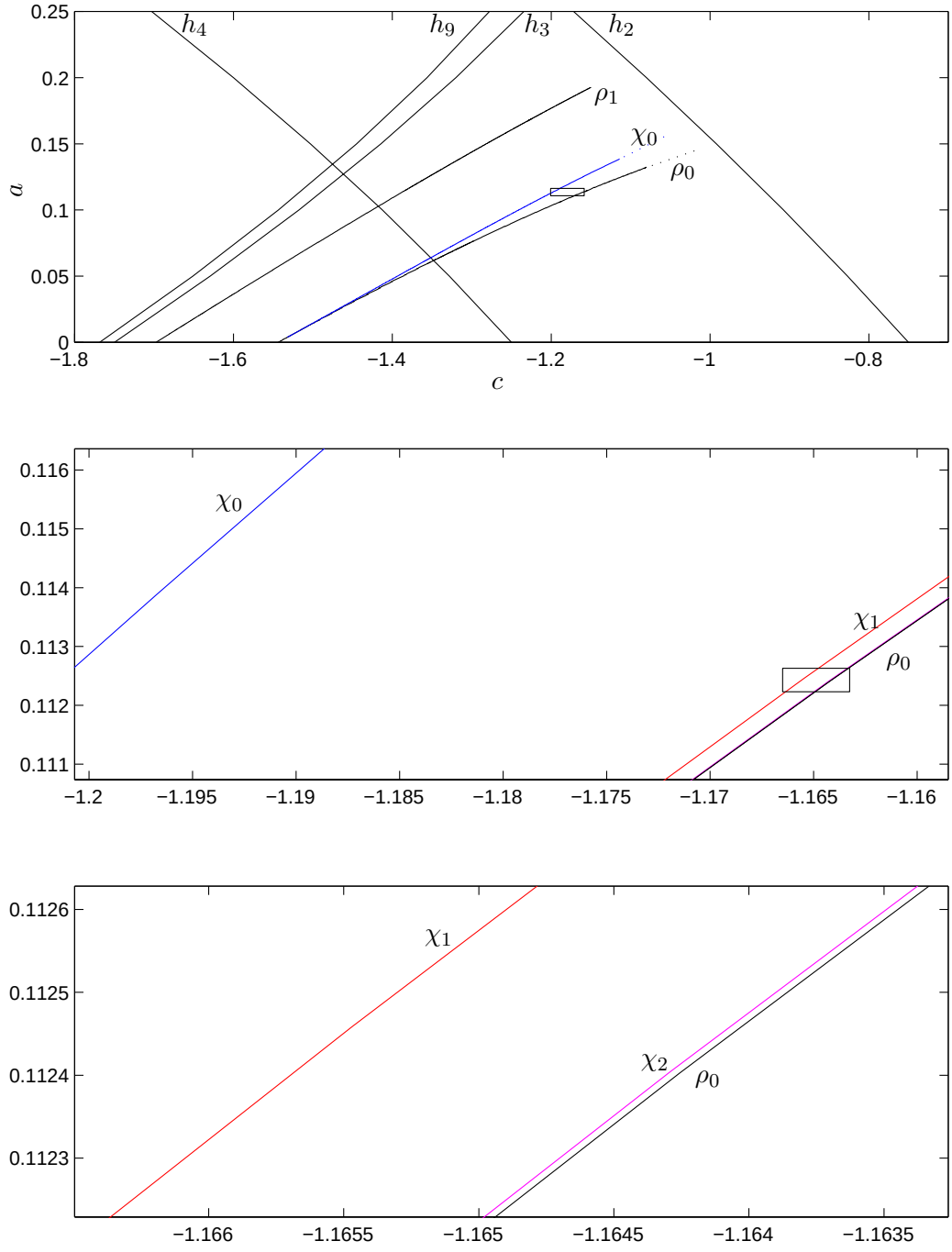

Figure 4.23: Two consecutive zoom showing χ_0, χ_1, and χ_2 approching ρ_0.

4.4 Disconnectivity of the connectivity locus.

Let $J_{a,c}$ denote the set J for the mapping $f_{a,c}$. We let $\mathcal{M}_a$ be the connectivity locus inside the $\mathbf{C} \times \{a\}$ slice in parameter space: $\mathcal{M}_a = \{c \in \mathbf{C} \ : \ J_{a,c} \text{ is connected } \}$. For example, $\mathcal{M}_0$ is the Mandelbrot set. A fundamental theorem in the study of quadratic polynomials, due to Douady & Hubbard, establishes the fact that $\mathcal{M}_0$ is connected. By contrast, our computer experiments have revealed that there exist $a \in (0,1) \subset \mathbf{R}$, such that $\mathcal{M}_a \cap \mathbf{R}$ is not connected: there is a "gap" between real values of the parameter c with connected $J_{a,c}$. The manner in which K_p^+ becomes disconnected is illustrated in figures 4.24 and 4.25. These figures are part of the evidence supporting the following conjecture.

Conjecture 5. *For $a_0 = 0.13610$ the set K_β^+ is disconnected for values of the parameter c in the interval $(-1.2240, -1.2215)$, but it is connected for $c = -1.2260$ and for $c = -1.2198$ on each side of this interval.*

We show in the following theorem that a rigorous verification of this 'gap" in $\mathcal{M}_{a_0} \cap \mathbf{R}$ would prove that $\mathcal{M}_{a_0}$ is not connected.

Theorem 8. *If Conjecture 5 holds then the set $\mathcal{M}_{a_0}$ is disconnected.*

Proof. Bedford and Smillie show in [BS3] that the Lyapunov exponent, Λ, is a pluri-subharmonic function of the parameters and satisfies $\Lambda_{a,c} \geq \log d$ for all a, c. Furthermore, the conditions $c \in \mathcal{M}_a$ and $\Lambda_{a,c} = \log d$ are equivalent when $|a| \leq 1$ ([BS6]). Then, by the maximum principle for sub-harmonic functions, the set $\mathbf{C} - \mathcal{M}_a$ does not have any bounded components when $|a| \leq 1$. In addition, for

$a \in \mathbf{R}$, the set $\mathcal{M}_a$ is symmetric with respect to reflection about the real-axis: $\Lambda_{a,c} = \Lambda_{a,\overline{c}}$ because the maps $f_{a,c} = f_{\overline{a},c}$ and $f_{\overline{a},\overline{c}}$ are smoothly conjugate and Lyapunov exponents are a smooth conjugacy invariant. This implies that if M is any component of $\mathcal{M}_a$, then M intersects the real axis in a connected set:

Suppose that there exits $c_1, c_2, c_3 \in \mathbf{R}$, $c_1 < c_2 < c_3$, such that $c_1, c_3 \in \mathcal{M}_{a_0}$ but $c_2 \in \mathbf{C} - \mathcal{M}_{a_0}$. It is known that the connectivity locus in $\mathbf{C}^2$ is compact ([HOV1]), hence $\mathcal{M}_{a_0}$ is compact. Let D be a disk containing $\mathcal{M}_{a_0}$. The component of $\mathbf{C} - \mathcal{M}_{a_0}$ containing c_2 is unbounded and symmetric with respect to reflection on the real axis. Thus there is a simple path $\gamma \in \mathbf{C} - \mathcal{M}_{a_0}$ from c_2 to a point $z \in \partial D$ such that γ is contained in the closure of the upper-half plane. By the symmetry with respect to complex conjugation $\overline{\gamma}$ is also a simple path from c_2 to ∂D. Then γ, $\overline{\gamma}$ and the clockwise oriented arc in ∂D from z to $\overline{z}$ form a simple closed curve in the open set $\mathbf{C} - \mathcal{M}_{a_0}$, separating the component of $\mathcal{M}_{a_0}$ containing c_1 from the component containing c_3. □

We have found "gaps" in the connectivity locus at several parameter values corresponding to complex bifurcations. We conjecture that such gaps occurs at all complex bifurcations, hence that each complex bifurcation curve corresponds to a thin band of disconnectivity in parameter space.

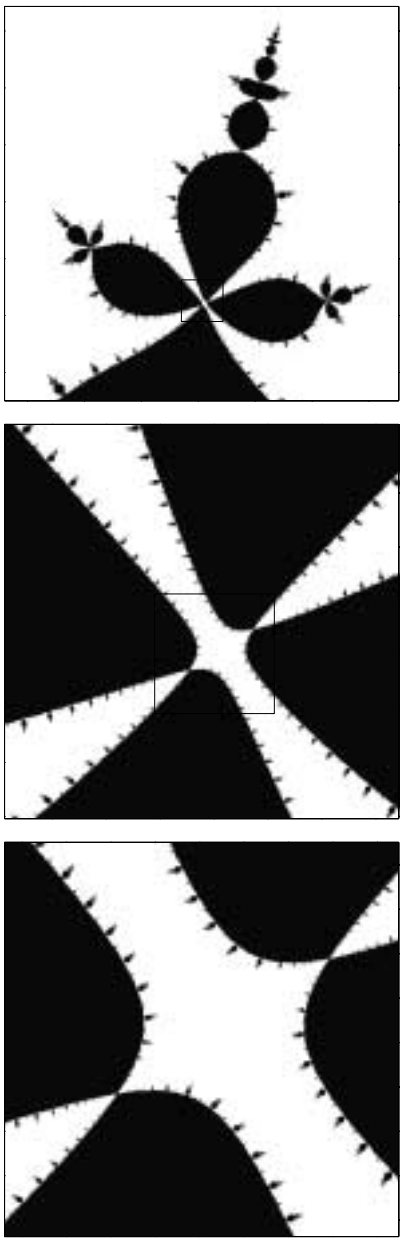

Figure 4.24: Details of a $W^u_{a,c}$ picture with disconnected K^+_p.

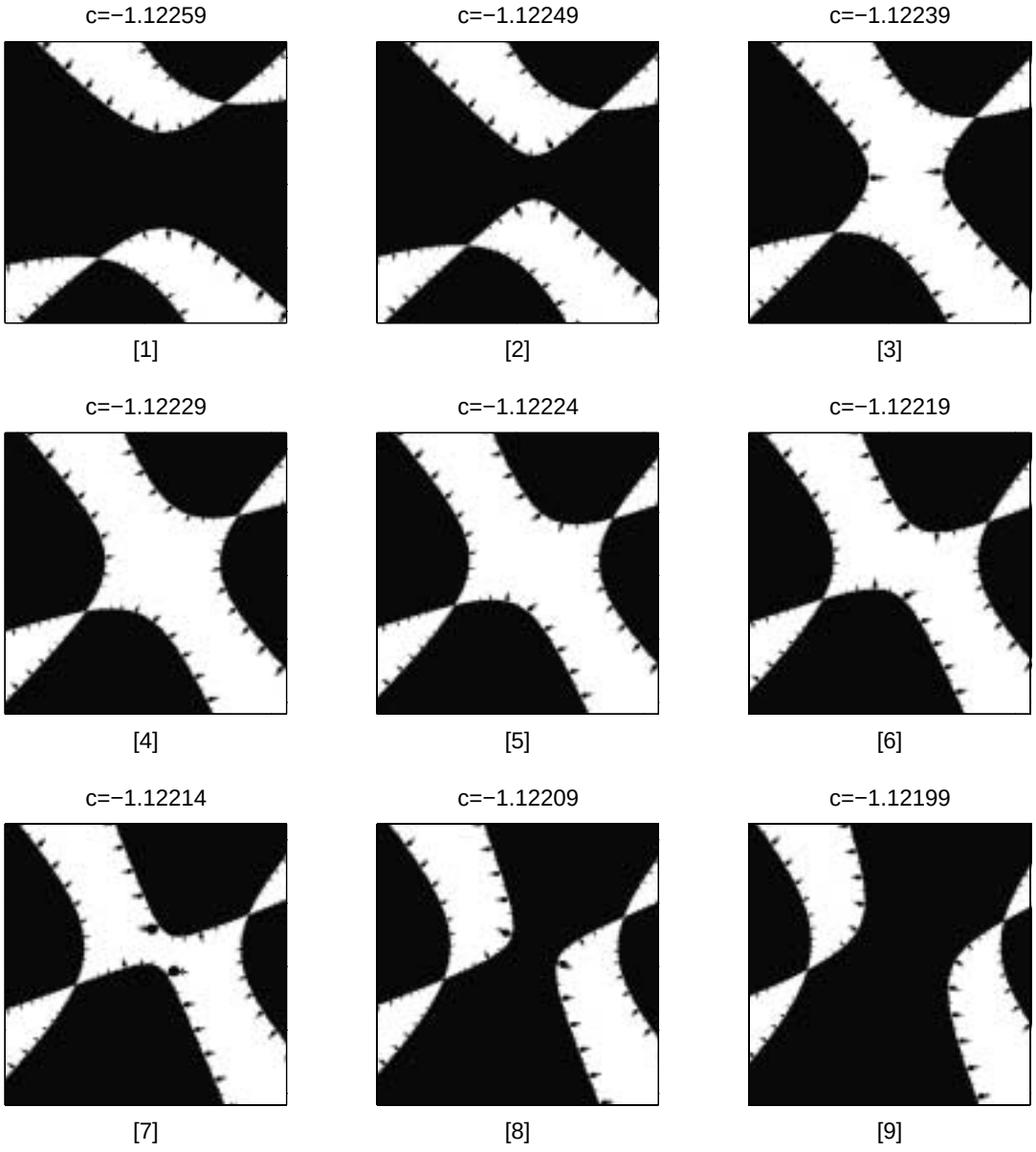

Figure 4.25: Sequence of W^u_β pictures with constant $a = 0.13610$ and decreasing c, illustrating a "gap" in $\mathcal{M}_a \cap \mathbf{R}$ (see figure 4.24 for a zoom-out of frame [4]).

APPENDIX

A Other bifurcation curves above region-$2'$.

In section §4.2.1 we computed the bifurcation curves ρ_0, χ_0, and ρ_1, defining Region 2.0 and 2.1 in parameter space, and in §4.3 we described a family of bifurcations between ρ_0 and χ_0.

Other bifurcations curves we have computed above ρ_1 are shown in figure A.26. Those curves labeled ρ_i correspond to real bifurcations (when the rays meet on the real axis of the W^u_β-picture before changing partners). On the other hand, χ' and χ_0 are complex bifurcations.

All of these curves except ρ_4 appear to continue up to the curve h_2. Our algorithm to compute the curves slows down considerably near h_2 so only a few points in each curve have ben computed near this boundary. The curve ρ_4, however, does not terminate on h_2, instead it bends and appears to becomes asymptotic to ρ_3 (although we have not yet extended ρ_4 to the level $a = 0$). Also we see that there are bifurcations curves such as the one labeled χ' which are asymptotic to two distinct bifurcation curves.

The rays corresponding to these bifurcation curves are given in figures A.27 to A.31 together with the W^u_β-pictures at parameter values below and above (but near) each curve.

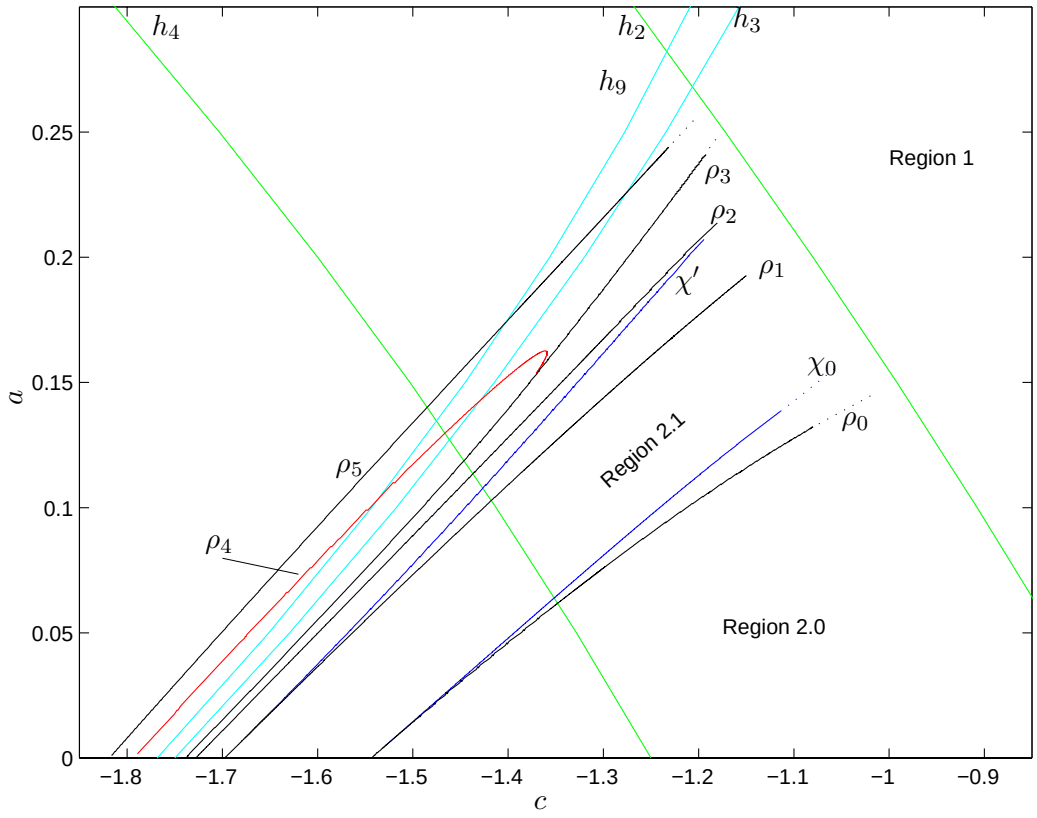

Figure A.26:

$$\begin{bmatrix} {}^{\infty}0.011100100(10)^{\infty} \\ {}^{\infty}0.011011011(01)^{\infty} \end{bmatrix} \qquad \begin{bmatrix} {}^{\infty}0.011100100(10)^{\infty} \\ {}^{\infty}0.100011011(01)^{\infty} \end{bmatrix}$$

$$\begin{bmatrix} {}^{\infty}0.100100100(10)^{\infty} \\ {}^{\infty}0.100011011(01)^{\infty} \end{bmatrix} \qquad \begin{bmatrix} {}^{\infty}0.011011011(01)^{\infty} \\ {}^{\infty}0.100100100(10)^{\infty} \end{bmatrix}$$

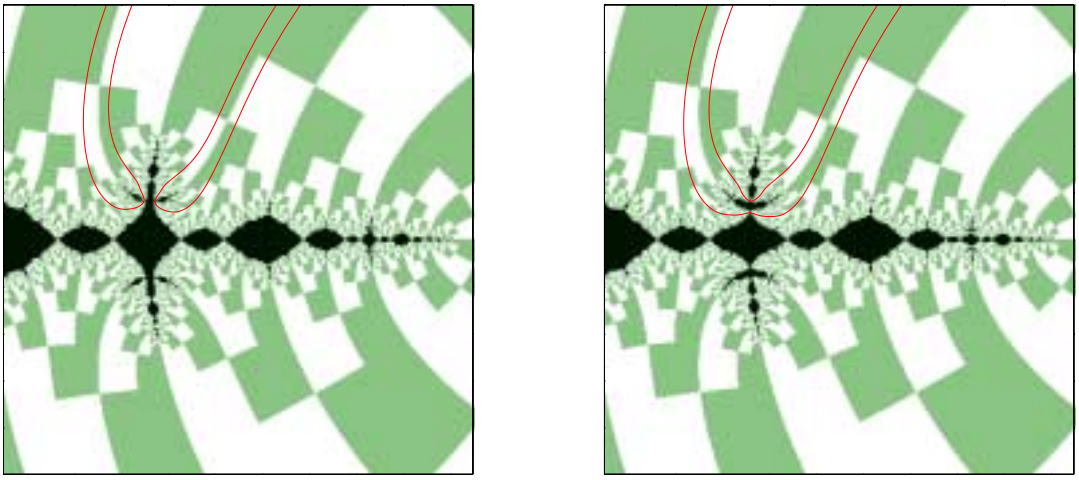

Figure A.27: Rays as identified below χ' (left) and above χ' (right).

$$\begin{bmatrix} {}^{\infty}0.011011011(01)^{\infty} \\ {}^{\infty}0.100100100(10)^{\infty} \end{bmatrix} \qquad \begin{bmatrix} {}^{\infty}0.011011011(01)^{\infty} \\ {}^{\infty}1.100100100(10)^{\infty} \end{bmatrix}$$

$$\begin{bmatrix} {}^{\infty}1.011011011(01)^{\infty} \\ {}^{\infty}1.100100100(10)^{\infty} \end{bmatrix} \qquad \begin{bmatrix} {}^{\infty}0.100100100(10)^{\infty} \\ {}^{\infty}1.011011011(01)^{\infty} \end{bmatrix}$$

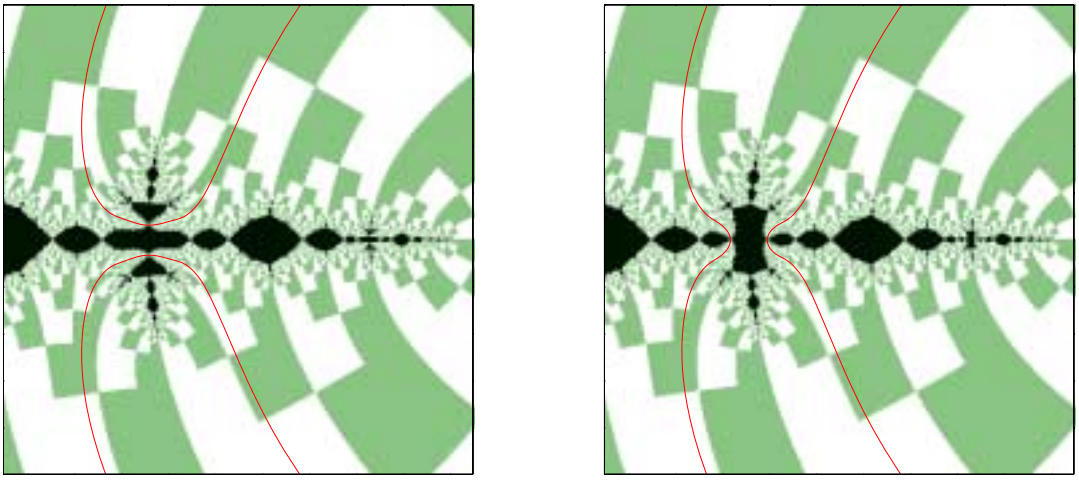

Figure A.28: Rays as identified below ρ_2 (left) and above ρ_2 (right).

$$\begin{bmatrix} {}^{\infty}0.011100100(10)^{\infty} \\ {}^{\infty}0.011011011(01)^{\infty} \end{bmatrix} \qquad \begin{bmatrix} {}^{\infty}0.011100100(10)^{\infty} \\ {}^{\infty}1.100011011(01)^{\infty} \end{bmatrix}$$

$$\begin{bmatrix} {}^{\infty}1.100100100(10)^{\infty} \\ {}^{\infty}1.100011011(01)^{\infty} \end{bmatrix} \qquad \begin{bmatrix} {}^{\infty}0.011011011(01)^{\infty} \\ {}^{\infty}1.100100100(10)^{\infty} \end{bmatrix}$$

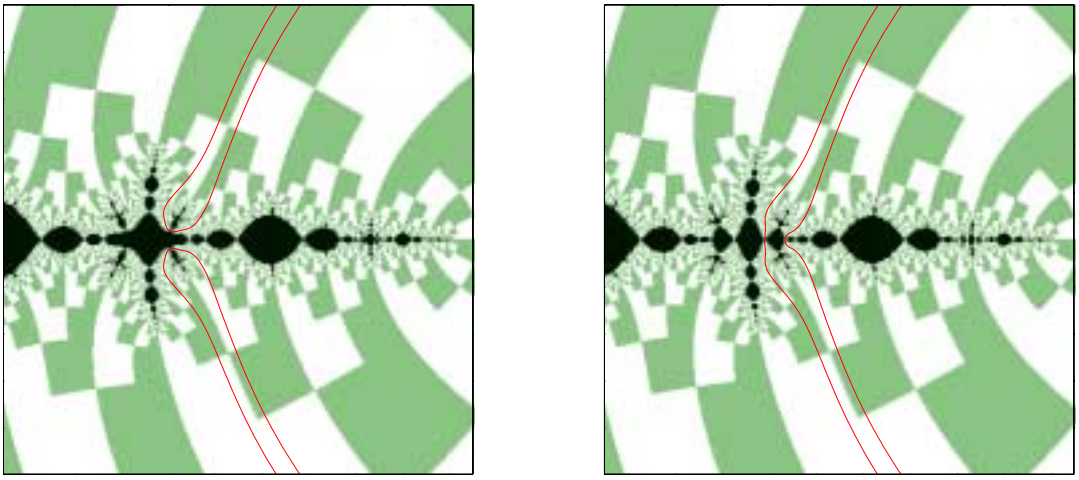

Figure A.29: Rays as identified below ρ_3 (left) and above ρ_3 (right).

$$\begin{bmatrix} {}^{\infty}0.011(100)^3(10)^{\infty} \\ {}^{\infty}0.100(011)^3(01)^{\infty} \end{bmatrix} \qquad \begin{bmatrix} {}^{\infty}0.011(100)^3(10)^{\infty} \\ {}^{\infty}1.100(011)^3(01)^{\infty} \end{bmatrix}$$

$$\begin{bmatrix} {}^{\infty}1.011(100)^3(10)^{\infty} \\ {}^{\infty}1.100(011)^3(01)^{\infty} \end{bmatrix} \qquad \begin{bmatrix} {}^{\infty}1.011(100)^3(10)^{\infty} \\ {}^{\infty}0.100(011)^3(01)^{\infty} \end{bmatrix}$$

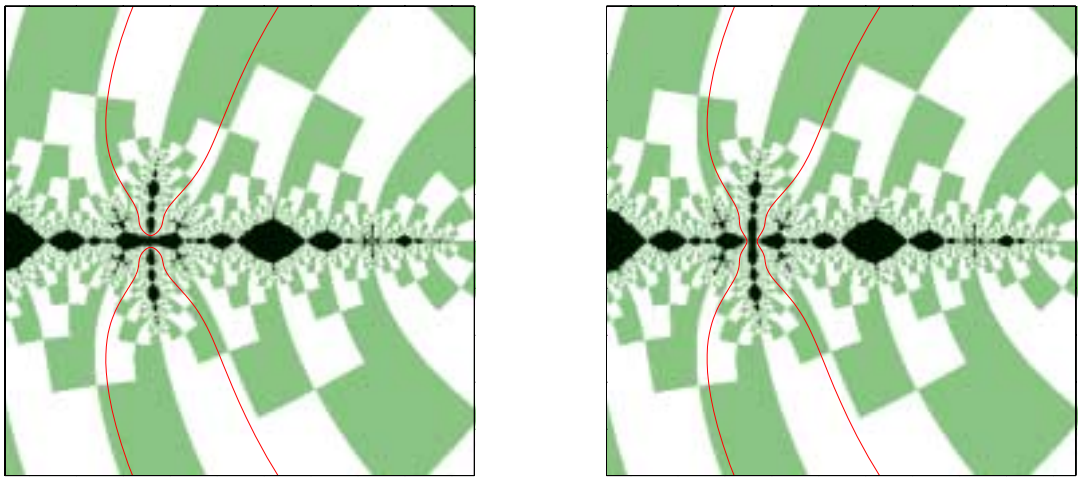

Figure A.30: Rays as identified "inside" ρ_4 (left) and "outside" ρ_4 (right).

$$\begin{bmatrix} {}^{\infty}0.011100(10)^{\infty} \\ {}^{\infty}0.100011(01)^{\infty} \end{bmatrix} \qquad \begin{bmatrix} {}^{\infty}0.011100(10)^{\infty} \\ {}^{\infty}1.100011(01)^{\infty} \end{bmatrix}$$

$$\begin{bmatrix} {}^{\infty}1.011100(10)^{\infty} \\ {}^{\infty}1.100011(01)^{\infty} \end{bmatrix} \qquad \begin{bmatrix} {}^{\infty}0.100011(01)^{\infty} \\ {}^{\infty}1.011100(10)^{\infty} \end{bmatrix}$$

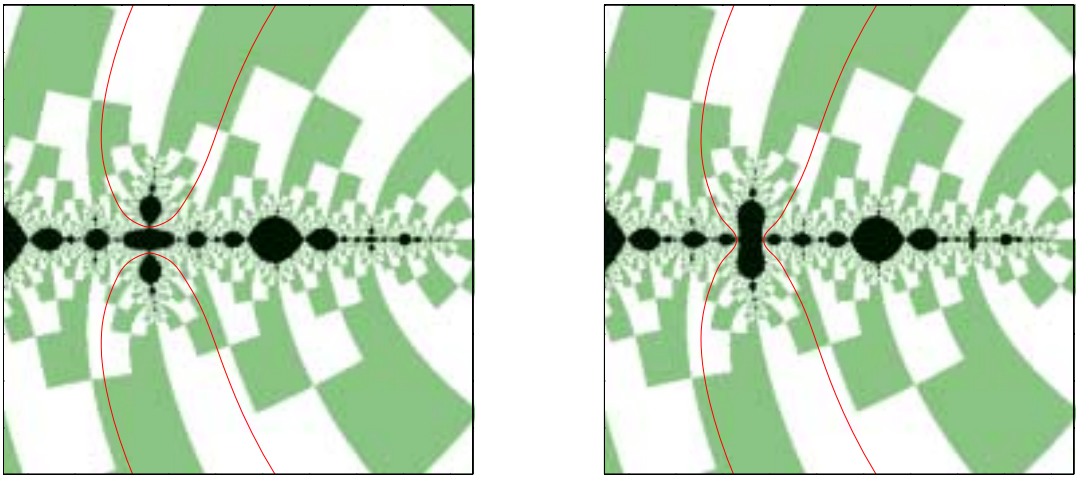

Figure A.31: Rays as identified below ρ_5 (left) and above ρ_5 (right).

B Notes on the algorithms.

B.1 Computing Unstable Manifolds.

The information contained in the W^u_p picture was explained in §2.5. We present here some further details of how these pictures are obtained. We let p be the β-fixed point (for other periodic points an appropriate iterate of f needs to be considered but the fundamentals are the same). An important piece of information we obtain from the W^u_p picture is the partition of $W^u(p)$ into points with bounded orbit, K^+_p, and their complement, U^+_p, pulled back to $\mathbf{C}$ via the uniformization map $\phi_p : \mathbf{C} \to W^u(p) \subset \mathbf{C}^2$ that parameterizes the unstable manifold. Except for the computation of $\phi_p(z)$, the problem of computing this partition is analogous to that of computing the filled Julia set of polynomials in the plane[5]. One of the simplest methods for obtaining this partition numerically is the "escape set" algorithm in which $z \in \mathbf{C}$ is assumed to be in K^+_p if $f^N(\phi_p(z)) \in W^u(p)$ does not escape a ball of radius R, where $N >> 1$ is some (fixed) large number of iterations. In practice this simple method gives a reasonable results for maps in the region we discussed here[6]. In our setting only a small neighborhood of 0 in $\phi_p^{-1}(W^u(p))$ needs to be computed since the W^u_p picture is invariant under multiplication by a constant λ. This self similarity was mentioned in §2.5 in connection with (2.23) which for the β-fixed point becomes

$$f \circ \phi_p(z) = \phi_p(\lambda z) \tag{B.1}$$

[5]Algorithms for this problem are discussed in detail in [PR, Mil2].

[6]In general the method is limited by the escape rate of points near K^+_p; more sophisticated methods take into account the orbits of neighboring points.

with λ the expanding eigenvalue of $Df(p)$. To compute ϕ_p we exploit the fact that it is an analytic map given by a power series, and use equation (B.1) to obtain a recursive formula for the coefficients in the Taylor expansion of ϕ_p. A truncated sequence can then be used to approximate ϕ_p after observing the behavior of the coefficients at the parameter values being considered.

B.2 Computing G^+ and its harmonic conjugate.

Additional information captured in the W^u_β picture are level sets of G^+ in U^+_p; (a third is is the coding of external rays given the binary decomposition of U^+_p, as explained in 2.5).

The function G^+ is the rate-of-escape function so $G^+ \equiv 0$ on K^+_p and on U^+_p it is well approximated numerically using the number of iterates it takes each point to escape a large ball. Specifically, for $q \in U^+_p$ we compute $\tilde{G}(q) \approx G^+(q)$ as

$$\tilde{G}(q) = \frac{1}{d^{n_q}} \log |X_{n_q}(q)|$$

where $X_n(q) = \pi_x f^n(q)$ for $n \geq 0$, and n_q is the first integer such that $|X_n(q)| > R$. In analogy with the one dimensional case, this computation is based on the relation $G^+ = \log|\varphi^+|$ and the asymptotic behavior of ϕ_p "at infinity": In our setting, $\varphi^+ \approx \pi_x$ on V^+ (more precisely $\varphi^+(x,y) = x + O(x^{-1})$ for $(x,y) \in V^+$). Then, for R large enough so that $|X_{n_q}(q)| > R$ implies $f^{n_q}(q) \in V^+$, we get $|X_{n_q}(q)| \approx |\varphi^+ \circ f^{n_q}(q)|$, and therefore $\tilde{G} \approx G^+$ since $G^+ \circ f = d\, G^+$.

Note that the error in the computed value for $G(q)$ is smaller for q near K^+_p, where n_q is large. Namely, if $|X_{n_q}(q)| = |\varphi^+(f^{n_q}(q))| + \varepsilon$, then $\tilde{G}(q) = G^+ + \varepsilon/d^{n_q}$.

The "improvement" in $\tilde{G}$ near K_p^+ will be useful in the computation of the landing point of external rays. This computation will require the ability to also compute a choice of harmonic conjugate H for G^+.

A numerical value for H cannot be obtained directly by iterating f. Instead, we get $\Theta_n = \arg(X_n) = \arg(\pi_x f^n)$. This quantity satisfies

$$\Theta_{n_q}(q) \approx d^{n_q} H(q) \mod 2\pi \tag{B.2}$$

where n_q is as in the computation of $\tilde{G}(q)$. Then, from a known value of $H(q_0)$ (initially 0 for q_0 in the fixed-ray), we obtain $H(q)$ for q near q_0 as follows:

1. Compute an initial linear approximation $H_I(q)$ based on the partial derivatives of $\tilde{G}$ at q_0 (this is a standard numerical integration step).

2. Determine the integer N that minimizes $\Delta = \Theta_{n_q}(q) + 2\pi N - H_I(q)$.

3. If Δ is adequately small, use N to compute $\tilde{H}(q) = (\Theta_{n_q} + 2\pi N)/d^{n_q} \approx H(q)$; else take steps to obtain a better H_I (there are many options).

In a sequence of these steps there is no cumulative error from the numerical integration, since H_I is only used to find N. Note also that if the error in (B.2) of size ε, after obtaining the correct N we get an error in $\tilde{H}(q)$ of size only $\varepsilon/2^{q_n}$.

B.3 Computing External Rays

Recall from §2.4 that when Theorem 1 holds, each component Ω of $W^u(p) - K^+$ is conformally equivalent to left-half-plane $\mathbf{H}$ with the Greens function $G = G^+|_{W^u(p)}$ and a choice of harmonic conjugate H as natural coordinates: The map $\omega : \Omega \to \mathbf{H}$,

$\omega = G + iH$ is a homeomorphism. Lines of constant-H correspond to external rays. In the W^u_p pictures, we visualize the inverse image of $\mathbf{H}$ under $h = \omega \circ \phi_p$, where ϕ_p is the natural parameterization of W^u.

To solve the problem of computing a specific external ray (or more precisely the landing point of the ray), we consider the more general problem of determining the point $z_* \in \mathbf{C}$ such that $h(z_*) = G_* + iH_*$ for some specified target values G_* and H_* (the case $G_* = 0$ corresponds to finding a landing point for the ray with $H = H_*$). One approach is to "linearly navigate" towards z_* adjusting the course at each step:

Adjust: Let s_k be a "small step" in the direction from $p_k = h(z_k)$ to p_*.

Advance: Compute $z_{k+1} = z_k + Dh(z_k)^{-1} s_k$.

To actually obtain a sequence that approaches the landing point $z_* = h^{-1}(0, H_*)$ one needs to deal with the paradigm of traveling with a reasonable step size while preventing the non-linearities near the fractal boundary at $G = 0$ from taking over.

Our approach exploits the fact that the computation of h improves as points approach the $G = 0$ region. Without giving all the details, the main idea is as follows:

1. Starting from a value z_0 such that $G_0 := G(z_0)$ is not too small, proceed along the G_0 level curve until reaching z_n such that $H(z_n)$ is near the target H_*.

2. Then, "descend" towards the the $G = 0$ level marching along the constant-H_* curve, stopping when $\tilde{G}$ becomes less than required accuracy.

The first stage can be done with a step that is a fixed and small fraction of the distance to the target H_*. The accuracy with which H_* is found is improved in the

second stage, and if the initial $G_0 > 0$ is chosen adequately the non-linearities have little effect in the march towards a neighborhood of $h^{-1}(G_0, H_*)$.

In the second stage one needs to adjust the step size to ensure that at each iteration step the new point z_k remains close to the H_*-ray. For instance, we check that the difference $\Theta + 2\pi N - H_I$ remains small in each step, and we also require that each new point descends only a few levels sets from the previous point (within a level set the integer n such that $|X_n(\phi_p(z))| > R$ is constant). This allows us to control the step size while assuring convergence towards the $G = 0$ level.

One nice feature of this approach is that plotting the points computed in the second stage is a way of visualizing external rays near their landing point.

Bibliography

[A] P. Atela, Bifurcations of dynamics rays in complex polynomials of degree two. *Ergod. Th. & Dynam. Sys.* (1991), 12:401-423. 2

[BK] C. Bandt and K. Keller, Symbolic Dynamics for angle-doubling on the circle I: The topology of locally connected Julia sets. *Lectures Notes in Math. 1514*, Springer, Berlin, (1992).

[Br] B. Branner, The Mandelbrot set. In *Chaos and Fractals, the mathematics behind the computer graphics*, R. Devaney & L. Keen, Eds. AMS Proceedings of Symposia in Applied Mathematics, (1989) 39:75–105. 2, 86

[BS1] E. Bedford and J. Smillie, Polynomial Diffeomorphism of $\mathbf{C}^2$ I: Currents, equilibrium measure and hyperbolicity, *Invent. Math.* (1990), 87:69-99.

[BS3] E. Bedford and J. Smillie, Polynomial Diffeomorphism of $\mathbf{C}^2$ III: Ergodicity, exponents and entropy of the equilibrium measure. *Math. Ann.* (1992) 294:395–420.

[BS5] E. Bedford and J. Smillie, Polynomial Diffeomorphism of $\mathbf{C}^2$ V: Critical points and Lyapunov exponents. *J. of Geometric Analysis* (to appear).

[BS6] E. Bedford and J. Smillie, Polynomial Diffeomorphism of $\mathbf{C}^2$ VI: Connectivity of J. (to appear). 10

[BS7] E. Bedford and J. Smillie, Polynomial Diffeomorphism of $\mathbf{C}^2$ VII: Hyperbolicity and external rays. (to appear). 2, 4, 4, 26, 120

[Bou] T. Bousch, Sur quelques problémes de dynamique holomorphique. Thése, Université de Paris Sud, Orsay, 1992.

[Buz] G. Buzzard and J. Smillie, Complex Dynamics in Several variables. In *Flavors of Geometry*, 1997.

[D] A. Douady Descriptions of compact sets in **C**. In *Topological Methods in Modern Mathematics: a symposium in honor of John Milnor sixtieth birthday.* L.Goldberg and A. Phillips, Eds., Publish or Perish, 1993. 7, 45, 51

[DH] A. Douady and J.H. Hubbard, Étude dynamique des ploynômes complexes I & II, Publications Mathématiques d'Orsay, 1984. 2, 86

[Fr] D. Fried, Finitely presented dynamical systems, *Ergodic Theory and Dyn. Sys.* (1987), 7:489–507. 37

[FS1] J.-E. Fornaess and N. Sibony, Complex Hénon mappings in $\mathbf{C}^2$ and Fatou-Bieberbach domains. *Duke Math. J.* (1992), 65:345–380.

[FM] S. Friedman and J. Milnor, Dynamical properties of plane polynomial automorphisms. *Ergodic Theory and Dyn. Sys.* (1989) 9:67–99. 7

[Hé] M. Hénon, A two-dimensional mapping with a strange attractor, *Comm. Math. Phys.* (1976) 50:69–77.

[Hig] P. Higgings, Introduction to topological groups. Cambridge University Press, (1974). 11

[Hub] J.H. Hubbard, Hénon mappings in the complex domain In *Chaotic Dynamics and Fractals*, M. Barnseley & S. Demko, eds. Academic Press, (1986).

[HOV1] J.H. Hubbard and R. Oberste-Vorth, Hénon mappings in the complex domain I: The global topology of Dynamical Space. *Publ. Sci. I.H.E.E.S.*, (1994), 79:5–46. 4, 8, 10, 124

[HOV2] J.H. Hubbard and R. Oberste-Vorth, Hénon mappings in the complex domain II: Projective and inductive limits of polynomials In *Real and Complex Dynamical Systems*, Branner & Hjorth, eds. Kluwer Academic Publishers (1995), 89–132. 30, 40, 43, 43

[KH] A. Katok and B. Hasselblatt, Introduction to the Modern Theory of Dynamical Systems, Cambridge University Press, (1995). 18

[LM] D. Lind and B. Marcus, An Introduction to Symbolic Dynamics and Coding Cambridge University Press, (1995). 18, 38

[Mil1] J. Milnor, Dynamics in one Complex variables. Preprint#1990/5. SUNY Stony Brook Institute for Mathematical Sciences.

[Mil2] J. Milnor. Self similarity and hairiness in the Mandelbrot set. In *Computers in Geometry and Topology*, M. Tangora, ed. Lect. Notes Pure Appl. Math. 114, Dekker (1989), 211-257. 134

[PR] H.-O. Peitgen and P. Ritcher, The beauty of fractals. Springer-Verlag (1986). 134

[Shu] M. Shub, Global stability of dynamical systems. Springer-Verlag (1987). 11

Addendum.

This is a slightly revised version of my doctoral thesis of 1998. Most changes are simple corrections of typing and spelling mistakes, but also I have re-worded a few sentences to improve legibility. Most noticeable, the title of section 3.3.2 has been shortened: the original title was "*A model for a map with an attracting fixed point as well as a period-3 sink: the (3-1)-graph*". The new shorter title allows hyperref to create a single link into this section when building the table of contents of the PDF document.